APPLICATION OF ENGINEERING PRINCIPLES TO THE DESIGN OF BIODEGRADABLE POLYMER MATRICES FOR CONTROLLED RELEASE

by

Sam N. Rothstein

B.S. Chemical Engineering, Bucknell University, 2005

Submitted to the Graduate Faculty of

Swanson School of Engineering in partial fulfillment

of the requirements for the degree of

Doctor of Philosophy in Chemical Engineering

University of Pittsburgh

2012

UNIVERSITY OF PITTSBURGH

SWANSON SCHOOL OF ENGINEERING

This dissertation was presented

by

Sam N. Rothstein

It was defended on

November 13, 2012

and approved by

Louis Falo, M.D., Ph.D., Professor and Chairman, Department of Dermatology

William Federspiel, Ph.D., W.K. Whiteford Professor, Departments of Chemical Engineering, Surgery, and Bioengineering

Robert Parker, Ph.D., Associate Professor, Department of Chemical Engineering

Nicolas Sluis-Cremer,Ph.D., Associate Professor, Department of Medicine, Division of Infectious Diseases

Dissertation Director: Steven Little, Ph.D., Chair, Department of Chemical Engineering, Associate Professor, Departments of Chemical Engineering, Bioengineering, Immunology

APPLICATION OF ENGINEERING PRINCIPLES TO THE DESIGN OF BIODEGRADABLE POLYMER MATRICES FOR CONTROLLED RELEASE

Sam N. Rothstein, PhD

University of Pittsburgh, 2012

Controlled release formulations improve drug safety and address patient adherence, barriers that are responsible for 10% of hospitalizations and over $100 billion in annual medical expenses. These benefits apply to medications that require consistent dosing over days, weeks, or months, a category accounting for over 90% of prescription drugs sales. Yet, the use of controlled release formulations remains comparatively sparse because their design requires months of costly experimentation.

Significant scholarship has been devoted to facilitating formulation development and to understanding controlled release behavior, particularly in the realm of mathematical modeling. However, each modeling study to date has only focused on predicting the performance of an extremely limited number of "drug"-polymer combinations, vehicle geometries and excipient types. Researchers have yet to arrive at one general theory of controlled release applicable to a wide range of drug delivery systems and have even begun to doubt that one will be developed.

To define the underlying mechanisms of controlled release, we studied data from formulations encapsulating a wide variety of agents. Analysis began with poly(lactic-co-glycolic) (PLGA) acid microparticles, yielding a set of equations that predicted the release behavior of neutral or anionic, water-soluble agents from small molecule drugs (~300Da) to viruses. Building from this foundation, new layers of diffusion/reaction equations were added to enable predictions for implant systems and sparingly soluble drugs. These predictions compared

favorably to *in vitro* data from implants that underwent either dissolution-limited or degradation-controlled release.

The new predictive models of controlled release enable analytical interpretation of *in vitro* release data. Their predictions have identified rates and durations of drug release in over 20 systems to date. Calculations of *in vitro* release also aid in targeting precise release behaviors ranging abrupt bursts to sustained, constant release. These behaviors were realized in a delayed release vaccine, capable of masking antigen from the body until a specific point in time, and as a sustained release formulation that delivered the HIV entry inhibitor, enfuvirtide, for one month. The *in vitro* and *in vivo* data from these two proof-of-concept applications support the use of predictive modeling in the design of long-acting controlled release formulations.

TABLE OF CONTENTS

PREFACE ..... **XVI**

1.0 INTRODUCTION: **1**

1.1 CONTROLLED RELEASE TECHNOLOGY **1**

1.1.1 Application to Drug Delivery **1**

1.1.2 Potential and Limitations **2**

1.1.2.1 Quality Assurance Considerations **3**

1.1.2.2 Summary of long acting controlled release formulations **4**

2.0 PRIOR ART IN THE EMPIRICAL DESIGN OF CONTROLLED RELEASE FORMULATIONS **5**

2.1 INTRODUCTION **5**

2.2 TUNING THE INITIAL BURST **8**

2.2.1 Modifying burst magnitude **8**

2.2.1.1 Dispersion of Drug in the Polymer Matrix **8**

2.2.1.2 Manipulation of Osmotic Pressure **9**

2.2.1.3 Manipulation of Matrix Size **10**

2.2.1.4 Manipulation of Drug Loading **11**

2.2.2 Tuning the kinetics of the initial burst **12**

2.2.2.1 Controlling Drug Dissolution Rate **12**

2.2.2.2 Effect of Radial Drug Distribution **13**

2.2.3 Initial burst summary **14**

2.3 TUNING THE LAG PHASE 14

2.3.1 Tools for tuning the duration of the lag phase 15

2.3.1.1 Setting of Initial Polymer Molecular Weight 15

2.3.1.2 Controlling Polymer Degradation Rate 16

2.3.1.3 Use of Catalytic Excipients 17

2.3.1.4 Post Fabrication Irradiation 17

2.3.2 Lag phase summary: 18

2.4 FINAL RELEASE 19

2.4.1 Tuning the rate of final release 19

2.4.1.1 Use of Polymer Blends 19

2.4.1.2 Control via Copolymer Ratio 20

2.4.2 Final release summary: 20

2.5 CONCLUSIONS: 21

3.0 DEVELOPING A PREDICTIVE MODEL OF RELEASE FROM BULK ERODING POLYMER MATRICES 22

3.1 INTRODUCTION 22

3.1.1 Evaluation of models addressing the initial burst by critical properties .. 23

3.1.1.1 Agent Loading and Copolymer Ratio: 23

3.1.1.2 Agent Loading, Solubility: 23

3.1.2 Evaluation of models addressing the burst and lag phases by critical properties 25

3.1.2.1 Initial Polymer Molecular Weight, Irradiation: 25

3.1.2.2 Polymer Initial Molecular Weight, Agent Distribution: 25

3.1.3 Evaluation of models of triphasic release by their critical properties..... 26

3.1.3.1 Microparticle Combinations: 26

3.1.3.2 Erosion, Degradation, Drug Loading, Posority, Particle Size, Solubility, and Polymer Chemistry: 27

3.1.4 Summary of Mathematical Models: 29

3.2 MODEL DEVELOPMENT 30

3.2.1 Release paradigm 30

3.2.2 Model Equations 33

3.2.2.1 Pore induction time distribution 35

3.2.3 Solution and Regression 37

3.2.4 Validation of math model 38

3.2.5 Regression-free predictions 41

3.3 MODELING RESULTS 42

3.3.1 Validation 42

3.3.2 Predictions 42

3.3.2.1 Predictions of Release Data 42

3.3.3 Theoretical Predictions 46

3.4 DISCUSSION 48

3.5 CONCLUSIONS 52

4.0 MATHEMATICS FOR HYDRATION LIMITED SYSTEMS 53

4.1 INTRODUCTION 53

4.2 METHODS 55

4.2.1 Release Paradigm 55

4.2.2 Model Development 56

4.2.2.1 Limiting Cases 59

4.2.3 Model Implementation 60

4.2.3.1 Critical length 61

4.2.4 Release Predictions 62

4.3 RESULTS 63

4.3.1 Matrix degradation kinetics 63

4.3.2 Dissolution controlled release 67

4.3.3 Degradation controlled release 69

4.4 DISCUSSION 73

4.5 CONCLUSIONS 78

5.0 IMPACT OF PREDICTIVE MATHEMATICAL MODELS ON *IN VITRO* CONTROLLED RELEASE ASSAYS 79

5.1 INTRODUCTION 79

5.2 MATERIALS AND METHODS 81

5.2.1 Materials 81

5.2.2 Microparticle fabrication 81

5.2.3 Microparticle characterization 82

5.2.4 *In vitro* release assay 82

5.2.5 Collection of published release data 84

5.2.6 Model predictions 84

5.3 RESULTS 85

5.3.1 Interpolation of release data sets with widely spaced sample points 86

5.3.2 Extrapolation of release data sets that terminate prior to completion 92

5.4 DISCUSSION 96

5.5 CONCLUSION 102

6.0 CASE STUDY: DELAYED RELEASE VACCINE PLATFORM 104

6.1 INTRODUCTION 104

6.2 MATERIALS AND METHODS 108

6.2.1 Materials 108

6.2.2 Polymer Selection 109

6.2.3 Formulation Production 110

6.2.4 Formulation Characterization 110

6.2.5 *In vitro* Release Assay 111

6.2.6 Mice 111

6.2.6.1 Immunization protocols 112

6.2.6.2 OT-II Proliferation Assay 112

6.2.6.3 Measurement of ova-specific CTL lysis 113

6.2.6.4 Titre measurement of IgG1a and IgG2c 113

6.3 RESULTS 114

6.3.1 Formulation Designs and *In vitro* Release 116

6.3.2 Formulations Properties 117

6.3.3 *In vivo* testing of the DRV 119

6.3.3.1 OT-II proliferation 120

6.3.3.2 OVA-specific CTL lysis 122

6.3.3.3 IgG1 and IgG2c titre 123

6.3.4 Results Summary 125

6.4 DISCUSSION 125

6.5 CONCLUSIONS 129

7.0 CASE STUDY: A SUSTAINED RELEASE FORMULATION 130

7.1 INTRODUCTION 130

7.2 MATERIALS AND METHODS 134

7.2.1 Materials 134

7.2.2 Microparticle Production 134

7.2.3 Microparticle Characterization 135
7.2.4 HPLC detection 135
7.2.5 Enfuvirtide (T20) Stability Calculations 136
7.2.6 T20 Activity Testing 136
7.3 RESULTS 137
7.3.1 Enfuvirtide Activity Results 142
7.3.1.1 Measurement of T20 stability 143
7.3.1.2 Measurement of T20 inhibition of viral replication 144
7.3.2 Results Summary 146
7.4 DISCUSSION 146
7.5 CONCLUSIONS 150
8.0 FUTURE WORK 152
APPENDIX 156
GLOSSARY OF ABBREVIATIONS 156
BIBLIOGRAPHY 158

LIST OF TABLES

Table 1: List of experimental systems used for model validation 39

Table 2: Interpolative Predictions 91

Table 3: Extrapolative Predictions 96

Table 4: Production Conditions 109

Table 5: Composition of 50:50 PLGA Mixture 137

Table 6: T20 Stability via Analysis of HPLC Peak Areas 143

LIST OF FIGURES

Figure 1: Microscopy images of particle matrix cross-sections and exteriors (insert). 6

Figure 2: Tri-phasic release profile 7

Figure 3: Comparison of burst magnitudes from microparticles of varying size. 11

Figure 4: Relationship between polymer molecular weight and lag duration. 16

Figure 5: Protein release predictions for PLGA & PLA particles. 28

Figure 6: Schematic depiction of a paradigm that can account for four-phase release. 31

Figure 7: Schematic depiction of the initial burst as it relates to occlusion size. 32

Figure 8: Correlations for D and M_{wr} developed from regressions to experimental data in Table 1. 40

Figure 9: Regression-free prediction for peptide release from PLGA microspheres. 43

Figure 10: Regression-free prediction for BSA release from polyanhydride microparticles. 44

Figure 11: Release predictions compared to *in vitro* data from blended PLGA polymer microspheres. 45

Figure 12: Theoretical release profiles for obtained by varying model parameters: R_p, R_{occ}, M_{wo}, $kC_w(n)$. 47

Figure 13: Degradation profiles (Mw relative to Mw_o as a function of distance and time) for various spherical matrices of 10kDa PSA. 65

Figure 14: Calculation of critical length 66

Figure 15: Predictions of dissolution-controlled, release of drug. 68

Figure 16: Predictions for degradation-controlled release of drug. 70

Figure 17: Predictions of release from (A) bulk eroding and (B) surface eroding POE matrices. 72

Figure 18: Testing model predictions for the interpolation of *in vitro* release data from enfuvirtide loaded 9kDa 50:50 PLGA, 20µm particles. 87

Figure 19: Evaluations of *in vitro* data for lysozyme encapsulated in 12kDa 50:50 PLGA[17]. 89

Figure 20: Evaluations of *in vitro* data for superoxide dismutase (SOD) 90

Figure 21*:* Testing an extrapolative prediction 93

Figure 22: Extrapolated SOD release from 106kDa poly(lactide) microparticles. 94

Figure 23: Release of rhGH from 45kDa 50:50 PLGA microparticles. 95

Figure 24: Comparison of dosing schedules 105

Figure 25: *In vitro* release of OVA from delayed release microparticles measured by spectraphotometry. 115

Figure 26: Microparticle formulations tailored for 2 and 4 week lag phases. 117

Figure 27: Comparison of OVA-alum microparticles A) pre- and B) post- wash. 118

Figure 28: Confocal microscopy analysis of 4 week DRV formulation. 118

Figure 29: **Sample sizing result from DRV particles.** 119

Figure 30: Comparison of OT-II cell proliferation from DRV microparticles and control vaccines 121

Figure 31: OVA-specific CTL lysis 122

Figure 32: **Titres of OVA-specific IgG2c and IgG1 antibodies.** 124

Figure 33: In vitro and in vivo enfuvirtide delivery profiles from a controlled release formulation.[78] 133

Figure 34: Scanning electron and confocal microscopy images of particles from SRF formulation. 138

Figure 35: *In vitro* release of DexTR from SRF microparticles. 139

Figure 36: *In vitro* release from the model defined mixture of DexTR microparticles. 140

Figure 37: *In vitro* release of T20 from three model-defined component microparticles of SRF 141

Figure 38: Detection of T20 by HPLC. 142

Figure 39: Luciferase expression of TZM cells exposed to HIV in the presence of T20. ... 144

Figure 40: The rate of active T20 release (green circles) follows model predictions (red lines). 145

PREFACE

My PhD research and its development in to a formulation design technology has been facilitated by a number of teams that require acknowledgment. First, I would like to thank my advisor Dr. Steven Little for giving the freedom to research a topic of my choosing, the modeling of controlled release. Steve and all of the Little Lab researchers have helped me transition this research from *in silico* to *in vitro* to *in vivo*. Second, I would like to thank my other advisors, Andrew Remes, Paul Petrovich and the Office of Technology Management as well as the teams at Idea Foundry, Innovations Works and the Pittsburgh Lifesciences Greenhouse helping me realizing my dreams as an engineer, moving a new technology from academica to industry. Finally and most importantly, I could not have completed this PhD without the love and support of my wife, Mary, and my family. You have always been my greatest support and helped me focus on the most important things in life.

1.0 INTRODUCTION:

1.1 CONTROLLED RELEASE TECHNOLOGY

Controlled release technology is a collection of tools, methods, or indeed technologies, for autonomously delivering an encapsulated payload at a desirable rate or with desirable timing. Products that rely on controlled release technology are found today in agricultural, food, consumables, personal-care, and pharmaceutical industries. Examples of these products include hormone supplements for cattle, nutrient-enriched drinks, microencapsulated enzymes in laundry detergents, moisturizing creams, and pills with once-daily dosing. These products range from the incredibly simple, like sandwiched layers of flavor in chewing gum, to the molecularly complex, like enyzme-degradable polymers for bio-responsive drug release.

1.1.1 Application to Drug Delivery

From the diversity of controlled release products, the drug delivery applications clearly represent the largest market segment with over $20 billion in annual sales[7]. In this niche, salts, sugars, polymers and other excipients are used to prolong bioavailability of a drug enabling less frequent administration. Successfully controlled release medications can command over $1 billion in annual sales[8]. Controlled release pills frequently reduce dosing from 2, 3, or 4 times a day to

once-daily. Biodegradable polymer matrices, such as nanoparticles, microparticles, film coatings and implants, allow dosing to be extended even further. A single injection of biodegradable polymer microparticles can provide weeks or months of dosing. An example of this type of medication is Risperdol Consta®, which provides two weeks of treatment for schizophrenic patients of whom fewer than 50% consume oral medications as prescribed[9]. In addition to improving adherence, long-acting formulations can also enable entirely new types of treatments. Gliadel wafer® a biodegradable disc that releases carmustine provides a hallmark example of such a treatment, by enabling the local treatment of neural glioblastoma after surgical resection. Use of this medication increased patient lifespan by 19-39% in clinical trials[10].

1.1.2 Potential and Limitations

The potential of controlled release medications, and in particular the long-acting dosage forms that provide weeks to months of drug delivery, is actually far greater than the size of the present controlled release technology market ($28 billion) indicates[7]. Controlled release technology addresses patient non-compliance (the failure to adhere to a prescription), which is a significantly larger market, accounting for $136 billion in annual medical expenses[11]. In practice, the field has not yet realized this enormous potential because generating a specific controlled release formulation (i.e. one customized to the dosing schedule demanded by any given medication) is extremely time consuming and costly. As such, only 11 controlled release formulations that extend dosing beyond 1 week have reached the market[12]. In each case, the associated drugs have clear compliance risks (elevating the need for extended dosing) or wide therapeutic windows (relaxing the requirement for stringent control over release). Yet, these medications represent

just a small fraction of drugs that could be improved with properly designed controlled release formulations. By one estimate, at least 90% of the top 100 best-selling prescription medications could further advance patient quality of life if they offered reduced dosing frequency[13,14]. From this viewpoint, the field can be said to have broad therapeutic applicability, but comparatively limited implementation.

1.1.2.1 Quality Assurance Considerations

In addition to being notoriously difficult to design, long-acting controlled release formulations are noted as being among the most complex of drug formulations to successfully consistently produce. The production of a biodegradable microparticles formulation brings into play a number of quality control considerations, including the properties of polymers and excipients, the removal of organic solvents, the lyophilization of powdered product, and the assessment of needle gauge[15]. Current practice is to assess the quality of a product batch post production. The most time consuming portion of this analysis is the *in vitro* release assay where a formulation's rate of drug release is measured in real time in order to determine if it is consistent with the FDA approved performance requirements. Research has been conducted on methods of accelerating the *in vitro* release assay by the means of elevated temperature[16]. For common hydrolysable polymers, such as poly(lactic-co-glycolic) acid, formulation degradation and in turn drug release is accelerated by increasing ambient temperature from 37^{o}C (standard) to values of between 40^{o}C and 60^{o}C. Once correlated to data from assays conducted at 37^{o}C, an elevated temperature assay can produce comparable results in a fraction of the time. At best, this approach has shortened the 2 month quality control assaying of Risperidol Consta® down to 1 week[17]. However, product safety and production efficiency can be further improved by a Quality by

Design (QbD) approach to quality control. In QbD knowledge of how variation in a formulations composition and production will affect its performance is used to determine if a given product is acceptable. This requires mapping of a formulation's performance across a design space spanning changes in both process parameters, such as mixing speed or lyophilization time, and material properties, such as polymer molecular weight or excipient concentration[18]. The state of the art in conducting such analysis is known as Design of Experiments (DoE), where statistical metrics are used to minimize the number of experiments needed to fully explore the combined impacts of various formulation properties and manufacturing parameters on drug release[19,20]. Even with the efficiency ensured by DoE, QbD analysis is very time consuming and costly to perform on long acting parenteral formulations because many different variations of a basic microparticle or implant design must be produced and then assayed over weeks or months until the full extent of their release behavior is known.

1.1.2.2 Summary of long acting controlled release formulations

Long acting formulations that deliver drug over weeks or months before being safely resorbed by the body are an area of tremendous potential for the field of controlled release technology. Such formulations have already made medical impacts addressing patient compliance and enabling entirely new types of treatments. They also have the potential to improve the large majority of medications, if cost and time issues associated with design and production can be addressed. Specific challenges come from an iterative experiment-driven design process and new quality assessment demands to improve formulation safety. Both of these challenges could be resolved with an in-depth quantitative understanding of parameters that effect formulation function.

2.0 PRIOR ART IN THE EMPIRICAL DESIGN OF CONTROLLED RELEASE FORMULATIONS

2.1 INTRODUCTION

Bulk eroding biodegradable polymer matrices have a track record of FDA approval that extends back more than 40 years. This record of clinical safety and efficacy encompasses not only long-acting controlled release formulations, but also surgical sutures and implantable devices, such as resorbable bone screws. Accordingly bulk-eroding polymer matrices, such as poly(lactic-co-glycolic) acid (PLGA) microparticles remain a first-choice in scenarios where drug must be autonomously released over weeks or months. However, because bulk eroding polymers, such as PLGA, were first developed for orthopedic and surgical applications, they are not optimally engineered for drug delivery performance.

Over the past two decades, a number of studies have aimed to increase the efficiency of designing degradable polymer drug delivery formulations. The earliest studies sought to identify key physical properties of the polymer matrices that determine release behavior[21,22]. Twenty years later, researchers are still experimenting with a variety of new formulation compositions, polymer chemistries and processing conditions in an attempt to tune this release behavior[23-26]. Over time, a number of system properties and processing conditions have emerged as potential tools for tuning the kinetics of delivery systems[14,27]. However, a standardized method of tuning

remains elusive due to the complexity that arises when factors, such as polymer chemistry, alter several properties that determine release simultaneously, such as matrix crystallinity, pH, degradation rate and hydrophobicity[24].

A review of empirical tools is essential in order to understand what is known about how biodegradable polymer matrices function as controlled release formulations. The most widely-studied biodegradable polymeric materials (i.e. polyesters, polyanhydrides, poly-ortho esters, etc…) offer the largest wealth of information on such tools given their long history of use and similarity of fundamental release behavior, which encompassed both the underlying mechanisms and resulting kinetics. Although the techniques that can be used to control release in these systems are generally applicable to any size, shape, and orientation of a degradable matrix, this chapter will most often refer to one of the most commonly reported configurations of these matrices, a spherical particulate system.(Figure 1) Studies on microparticles have empirically varied independent system properties (such as matrix size, degradation rate or polymer molecular weight) or processing conditions (such as emulsion type, solution osmolality, or solvent choice)

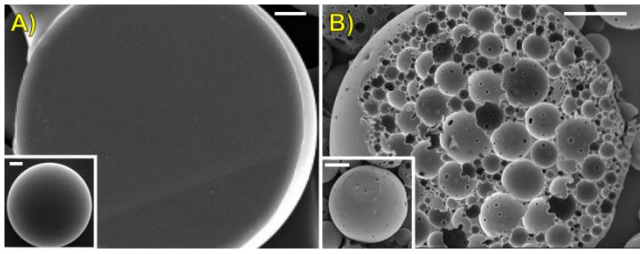

Figure 1: Microscopy images of particle matrix cross-sections and exteriors (insert).

A) In homogenous systems (like single emulsion microparticles) the drug resides in-phase with the polymer matrix (adapted with permission from[1]). B) In contiguous systems (like double or water-in-oil-in-water emulsion microparticles), the drug resides in pockets that are separated from the polymer matrix.

and documented their effects with *in vitro* assays. Each of these experimental variations can be evaluated for its potential as a design tool that a engineer can use to tune release behavior.

As a general rule, drug delivery vehicles can be tuned to provide a specific rate and duration of release independently. However, biodegradable matrices have been commonly observed to produce up to three distinct phases: 1) an Initial Phase (a.k.a. "Initial Burst") that is typically categorized by the rapid delivery of drug upon hydration, 2) a "Lag Phase" marked by a near-zero rate of release for some period of time. and 3) a "Final Phase" where measurable release resumes, typically in a Fickian fashion. Therefore, it would be useful to classify tools by their suitability for tuning the magnitude and/or duration of each individual phase in order to gain complete control over release.(Figure 2) Further, by analyzing the attempts to control these fundamental system phenomena and documenting their effects on release behavior, a picture of formulation function can be developed.

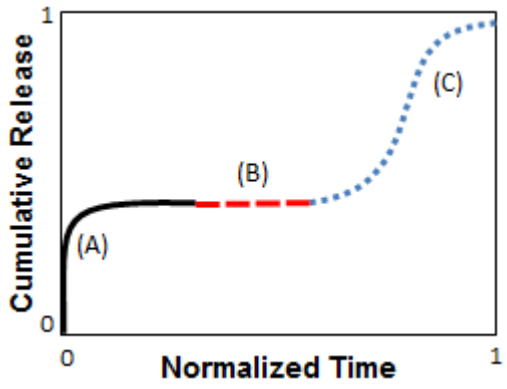

Figure 2: Tri-phasic release profile

Diagram of the A) Initial Burst, B) Lag Phase and C) Final Release. Note that any one of these phases may or may not be apparent depending upon the properties of the release system.

2.2 TUNING THE INITIAL BURST

Numerous studies have addressed the "Initial Burst" and a summary of findings have been the focus of two reviews in the past decade[28,29]. Both of these reviews discuss hypothetical mechanisms of "burst" release and potential strategies for preventing or eliminating it. Maintaining the theme of this review, we will focus on the impact that individual "design tools" have on the magnitude and/or kinetics of the initial burst.

2.2.1 Modifying burst magnitude

The initial burst can easily encompass all of release or even be completely eliminated. However, no one method exists for precisely targeting values across this entire range. Instead, studies put forth a variety of techniques that change burst magnitude with varying degrees of sensitivity.

2.2.1.1 Dispersion of Drug in the Polymer Matrix

Several studies have succeeded in creating dramatic reductions in burst magnitude by forcing hydrophilic proteins to disperse in the hydrophobic polymer matrix. For example, Fu et al eliminated the initial release of a water-soluble protein (human Glial-cell line derived neurotrophic factor) by using an ionic surfactant to dissolve the hydrophilic protein in-phase with the polymer[30]. In contrast, an equivalent double emulsion formulation (with polymer entrapping pockets of aqueous protein) produced more than 70% initial release[30]. A similar approach was adopted to eliminate the burst release of insulin using PEGylation, which aided the dissolution of

the protein in dichloromethane[31]. Practically, partitioning experiments can be used to determine if other agents will dissolve/disperse in the same phase as the polymer (e.g. organic phase) with the aid of surfactants or other modifications[32]. Since this design tool simply involves the dispersion of drug and polymer in a matrix, it should readily apply to any number of systems.

Interestingly, less predictable results are observed when a cosolvent is used to stabilize hydrophilic drugs in the same phase as the hydrophobic polymer matrix[33,34]. Using this approach on insulin-loaded PLGA microparticles reduced burst magnitude from 65 to 20%[34]. However, when applied to another protein (granulocyte colony stimulating factor), this technique actually increased the magnitude of the initial burst[33]. Yet both of these studies produce single emulsion systems by dissolving a protein in the co-solvent, dimethylsulfoxide, before mixing it with a polymer-dichloromethane solution. It is unknown as to the source of the disparity, but it may be possible that this process may cause protein molecules to aggregate into a separate phase, giving rise to a measurable burst magnitude.

2.2.1.2 Manipulation of Osmotic Pressure

Subtle changes in burst magnitude have also been achieved by changing the osmotic pressure during the processing of systems that are intentionally fabricated with an internal aqueous phase (e.g. double (water-in-oil-in-water) emulsion systems, see Figure 1B). Accordingly, Jiang et al tuned the initial burst of bovine serum albumin (BSA) to values between 30% and 80% of total release by adding salt or sucrose to the outermost aqueous phase during microparticle fabrication[35]. The same technique has been used in other macromolecule-loaded systems to reduce the magnitude of the initial burst[17,36]. Within each study, the reduction in burst magnitude was proportional to the amount of NaCl added to the outermost aqueous phase, (i.e.

the strength of the osmotic pressure gradient driving water out of the microparticles). Because osmosis is a fundamental process, this design tool should extend to a wide range of contiguous systems, and is particularly important to account for in systems where the drug itself dramatically affects the osmotic pressure (such as plasmid DNA)[37,38].

2.2.1.3 Manipulation of Matrix Size

A number of studies have also varied matrix size to tune the magnitude of burst release in double emulsion systems[2,6,36,39]. While this property is particularly easy to tune during fabrication, its effectiveness at controlling the magnitude of initial release varies from agent to agent. For example, initial release of the small molecule, lidocaine from polymeric microparticles dropped 30% as particle size increased 10 fold[2]. This trend is echoed over a larger size span by polyanhydride particles loaded with Butorphanol[39]. However, the release of insulin was more sensitive to changes in particle size, dropping 35% in magnitude from just a 3 fold change in particle size[36](Figure 3). Limitations arise as matrix size is reduced to below 5μm because such small bodies are readily cleared *in vivo* by the reticuloendothelial system (RES, consisting of phagocytic cells like macrophages)[40] or above 500μm in diameter as matrix hydration begins to affect the kinetics of the initial burst[41,42]. However, for median sizes, this method presents an effective approach to tuning the magnitude of initial burst release.

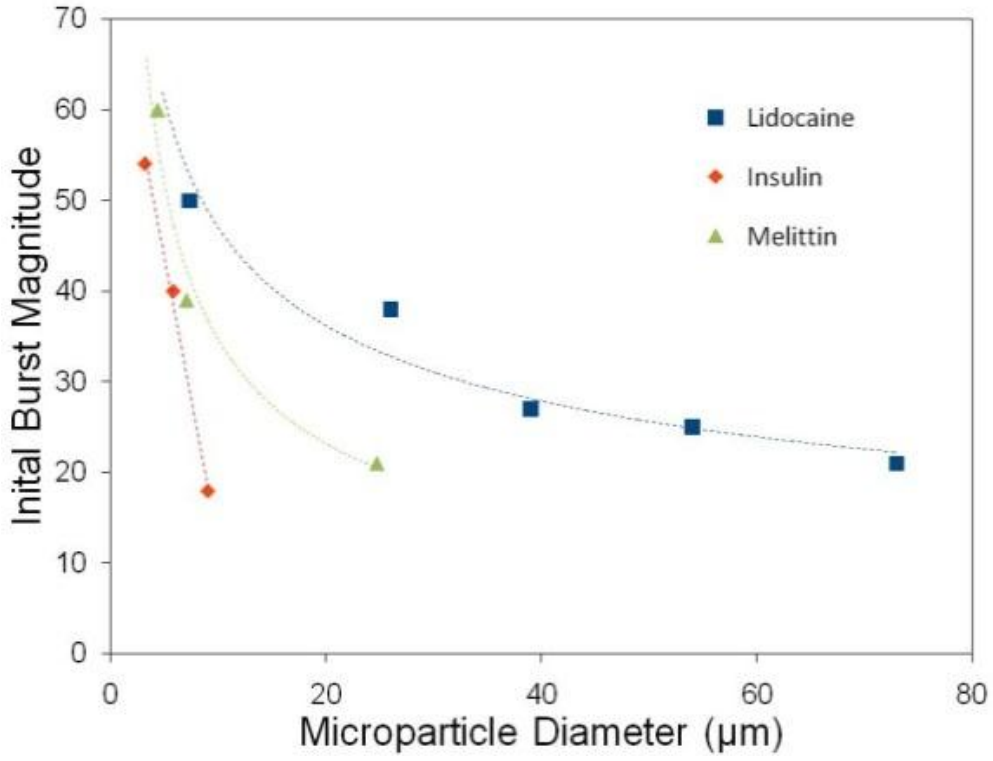

Figure 3: Comparison of burst magnitudes from microparticles of varying size.

Analysis was conducted on data from three different studies: Small molecule Lidocaine[2], Insulin protein[5] and Melittin peptide[6]. The burst magnitude of each system was affected to different extents by changes in matrix size.

2.2.1.4 Manipulation of Drug Loading

Discrete changes in initial burst magnitude have also been produced by altering the drug loading. Working with a variety of model proteins (lysozyme, carbonic anhydrase, alcohol dehydrogenase), Sandor et al noted that decreasing drug loading from 7 to 1wt% reduced the initial burst from a high of roughly 80% to just 15-40% of total release[43]. Equally dramatic reductions in burst magnitude have been observed following changes in peptide loading[6,36]. Studies on small molecule release from polyester and polyanhydride implants have also reported

similar trends[44-48]. Limitations to this technique do arise at low loadings (lower payload) or high loading (breakdown of matrix structure, e.g. percolation)[49]. However, the simplicity and broad applicability of this tool still make it very attractive for inducing measurable changes to burst magnitude.

2.2.2 Tuning the kinetics of the initial burst

Methods for altering the rate (kinetics) of the initial burst may also prove useful if it can be manipulated to benefit the delivery strategy. For example, rapid delivery of an antigen might be necessary for the successful function of a controlled release vaccine. Alternatively, slowing the initial burst rate may bring the initial delivery of a prescription in line with its optimal, constant (zero order) release profile.

2.2.2.1 Controlling Drug Dissolution Rate

One way to influence burst release kinetics is to alter the encapsulated agent's dissolution rate. This has been accomplished by co-encapsulating an agent with a variety of excipients[50,51]. Experimenting with different clycodextrin excipients, Wang et al was able to tune the duration of initial release of beta-lapachone (a hydrophobic chemotherapeutic) to values between 1 week and 1 day by complexing it with hydrophilic cyclodextrin of varying size[50]. This approach to increasing burst rate should also apply to other hydrophobic, small molecules, that readily complex with cyclodextrin or other hydrophilic agents[29].

Interestingly, reports describing the use of excipients to decrease the rate of early release (rendering hydrophilic molecules more hydrophobic) are absent from the literature, possibly

because evidence suggests that these types of systems exhibit little to no initial burst[30]. Further, a study intending to reduce dissolution rate by switching from amorphous to crystalline drug reported a similar change in burst magnitude, but not kinetics[52]. However, studies comparing agents with different intrinsic dissolution rates have noted a correlation to burst kinetics in polyanhydride implants[53,54]. This suggests that methods for reducing an agent's dissolution rate could slow its burst release. However, until such methods are realized, excipients remain a reliable tool for increasing burst release rate of hydrophobic agents.

2.2.2.2 Effect of Radial Drug Distribution

A number of different fabrication methods have been used to control the radial distribution of drug within biodegradable polymer matrices, thereby altering their initial burst kinetics. Such heterogeneous distributions have been achieved with double-walled microparticles which are formed by using multiple immiscible solvents to separate polymers of differing solubility into core and shell phases. These systems consistently show reduced protein burst kinetics when the drug is trapped in the matrix core rather than when it is in the shell or loaded throughout[55,56]. Further, the extent of this reduction is proportional to the thickness of the shell separating the drug-loaded core from the outside environment[55]. Coated implants (tablets, discs, or spheres) made from polyesters or polyanhydrides have produced similar results[57-60]. Mixed results were observed in some small molecule loaded matrices, which could be explained by the preferential partitioning of such agents into the coating shell instead of the matrix core[61-64]. Fortunately, studies have reported controlling the radial distribution of small molecules through an electrospray fabrication process[3,65,66]. Piroxicam and Rhodamine loaded microparticles produced by this method showed significantly slower initial release kinetics when drug was concentrated

at the matrix core than when it was distributed closer the particle surface[3].(**Figure 4**) This technique was also recently applied to macromolecule loaded (Rhodamine-BSA or FITC-dextran), double emulsion microparticles, but only the magnitude of the initial burst was altered[67], as discussed in section 2.2.1. Between electrospray fabricated microparticles and systems such as double-walled particles or implants, radial drug distribution can successfully modified for a diverse array of active agents.

2.2.3 Initial burst summary

A number of different techniques make it possible to tune the magnitude and duration of the initial release phase. By altering processing methods, matrix size, osmotic pressure, or drug loading, the magnitude of the initial release can be tuned to nearly any value between 0 and 100%. By altering the agent dissolution rate or radial drug distribution, it is possible to tune kinetics of initial release as well. Despite the encompassing applicability and diversity of these tools for tuning burst release, future research into mechanism of the bust and its relation to drug chemistry is needed to tune it *a priori*.

2.3 TUNING THE LAG PHASE

Following the initial burst, a lag (or pause in release) may occur before the remaining encapsulated drug is released. By definition, this phase lacks measurable kinetics, but may possess significant duration. However, particularly slow initial release or, conversely, early

onset of final release may serve to disguise this phase. Hence, for the purposes of this chapter, the duration of the lag phase is defined as time elapsed prior to the onset of final release (day 0 to the resumption of drug delivery).

2.3.1 Tools for tuning the duration of the lag phase

2.3.1.1 Setting of Initial Polymer Molecular Weight

Many studies have shown that the duration of the lag phase can be altered by varying the polymer's initial molecular weight (Mw_o). For example, Friess et al. induced a 10 day lag phase in gentamicin loaded microparticles by switching from a 13.5kDa PLGA to a higher molecular weight of 36.2kDa[68]. Comparable results have been reported for small molecule loaded polyester implants[69]. This relation also holds true in peptide loaded microparticles[5,70,71]. Macromolecule release data from different studies also confirms a clear trend between lag phase duration and the molecular weight of the PLGA matrix (Figure 5) [5,30,35,43,72-78]. This fundamental trend is only preserved with a given class of agents, suggesting that the effect of polymer molecular weight is dependent, at least in part, upon some property (or properties) of the encapsulated agent[68,70,75].

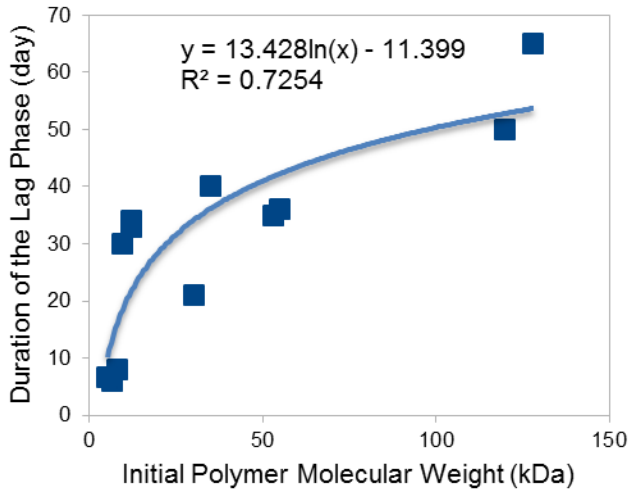

Figure 4: Relationship between polymer molecular weight and lag duration.

Duration of the lag phase (*squares*) was determined by analyzing macromolecule release data from a number of different studies[5,30,35,43,72-78]. The results fit a power expression (*line*).

2.3.1.2 Controlling Polymer Degradation Rate

Another well-documented tool that can be used to alter the duration of the lag phase is the polymer's degradation rate. For copolymers, this is simply controlled by altering the ratio of the two monomers, with degradation rate typically being inversely proportional to hydrophobicity of the resulting polymer chain. For example, in work by Cui et al where 9.5kDa 50:50 PLGA microparticles produced a melittin release profile with an 8 day lag phase, 10kDa 75:25 PLGA microparticles presented a 14 day lag phase[6]. Similarly, Wang et al tested ethacrynic acid loaded films of 110kDa 50:50 PLGA and PLA, which produced lags of 1 or 6 days, respectively[79]. This trend has also been echoed by polyanhydride copolymer microparticles loaded with BSA[80], PLGA and PLA fibers loaded with BSA [81] as well as other polyester implants loaded with small

molecule drugs[82,83]. The consistent performance of the polymer degradation rate and initial molecular weight as tools for controlling lag phase duration suggests that the two may act in concert via a common property such as polymer lifespan.

2.3.1.3 Use of Catalytic Excipients

When a specific polymer chemistry or molecular weight is desired (and therefore not accessible as a tool to tune release), the degradation rate and, in turn, duration of the lag phase can also be modified by using an excipient. This is evident in one study where proteinase K increased the degradation rate of PLA fibers eliminating all lag from the release of paclitaxel and doxorubicin[84]. This enzyme will also catalyze the degradation of l-lactic linkages in PLGA copolymers and consequently should shorten the duration of lag phase in said systems as well[85]. An anhydride (acid) has also been used as a catalyst to hasten the degradation of poly-ortho-ester matrices, completely eliminating a 2-day lag phase[86]. This mechanism should apply equally well to polyester or polyanhydride matrices whose hydrolysis is also affected by the presence of acid[41]. Future work is needed to determine if acidic excipients will cause measurable damage to peptides or proteins.

2.3.1.4 Post Fabrication Irradiation

The duration of the lag phase can also be reduced by gamma irradiation[87,88]. The most dramatic changes produced by this method were reported for the release of progesterone from PLA microspheres, where 100kGY of radiation reduced the lag duration from nearly 200 days (prior to exposure) to just 50 days [88]. Working with small molecule loaded PLGA microspheres, Fasiant et al also reported a short lag duration when 5-Fluorouracil loaded PLGA microparticles

were irradiated (4-33kGy)[87]. These changes in lag duration can likely be attributed to the cleavage of polymer chains in the encapsulating matrix (e.g. reduction in initial polymer molecular weight), a phenomena whose effects are described earlier in this section. Interestingly, both studies also noted an increase in burst rate, a phenomena not observed with other degradation-based methods of altering the duration of the lag phase. While this method for altering lag phase should apply to a wide range of polyester matrices, its utility may be limited because: 1) it simultaneously alters the kinetics of the initial burst, 2) it appears to be only capable of shortening the lag phase (not lengthening it) and 3) it may degrade sensitive agents such as peptides and proteins.

2.3.2 Lag phase summary:

Controlling the duration of the lag phase can be simply a matter of tuning the encapsulating polymer's lifespan. This can be accomplished by adjusting polymer initial molecular weight or degradation rate, as well as by using a catalytic excipient or gamma irradiation. By carefully tuning the lag phase it is possible to either merge initial and final release into one seamless phase or separate them by considerable delay. As lag phases were rarely observed in system releasing small molecules (< 300Da), further study is warranted to determine how best to induce and tune this phase in such systems.

2.4 FINAL RELEASE

Control over the final release phase can help extend drug delivery or even determine how pronounced the effects of the initial burst and lag phase will be on the overall release profile. Because this phase is responsible for the delivery of the remainder of drug in the polymer matrix, its magnitude is (by definition) predetermined by the magnitudes of the prior release phases. However, the kinetics of this phase can still be readily tuned by several methods.

2.4.1 Tuning the rate of final release

2.4.1.1 Use of Polymer Blends

Firstly, the rate of final release can be reduced (or its duration extended) by blending together like polymers[68,70,89-92]. For example, by adding together equal measures of 36.2kDa PLGA and 13.5kDa PLGA, Friess et al was able to extend the final release of gentamicin (small molecule) from just 3 days to 7 days[68]. Similar mixtures have also been used to extended the release of peptides and proteins[70,90]. This tool has even been used to sustain protein (lysozyme) release from polyanhydride microspheres[92]. Interestingly enough, this method of reducing the final release rate extends directly from methods for tuning the lag phase duration (which also marks the time until final release). For instance, mixing together polymers with different lag phases could stagger the onset of final release, yielding an overall slower final release rate than either polymer could achieve alone. Hence this technique for modulating the rate of final release should prove effective for any matrix system with an adjustable lag phase.

2.4.1.2 Control via Copolymer Ratio

Data also suggests that duration of final release in polyester systems is dependent on the copolymer ratio of PLGA. Studies on melittin release show that 50:50 PLGA microparticles complete final release in just 2 weeks, while comparable 75:25 PLGA microparticles take 3 weeks to deliver nearly the same amount of drug[6]. A similar observation can be made for the ethacrynic acid loaded films[79]. (Note, in all aforementioned cases altering copolymer ratio also adjusted the duration of the lag phase via the polymer degradation rate, as described in section 2.3.1) While, this effect appears consistent across PLGA copolymers, further research is needed to better understand its mechanism and the breath of its applicability. Tuning common factors such as polydispersity in the polymer molecular weight or semicrystallinity of the polymer matrix (which can lead to variance in the polymer lifespan[93]) may produce comparable effects in other polymer types[94].

2.4.2 Final release summary:

A relatively limited number of techniques are able to alter the kinetics of the final release phase for a number of different systems. Both blending like polymers and altering copolymer chemistry (for greater lactic content) decreases the rate of final release, allowing for more extended delivery. Similarly reducing the polydispersity in polymer initial molecular weight or reducing the copolymer's lactic acid content can increase the rate of final release.

2.5 CONCLUSIONS:

Many methods for tuning the release kinetics of biodegradable polymer matrices have been tested in carefully designed experiments on a variety of different drugs. The result is a set of independent methods for tuning the magnitude or kinetics of the initial burst, the duration of the lag phase and the rate of final release. When used in combination, these design tools can produce release profiles ranging pure the Fickean diffusion to complex tri-phasic behaviors. Further progress can be made towards quantifying the changes in release produced by these tools with mathematical modeling.

3.0 DEVELOPING A PREDICTIVE MODEL OF RELEASE FROM BULK ERODING POLYMER MATRICES

3.1 INTRODUCTION

Spurred by a desire to hasten the development of new formulations, many efforts have been made to model degradation-controlled release profiles based on the physical properties of the matrix, drug, and polymer[4,95-101]. The most notable of these models not only accurately describe release data, but also provide a means of predicting how to control it (i.e. predicting how changes in system properties will affect the release of a given drug). This is an important distinction, as many models, through regression, will fit tri-phasic release data, while only predicting how one or two system properties will affect release. As most system properties only alter a single aspect or phase of release kinetics, this would limit a model's ability to tailor release kinetics. On the other end of the spectrum, when a model accounts for too many system properties, its utility for formulation design is limited by the number of properties that can actually be tuned during matrix fabrication. Common ground for more specific characterization of mathematical models as design tools can be found in the phase or phases of release that they effectively be used to tune. Compared on the basis of the phases that they describe, models can be evaluated for their accuracy, applicability to formulation design, and ease of implementation.

3.1.1 Evaluation of models addressing the initial burst by critical properties

3.1.1.1 Agent Loading and Copolymer Ratio:

Wong et al. modeled the initial burst release of Immunoglobulin G from PLGA microparticles with varying drug loading and copolymer composition[102]. Analytical solutions to this diffusion-dissolution model revealed a strong agreement to the first 50 days of release data when values for the agent diffusivity and dissolution rate constant were optimized to minimize sum-squared error. The low variance in these optimized values may allow for the prediction of burst release in systems with different loadings or copolymer ratios. (As some of the collected data was lacking a lag phase, at times, both of these properties appeared to impact the initial burst kinetics.) Further work is required to determine if values for agent diffusivity and dissolution rate will have to be calculated anew when attempting to predict the burst kinetics of other proteins or polymer chemistries.

3.1.1.2 Agent Loading, Solubility:

Small molecule release from PLGA has been captured by a model that combines a Monte Carlo description of dissolution and erosion with partial differential equations describing pore-mediated diffusion[100]. This model was successfully applied to 5-fluorouracil release data from 104kDa PLGA microspheres by optimizing values for mean polymer lifespan and agent diffusivity. Importantly, values for loading, drug solubility and matrix size were specified for the given microparticle system instead of being computed by regression from release data. This should allow the model to predict how changes in these system properties affect release, provided that their perturbation does not significantly alter the optimized values for mean

polymer lifespan and agent diffusivity. While this predictive ability has yet to be tested, experimental studies suggest that altering the loading will affect the magnitude of the initial burst (section 2.2.1) and varying drug solubility will affect burst kinetics (section 2.2.2). (In like systems, matrix size has been reported to affect the polymer degradation rate and, in turn, its lifespan, while having little impact on release kinetics[1].) Future implementation of this model on single emulsion systems (where agent solubility and loading have been experimentally varied) would promote its utility as a design tool.

Zhang et al. have derived a detailed model for describing mono-, bi-, and tri-phasic protein release profiles[103]. To account for this diversity in release behavior, this model actually contains three different versions of its core equations optimized to approximate a diverse range of experimentally observed erosion behavior. Each version of the model's equations was tested on release data from systems with different erosion profiles. By fitting the model first to mass loss (erosion) data, the most appropriate version of its equations was determined and values were computed for erosion rate constants. Then release data was described by optimizing values for the initial tortuosity and dissolution rate constant. Values for the remaining system properties (agent solubility limit, initial diffusivity, microparticle radius, drug loading, initial tortuosity and initial porosity) were taken from the literature. Because sensitivity analysis shows that the erosion mechanism can have a dramatic effect on release kinetics, matrix-specific properties that are likely to affect erosion (e.g. microparticle radius, initial porosity or initial tortuosity) may prove a difficult means of precisely altering release. Fortunately, this model still accounts for agent-specific system properties such as agent loading and solubility which can be used to tune the magnitude and kinetics of the initial burst, respectively (sections 2.2.1 and 2.2.2).

3.1.2 Evaluation of models addressing the burst and lag phases by critical properties

3.1.2.1 Initial Polymer Molecular Weight, Irradiation:

Diffusion-erosion equations have been combined with empirical correlations to predict the effects of post-fabrication, gamma irradiation on release[104]. This model accurately fit bi-phasic release data from aclaribicin or progesterone-loaded, polyester PLA microparticles of varying molecular weight or irradiation exposure, respectively. Optimized parameter values for agent diffusivity, degradation rate, lag-phase duration, erosion and auto-catalysis were successfully correlated to irradiation exposure. Based on these correlations a further regression-free prediction was made for a more heavily irradiated set of PLA microparticles. This demonstrates that the model can successfully predict the experimentally observed effects of irradiation exposure on release, namely increased burst rate and decreased lag duration. It is likely that similar predictions could be made for other agents and polyester matrix formulations if their system-specific parameters (agent diffusivity, erosion half-life and degradation rate) are recalculated. With such adjustments, this model could aid in the prediction of initial burst kinetics and lag phase duration following irradiation exposure. It is possible that equivalent correlations could be developed and used to predict the effects of varying initial polymer molecular weight as well.

3.1.2.2 Polymer Initial Molecular Weight, Agent Distribution:

Raman et al modeled the effects of polymer initial molecular weight and drug dispersion on piroxicam release from single emulsion microparticles[101]. The model combines diffusion-reaction expressions with a correlation relating piroxicam diffusivity to polymer molecular weight (*D(Mw)*) in order to predict release while only needing to optimize one constant (initial

drug diffusivity), which accounts for the kinetics of initial release. Its descriptions of release were accurate for the initial burst and the lag phase, but deviated from the data as much as 15% at later points in time. This likely occurred because the *D(Mw)* correlation requires extrapolation for polymer molecular weights less than 5kDa, an issue which could be resolved by gathering data from lower molecular weight polymer matrices. As implemented, this model can predict changes in burst kinetics arising from drug distribution and changes in the lag phase duration due to polymer initial molecular weight. With an agent specific *D(Mw)* correlation and recalculated values for initial diffusivity in place, this model could be used to predict the performance of different drugs as well.

3.1.3 Evaluation of models of triphasic release by their critical properties

3.1.3.1 Microparticle Combinations:

The aforementioned model of piroxicam release has recently been extended by Berchane et al with an algorithm for tuning release kinetics by mixing together different microparticle formulations at different ratios[105]. This algorithm was used to optimize (using weighted sum squared error) the component mass fractions in a mixture of piroxicam loaded microparticles with different release behaviors to produce entirely new profiles, from linear to multi-phasic patterns. This technique could readily be adapted to generating specific release profiles for any number of drugs provided that a library of formulations with suitably diverse release behaviors could be developed.

3.1.3.2 Erosion, Degradation, Drug Loading, Posority, Particle Size, Solubility, and Polymer Chemistry:

Batycky et al modeled tri-phasic protein release by piecing together a number of analytical equations[4]. This model successfully predicted the release of glycoprotein 120 from PLGA microspheres based on measured values for 19 different parameters (Figure 5A). Less rigorous predictions (using a number of estimated parameters) for tetanus toxin release captured the initial burst and lag phases but showed systematic deviations arising at just 15 to 45% of completion (Figure 5B). This suggests that it is important to precisely measure or derive values for all model parameters if accurate predictions are to be made. Eight of these parameters, such as effective drug diffusivity, rate of mesopore formation or burst release fraction, can only be determined through observation of the polymer matrix during *in vitro* degradation, erosion and release assays. However, the remaining eleven parameters correspond to system properties that are commonly known or readily measured, namely microparticle radius, initial porosity (micro, meso, and occlusion), pore size distribution, polymer degradation rate, monomer molecular weights, soluble oligomer number, drug radius, drug molecular weight, and drug loading. Parametric sensitivity analysis, where each of these parameters is independently varied, will help determine which system properties specified in this model can be used to tune release[106].

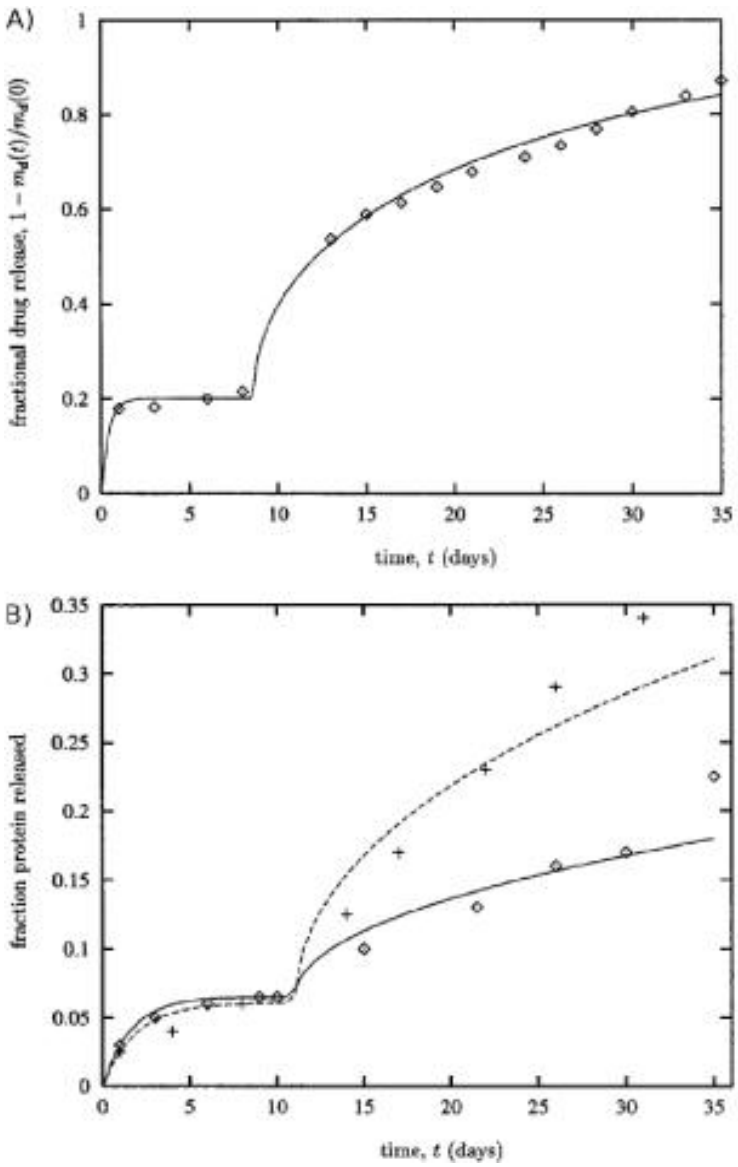

Figure 5: Protein release predictions for PLGA & PLA particles.

A) Model's prediction (solid line) compares favorably with Glycoprotein release data (diamonds). B) Estimations of tetanus toxin release (solid line) capture the initial burst and lag phase of the data from PLGA (crosses) and PLA (diamonds) microparticles. Reproduced with permission of ref. [4]

3.1.4 Summary of Mathematical Models:

Each of the aforementioned models takes steps towards enabling the rational design of biodegradable controlled release matrices. In order to supplant the need for exploratory *in vitro* release experiments in the design of controlled release therapeutics, though, a model must satisfy three requirements. 1) The model must apply to a wide range of agents because each new therapeutic must deliver a unique drug[11,23]. 2) The release of such agents must be described entirely from readily attainable design parameters, thereby allowing researchers to acquire specifications for a matrix from a given release profile or dosing schedule[107]. 3) The model must be robust enough to capture the breadth of release behaviors that have been documented for the system in question, in this case, bulk eroding polymer matrices[5,6,30,43,68,70,72,73,79,80,108-111].

This chapter documents the development and implementation of a new controlled release model designed to meet the criteria specified above. This work was summarized in a manuscript by Rothstein et al. that was published in the Journal of Materials Chemistry in 2008{Rothstein 2008}. This model uses new methods to describe the release of water-soluble agents that are discretely encapsulated in bulk eroding, polymer matrices and that dissolve rapidly, relative to the time scale of release. In addition fundamental descriptions of release, the model includes two correlations that enable predictions with knowledge of just five parameters, all commonly known or easily measured prior to release. These parameters are microsphere radius R_p, occlusion radius R_{occ}, polymer degradation rate kC_w, polymer initial molecular weight M_{wo}, and agent molecular weight M_{wA}. As a test of the model, regression-free predictions were compared to multiple sets

of published experimental data. Furthermore, the range of attainable dosing schedules is explored by varying the matrix-specific parameters.

3.2 MODEL DEVELOPMENT

3.2.1 Release paradigm

Consider an initially uniform matrix of known geometry comprised of a biodegradable polymer, such as a polyester or polyanhydride, and with randomly distributed entrapped release agent (*e.g.* drug of concentration C_{Ao}), loaded below its percolation threshold (such that agent remains discrete) to ensure matrix mediated release. This agent can either be dispersed as crystals (such as in the case of uniformly loaded systems, *e.g.* single emulsion-based particulates) or housed as a solution in occlusions (*e.g.* double emulsion-based particulates).[107] At time zero, an aqueous reservoir begins to hydrate the matrix, a process which happens quickly for the bulk eroding polymers matrices considered herein[4,41]. As the matrix hydrates, encapsulated agent adjacent to the matrix surface (with a direct pathway for egress) diffuses into the reservoir in a phase typically dubbed "the initial burst" (Figure 6, phase 1). The relative size of the occlusion (R_{occ}) occupied by the encapsulated agent is proportional to the magnitude of the initial burst as illustrated in Figure 7.

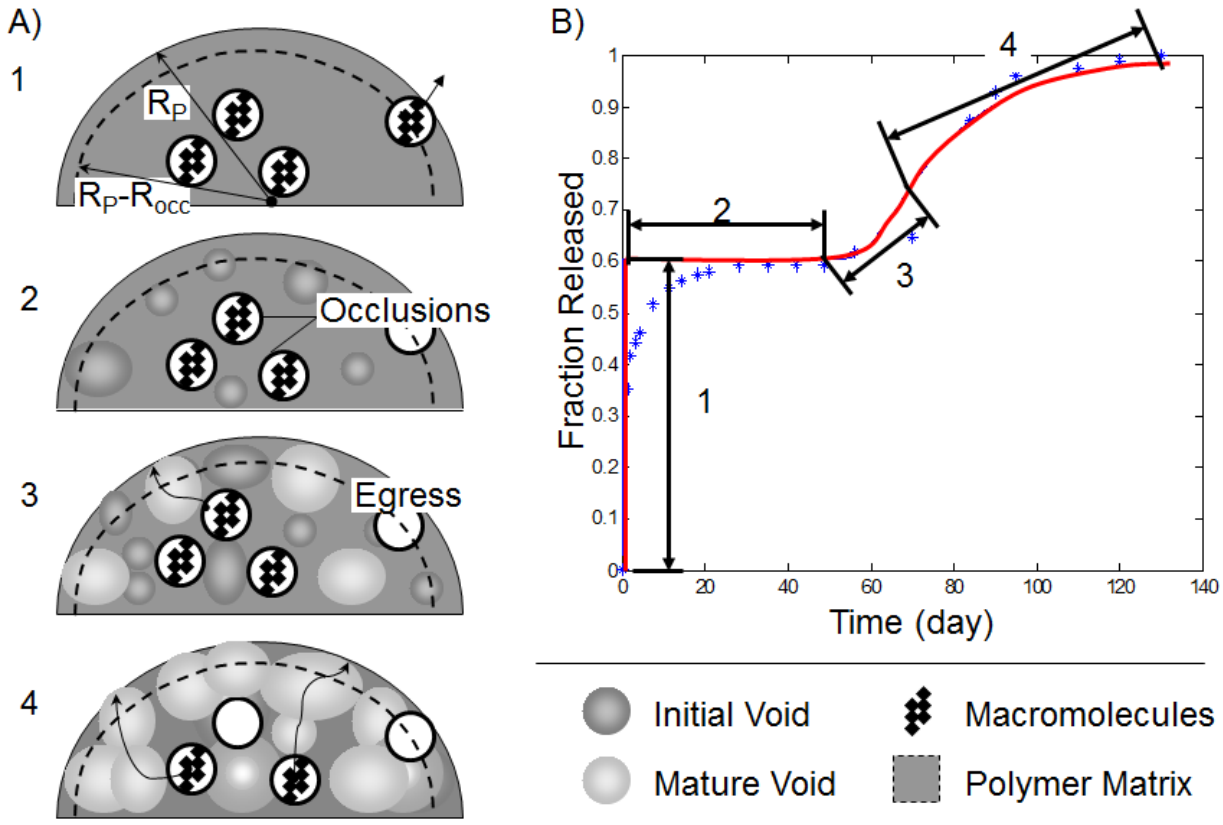

Figure 6: Schematic depiction of a paradigm that can account for four-phase release.

A) Cross section diagrams depicting the four phases of release for a double emulsion microparticle with agent encapsulated heterogeneously in occlusions. Initially, agent abutting the matrix surface is released (1). The remaining agent requires the growth and coalescence of pores for further egress (2–4). B) Release profile for macromolecular drug encapsulated in biodegradable polymer matrix with four phases of release labeled. The numbers associated with each cross section diagram (A) indicate which phase of the release profile is illustrated. These phases are 1) initial burst, 2) lag phase, 3) secondary burst and 4) final release.

As the initial burst release commences, degradation of the polymer begins, increasing chain mobility and effectively leading to the formation of pores in the polymer matrix[32] (Figure 6, phase 2). Although a number of mechanisms have been proposed for this heterogeneous degradation profile, one hypothesis, which has been reinforced by experimental data, is based upon regions of varying amorphicity and crystallinity[93,112,113]. It is believed that amorphous regions of polymer erode first, leaving behind pores (as shown using scanning electron microscopy)[1]. These pores appear to be essential for subsequent release[114](Figure 6, phase 3).

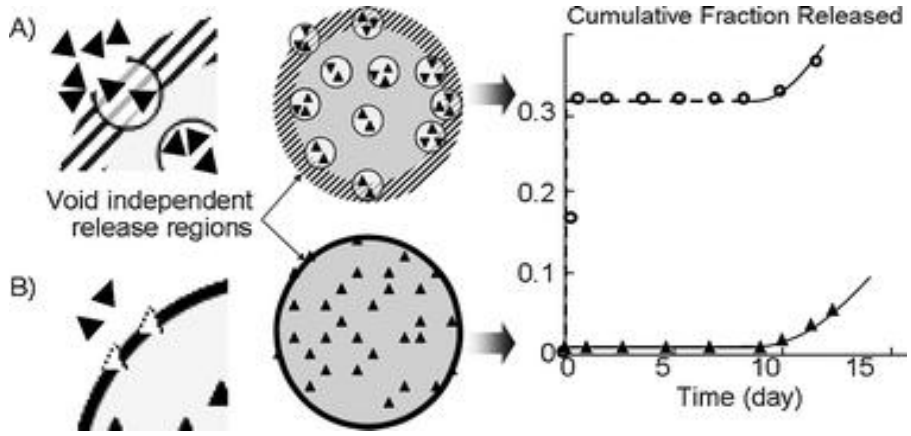

Figure 7: Schematic depiction of the initial burst as it relates to occlusion size.

A) The double emulsion particle contains large occlusions filled with drug solution and produces a significant initial burst. B) The more uniformly loaded (e.g. single emulsion particle, melt cast matrix) contains small granules of drug and has minimal initial release

With the cumulative growth and coalescence of these pores, agents are able to diffuse towards the surface of a polymer matrix that would otherwise be too dense to allow their passage[114] (Figure 6, phase 4). Thus, a pore is defined as a region of polymer matrix with an average molecular weight low enough to allow the release of encapsulated agent. (This is in contrast to the occlusion, which is defined as a region occupied by dissolved or solid agent, marked by the *absence* of polymer matrix.) Further, the molecular weight associated with release may vary for each encapsulated agent type (small molecule, peptide, protein, *etc*.), leading to a size-dependent restriction for agent egress.

With a size-dependent restriction on egress established, the degradation controlled release of any encapsulated agent can only occur when the following four conditions are satisfied. 1) The release agent must be present in the polymer matrix. 2) A pore must encompass the release agent. 3) That release agent must be able to diffuse through the encompassing pore. 4) The pore must grow and coalesce with others to create a pathway for diffusion to the surface.

3.2.2 Model Equations

Agent concentration within a matrix (such as a microsphere, rod, or thin film) can be calculated from Fick's second law (Equation 1) for any point in time (t) or space (r), provided that the agent is not generated or consumed in any reactions while within the matrix[96-98,100].

$$\frac{\partial C_A}{\partial t} = \nabla \cdot D_{eff} \nabla C_A \qquad (1)$$

Here D_{eff} is an effective diffusivity term. Integrating C_A/C_{Ao} over the entire matrix volume yields the cumulative fraction of agent retained in the matrix ($P(t)$) (Equation 2).

$$P(t) = V^{-1}\int C_A/C_{Ao}dV \qquad (2)$$

For a sphere:

$$P(t) = \int_0^{Rp} \frac{C_A}{C_{A,o}} \cdot \frac{r^2}{3 \cdot {R_p}^3} dr$$

In turn, the cumulative fraction of agent released ($R(t)$), a metric commonly used to document formulation performance, is simply (Equation 3):

$$R(t) = 1 - P(t) \qquad (3)$$

At the center point, line, or plane of the matrix ($r = 0$) symmetry conditions are defined such that $dC_A/dr = 0$. At the matrix surface ($r = R_p$) perfect sink conditions are specified. (The impact of sink conditions has been explored in prior experimental work {Klose 2011}.) A boundary also exists at a depth of R_{occ} in from the matrix surface ($r = R_p - R_{occ}$) where continuity conditions are defined. In the subdomain from R_p to $R_p - R_{occ}$ (terminating one occlusion radius in from the particle surface), agent is subject to the initial release, such that D_{eff} is simply a constant (D), reflecting the movement of agent through the hydrated occlusions abutting the matrix surface. In the subdomain from 0 to $R_p - R_{occ}$, agent is subject to pore-dependent release, such that $D_{eff} = D\varepsilon$ where D is the diffusivity of the agent through the porous matrix and ε is the matrix porosity.

For a system of like matrices, such as microspheres or sections in a thin film, that degrade randomly and heterogeneously, the accessible matrix porosity is simply a function of time as a discrete pore has, on average, an equal probability of forming at any position in the polymer

matrix. Hence, the time until pore formation can be calculated from the degradation of the polymer matrix, as any differential volume containing a pore would have a lower average molecular weight than its initial value. Assuming that the polymer degradation rate is normally distributed,[112] the induction time for pore formation will also follow a normal distribution. As this pore formation is cumulative, the time-dependent matrix porosity ($\varepsilon(t)$) can be described with a cumulative normal distribution function (Equation 4).

$$\varepsilon(t) = \frac{1}{2}\left[erf\left(\frac{t - \bar{\tau}}{\sqrt{2\sigma^2}} \right) + 1 \right] \quad (4)$$

Here, $\bar{\tau}$ is the mean time for pore formation and σ^2 is the variance in time required to form pores.

3.2.2.1 Pore induction time distribution

Calculating the cumulative normal induction time distribution ($\varepsilon(t)$) requires values for $\bar{\tau}$ and σ^2. For polymers that obey a first order degradation rate expression, the mean time for pore formation ($\bar{\tau}$) can be determined as follows:

$$\bar{\tau} = \frac{-1}{kC_w} \ln \left| \frac{M_{wr}}{M_{wo}} \right| \quad (5)$$

where kC_w is the average pseudo-first order degradation rate constant for the given polymer type, M_{wo} is the initial molecular weight of the polymer, and we define M_{wr} as the average polymer molecular weight in a differential volume of matrix that permits the diffusion of the encapsulated agent. For blended polymer matrices, the value for $\bar{\tau}$ was calculated by averaging the results obtained from equation 5 for each component.

It is reasonable to believe that the matrix molecular weight at release (M_{wr}), which dictates how much degradation is required before release can occur, would vary depending on the size of the encapsulated agent. Macromolecules or larger agents can only diffuse through a section of matrix if it is almost entirely free of insoluble polymer chains. Hence the M_{wr} for such agents is considered the polymer solubility molecular weight (668 Da for 50:50 PLGA as provided by Batycky *et al.*)[4]. As agent size decreases (as indicated by M_{wA}), however, egress can occur through more intact sections of polymer matrix (higher M_{wr}), as less free space is needed to allow their passage.

The distribution of polymer degradation rates ($kC_w(n)$) attributed to matrix crystallinity is needed to calculate the variance (σ^2) in the induction time distribution for pore formation ($\varepsilon(t)$)[93]. To determine $kC_w(n)$, the first order degradation rate equation $M_w = M_{wo}e^{-kCw \cdot t}$ was linearly fitted at three different time periods to published degradation data for the desired hydrolysable polymer. Fitting the initial slope of the degradation profile provides the degradation rate constant of amorphous polymer as degradation occurs faster in amorphous regions of the matrix[93]. Fitting data from the final weeks of degradation produces a rate constant for the crystalline material, as amorphous regions are largely eroded by this point. Finally, a fit of the entire degradation profile yielded a rate constant indicative of the overall morphology.

With values for $kC_w(n)$ defined, a distribution of induction times ($\tau(n)$) was calculated using equation 5. For blended polymer matrices this $\tau(n)$ includes values calculated at all component $kC_w(n)$ and M_{wo}. The standard deviation was taken for $\tau(n)$, then divided by a crystallinity-based factor and squared, yielding an adjusted variance (σ^2), which conforms with lamellar size data.

This crystallinity-based factor adjusts the probability of finding pores formed from the fastest degradation rate in $kC_w(n)$ to match the probability of finding a differential volume of matrix containing purely amorphous polymer. For all modeled cases, this differential volume is defined as a region large enough to allow the passage of a small virus or protein complex (20 nm diameter). As multiple lamellar stacks can fit into this differential volume, the probability that such a volume is purely amorphous can be calculated from of the number of stacks per differential volume and the average crystallinity of the matrix. From crystallinity data on 50 : 50 PLGA matrices, [93,112] the probability of finding a purely amorphous differential volume is calculated as 0.05%. Thus, to ensure that the probability of finding a pore formed from the fastest degradation rate in $kC_w(n)$ also equals 0.05%, the standard deviation in the induction time distribution for pore formation was adjusted by a factor of 5. Similarly, factors of 4 and 2 were calculated from crystallinity data for 75:25 PLGA and polyanhydride matrices, respectively[112,115,116]. Because each of these parameters is calculated from published x-ray diffraction crystallinity data, it provides a materials-based input (independent of encapsulated drug) for the model's for solution

3.2.3 Solution and Regression

With values for $\bar{\tau}$ and σ^2 selected (defining $\varepsilon(t)$), a finite element solution to equation 1 was calculated (Comsol®, v3.3) for the given matrix geometry, using default solver settings. (To decrease computation time, the matrix geometry was simplified to one dimension based on symmetry, for a sphere, or high aspect ratio, for a thin film.) The resulting concentration profiles were numerically integrated to calculate the cumulative fraction of agent released (equations 2

and 3). For validation, the numerical solutions of the model were fit to experimental data sets by varying M_{wr} and D. (It should be noted that data points charting the kinetics of the initial burst were omitted from these regressions, as the model only predicts the magnitude of this phase.) Each fit was optimized using the *fminsearch* function (Matlab®, R2007a), which minimized sum-squared error (SSE) or weighted sum-squared error (wSSE) when error bars were provided.

3.2.4 Validation of math model

As derived above, values for D and M_{wr}, while not easily quantifiable, are needed to solve the fundamental model equations 1–5. Hence, to further develop the model, regressions to multiple data sets were conducted to relate these parameters to more readily attainable system properties[5,6,30,43,68,70,72,73,79,80,108-111]. For these regressions, values for the readily attainable model parameters, M_{wo} and R_p, were taken from the published data sets[5,6,30,43,68,70,72,73,79,80,108-111]. $kC_w(n)$ was calculated and averaged from several different sources[78,101,117-119] as described above. Data points documenting the kinetics of the initial burst were not included for fitting, as the model, in its current form, only predicts the magnitude of this phase. (This current limitation is discussed further in Section 3.4.) Properties for the experimental systems described by these regressions are listed in Table 1. Each fit to published data yielded optimized values for D and Mwr that were subsequently correlated to M_{wo} and R_p (Figure **8**).

Table 1: List of experimental systems used for model validation

Agent	M_{wA}/Da	Polymer	M_{wo}/kDa	R_p/μm	Ref.
Metoclopramide	297	50:50 PLGA	98	75	[111]
Ethacrynic acid	303	50:50 PLGA	110	35 (film)	[79]
Betamethasone	392	50:50 PLGA	41.8	19.5	[110]
Gentamicin	477	50:50 PLGA	13.5, 36.2	133, 276	[68]
Leuprolide	1 209	50:50 PLGA	18, 30	20	[70]
Melittin	2 860	50:50 PLGA	9.5	2.15, 3.5	[6]
SPf66	4 700	50:50 PLGA	100	0.6	[109]
Insulin	5 808	50:50 PLGA	6.6, 8	1.5	[5]
Neurotrophic factor	12 000	50:50 PLGA	9.3	8.85	[30]
BSA	69 000	PSA	37	10	[80]

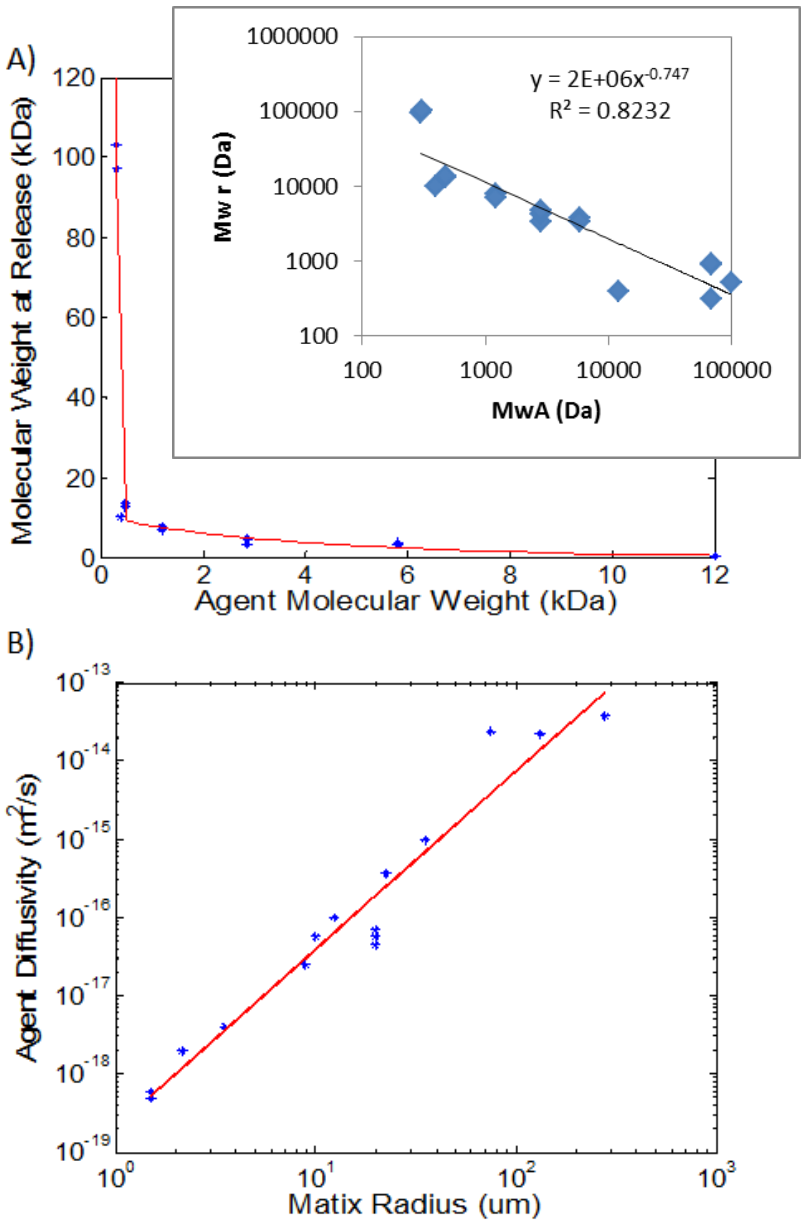

Figure 8: Correlations for *D* and M_{wr} developed from regressions to experimental data in Table 1.

A) Plot of polymer molecular weight at the onset of drug release (M_{wr}) *vs.* release agent molecular weight (M_{wA}), (equation in insert). The data used to form this correlation comes from 50:50 PLGA systems. B) Plot of *D versus* R_p. The line indicates the power expression, $D = 2.071 \times 10^{-19} R_p^{2.275}$ which fits the estimations with an $R^2 = 0.95$.

3.2.5 Regression-free predictions

To test the model, regression-free predictions were made for a variety of biodegradable matrix systems, each with published controlled release data[6,68,80]. Values for the parameters needed to make these predictions were all taken from the literature[5,6,30,43,68,70,72,73,79,80,108-111]. Values for kCw were kept consistent with values used in the validation optimizations, as these were assumed to depend wholly on polymer chain chemistry. Values for Mw_o, Mw_A, and R_p were taken directly from the published work under consideration. The occlusion radius (R_{occ}) was found by averaging the sizes of 10 occlusions, randomly selected from scanning-electron or fluorescence microscopy images of the microspheres.

The model's predictive capabilities were explored by specifying *a priori* conditions such as occlusion (R_{occ}) and matrix (R_p) sizes as well as the mean polymer molecular initial weight (M_{wo}) and its distribution. Specifically, occlusion size was varied from that of a matrix with a homogeneously loaded, small molecule (R_{occ} < 1 nm) to a larger occlusion containing drug (800 nm), as could be found in double emulsion formulation, R_p was set between 8 and 150 μm and M_{wo} was varied from 7.4 to 100 kDa. In addition, blends of common polyesters were considered such as a 2:1 ratio of 7.4 kDa 50:50 PLGA and 60 kDa PLA or a 1:1 ratio of 10 kDa and 100 kDa PLGA. To provide continuity all predictions were generated for a short peptide (900 Da) encapsulated in a spherical matrix.

3.3 MODELING RESULTS

3.3.1 Validation

Solving the fundamental model equations requires values for D and M_{wr}, which are difficult to directly measure. Fitting the model to release data for a wide range of agents generated values for molecular weight of release (M_{wr}) that display a strong correlation with agent molecular weight (M_{wA}) as shown in Figure **8**A. Fitting a power expression ($y = ax^b$) to the plot of the regressed diffusivity values *versus* particle size data (R_p), as suggested by Siepmann *et al.*,[1] resulted in $a = 2.071 \times 10^{-19}$ and $b = 2.275$ ($R^2 = 0.95$) (Figure **8**B). These correlations compile data from multiple agents, polymer molecular weights and matrix sizes (Table 1).

3.3.2 Predictions

3.3.2.1 Predictions of Release Data

Regression-free model predictions for experimental data capture the magnitude of the initial burst, the duration of the lag phase, the onset of the secondary burst and the final release phase. Figure 9 displays one set of predictions for peptide release from various PLGA copolymer microspheres[6]. These predictions appear to extend to polymer matrices other than PLGA, such as polyanhydride microspheres (which, if sized less than 75 μm, are theorized to be entirely hydrated for the duration of release)[41]. The prediction for BSA release from 20:80 CPH:SA polyanhydride microspheres ($R_p = 10$ μm)[80] illustrates this broader applicability (Figure **10**). In

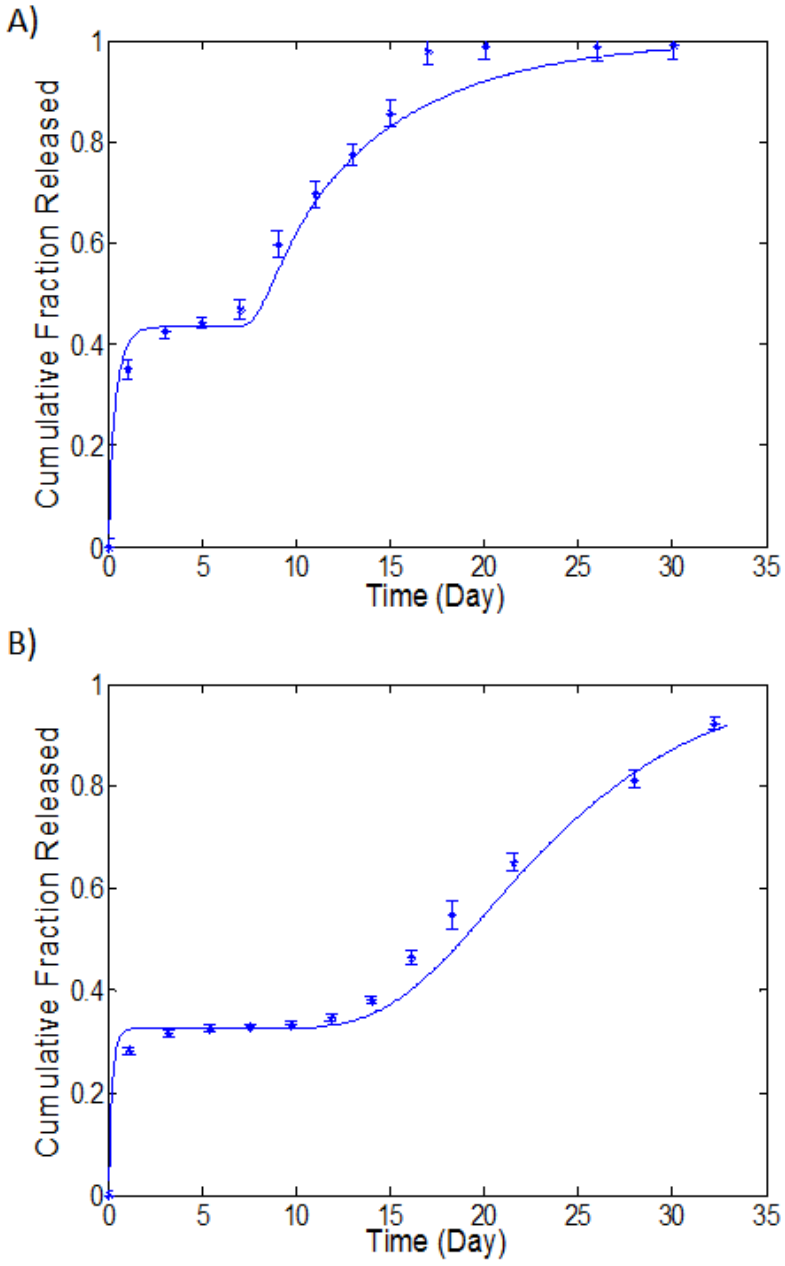

Figure 9: Regression-free prediction for peptide release from PLGA microspheres.

The M_{wr} for melittin (M_{wA} = 2.86kDa) was calculated at 4.68kDa from the correlation in Figure **8**. A) For the 9.5kDa 50:50 PLGA microsphere (R_p = 3.7μm, R_{occ} = 0.52μm) D was correlated at 4.06×10^{-18}m^2/s. B) The D for 9.3kDa 75:25 microspheres (R_p = 4.5μm, R_{occ} = 0.54μm) was calculated at 6.34×10^{-18} m^2/s.

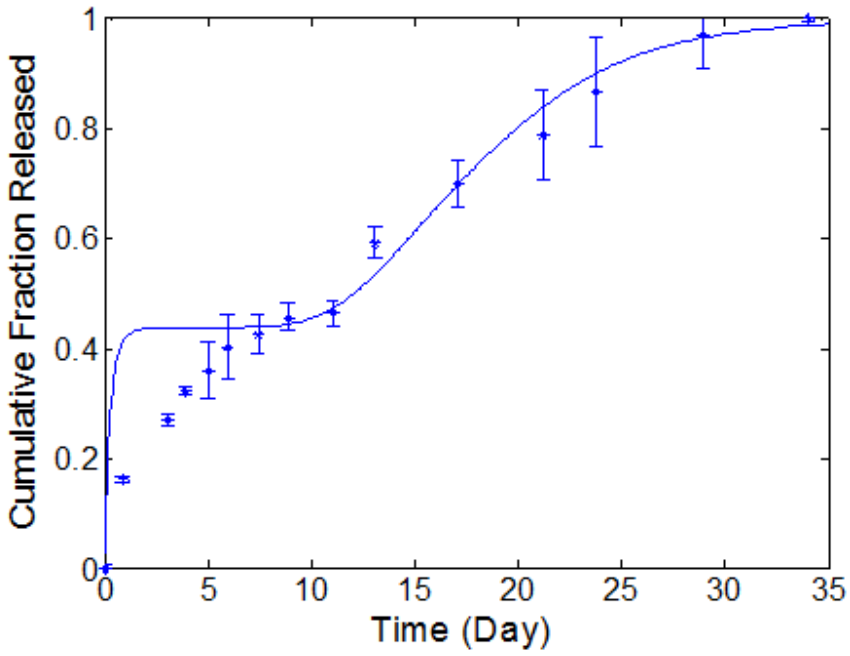

Figure 10: Regression-free prediction for BSA release from polyanhydride microparticles.

System is composed of 20:80 CPH:SA polyanhydride (M_{wo} = 18 kDa, R_p = 10 μm and R_{occ} = 1.54 μm). As the M_{wr} values presented in Figure **8**A are specific to PLGA copolymers, the M_{wr} for this prediction (940 Da) was acquired by fitting the model to data from microparticles fabricated in an identical manner using polysebacic acid (data not shown). In accordance with the correlation in Figure **8**B, D was set at 3.67×10^{-17} m^2/s.

addition, release predictions have also been made for matrices formulated from a blend of two different polymers[68] (Figure 11). All of these predictions serve to confirm that the model can describe: 1) the magnitude (but not the kinetics) of the initial burst from known occlusion size; 2) the duration of the lag phase from known polymer initial molecular weight, degradation rate and release agent molecular weight; 3) the onset of the initial burst from the matrix crystallinity derived rate distribution; and 4) the rate of subsequent release from the agent diffusivity (D) correlated to the matrix size.

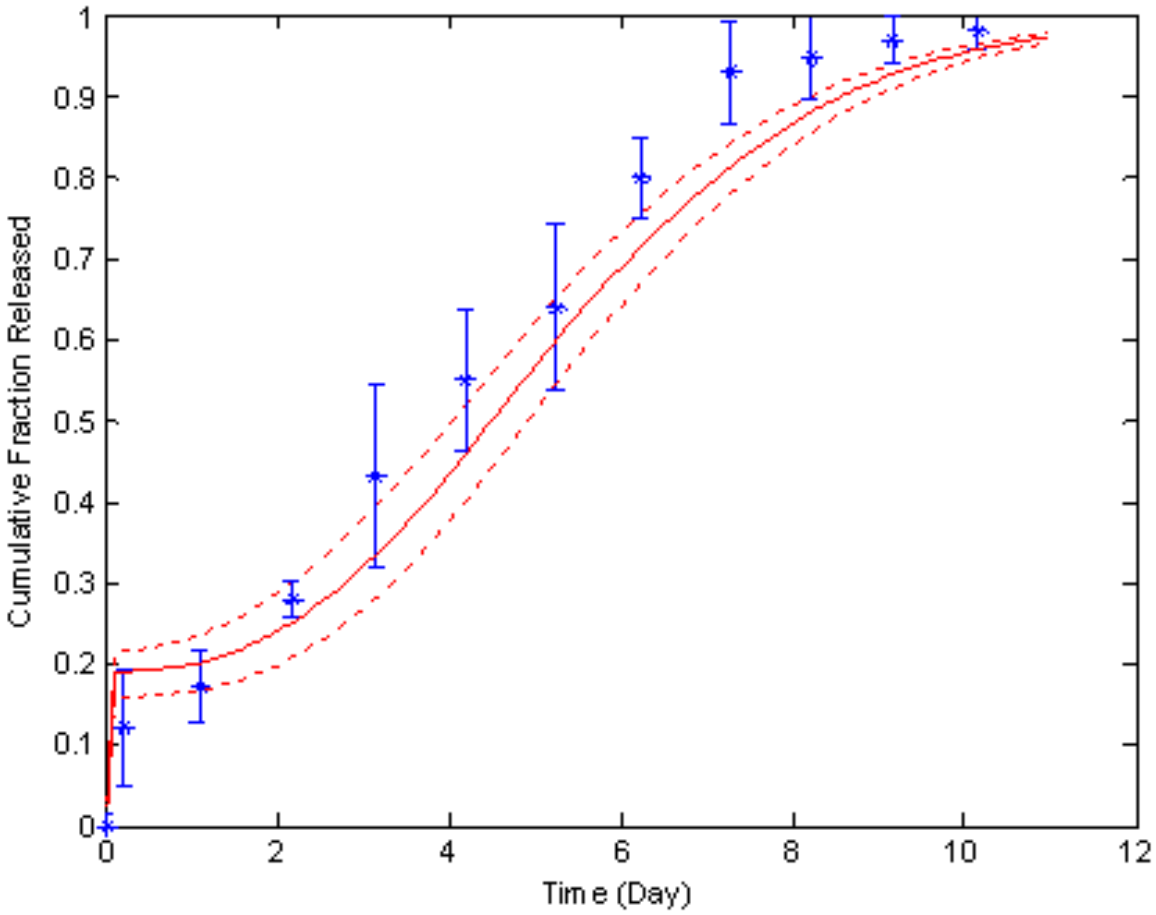

Figure 11: Release predictions compared to *in vitro* data from blended PLGA polymer microspheres.

Gentamicin was release from microspheres (R_p = 374.6 μm and R_{occ} = 24.7 μm) composed of a 1:1 blend of 13.5 and 36.2 kDa 50:50 PLGA (asterisks). As the R_{occ} could not be determined from the published SEM images, the value of 24.7 μm was acquired from different sized gentamicin-loaded microspheres fabricated under like conditions. The M_{wr} and D were correlated at 13.3 kDa and 1.48×10^{-13} m^2/s, respectively. Bounds of the predictions reflect inherent error, propagated from variances in the model's input parameters (dashed lines).

3.3.3 Theoretical Predictions

By varying the readily attainable model parameters within physically relevant bounds for controlled release formulations, it was possible to predict behaviors ranging from a four phase release profile to zero order release (Figure 12). Changing the ratio of occlusion size (R_{occ}) to particle size (R_p) (representing the fraction of matrix volume defined as "near the surface") affected the magnitude of the initial burst (Figure 7). The ratio of the polymer molecular weight at release (associated with the molecular weight of the release agent) to its initial molecular weight (Mw_r/Mw_o) and the mean reaction rate (associated with polymer type) were collectively found to be responsible for the duration of the lag phase. Lastly, modifying the distribution of degradation rates ($kC_w(n)$) or incorporating an Mw_o distribution (used to calculate the induction time distribution for pore growth) influenced the rate of onset for the secondary without affecting the initial burst. Tuning these parameters in combination can minimize the magnitude of the initial burst and the duration of the lag phase, while simultaneously slowing the rate of onset of the second burst, leading to a more linear release profile.

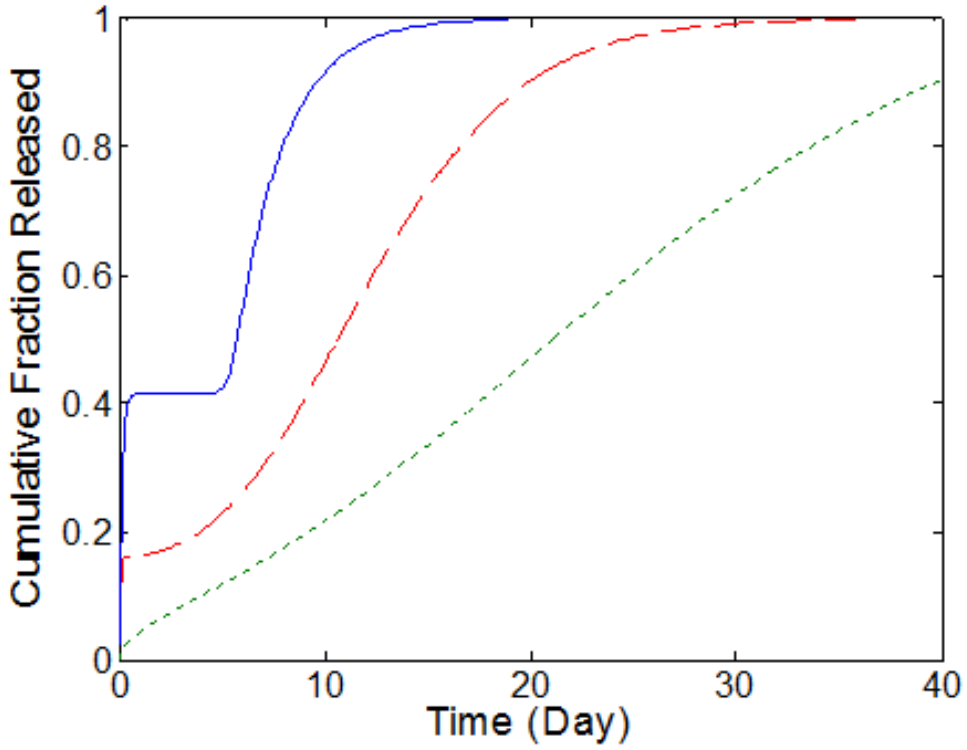

Figure 12: Theoretical release profiles for obtained by varying model parameters: R_p, R_{occ}, M_{wo}, $kC_w(n)$.

The profiles progress from a typical four phase release pattern (solid) to zero order release (dotted). For the solid line a 13kDa 50:50 PLGA matrix was considered with R_p = 150μm, and R_{occ} = 23.5μm. The dashed line was generated based on a 1:1 blend of 10kDa and 100kDa 50:50 PLGA (R_p = 20μm, R_{occ} = 1μm). For the dotted line a 2:1 ratio of 7.4kDa 50:50 PLGA and 60kDa PLA was considered in a single emulsion matrix with R_p = 8μm.

3.4 DISCUSSION

In the effort to hasten the development of biodegradable matrix-based, controlled release therapeutics, many models have been developed to describe the release of specific classes of agents, such as small molecules or proteins[4,95,97-101]. In general, these models require parameters that can only be obtained by fitting controlled release data,[99,100] or otherwise by carefully observing controlled release experiments[4]. In order to eliminate the need for exploratory *in vitro* experiments, which investigate the drug dosing schedules supplied by controlled release formulations, a model must be able to predict, without regression, a broad range of release behaviors for a wide array of agents, entirely from tunable matrix properties. To meet this goal, the model developed in the chapter includes new methods of calculating the magnitude of the initial burst release and the duration of the subsequent lag phase, which allow these features to be predicted with commonly known parameters regardless of the encapsulated agent type, be it small molecule, peptide or protein. This model was also applied to numerous sets of published data to generate values for two correlations. These correlations complete a set of readily attainable parameters for making regression-free predictions of drug release from uniformly hydrated biodegradable matrices. Finally, by varying the tunable parameters over rational bounds, the range of potential release behaviors attainable with such systems were explored.

The comparison of model predictions and experimental data strongly suggests that the magnitude of the initial burst is directly proportional to the amount of agent localized to occlusions residing just *inside* the matrix surface. This region is defined over the entire surface of

the matrix to a depth of $R_p - R_{occ}$, such that any occlusion localized to this region would abut the matrix–reservoir interface. Prior models attributing the initial burst to the amount of agent adsorbed to the matrix surface required the fitting of empirical parameters for the absorption/desorption of each new drug type[4,95]. Further, results from several studies examining release from particles of uniform size and surface morphology, but varying occlusion size (based on the formulation method), suggest that it is unlikely that desorption from the surface (with surface area being proportional to the magnitude of the initial burst) is responsible for the initial burst phase of release[30,70].

Regression-free predictions of published experimental data also suggest that the model consistently calculates the duration of the lag phase for release agents ranging from small molecules to proteins. Prior models have only accurately predicted the duration of the lag phase for either small molecules[100,101,120] or proteins[4]. The current model establishes a polymer molecular weight associated with release (Mw_r) and inversely correlates it to agent molecular weight (Mw_A) (Figure **8**A). The concept that small molecules can diffuse more readily through a higher molecular weight polymer matrix than larger molecules is supported by both diffusion flow cell studies[114] and careful analysis of release data[5,6,30,43,68,70,72,73,79,80,108-111]. In addition, scanning electron microscopy[1,119] and other morphological[121] studies have shown that with degradation, PLGA matrices become increasingly porous solids. The current model attributes this heterogeneous degradation to matrix crystallinity, a mechanism also supported by previous models[120,122].

The model predicts the onset of the secondary burst (Figure 6) using expressions that have both similarities and fundamental differences with those presented in the literature[4,95-101]. Like prior models, the current work employs Fick's second law with an D_{eff} dependent on matrix

porosity. Saltzman and Langer first derived this expression to predict protein release from non-degradable porous polymers[98]. Their lattice-based percolation calculations yield an accessible porosity that fits a cumulative normal distribution, a feature that our model is able to implement without estimated parameters. Recent controlled release models based on stochastic methods have also successfully employed a version of this equation to describe the egress of small molecules from regressed degradation rate constants[99,100]. The current work is, however, fundamentally different from these prior models[99,100] as it describes pore formation in biodegradable matrices entirely from known parameters and applies to a broad range of agents, including small molecules, peptides, and proteins.

As mentioned in section 3.3, the diffusivity values calculated for Figure **8**B are consistent with those found in the literature[1,4,100,114]. These diffusivities display a power dependence on the size of the encapsulating matrix, where $D = aR_p^b$. This expression was originally developed by Siepmann *et al.*[1] to compensate for the size-dependent increase in degradation rate that occurs in autocatalytic polymers such as PLGA[123]. Notably, this effect would be more realistically represented with a degradation rate expression that correctly accounts for the impact of size dependent autocatalysis on pore formation. However, the present relation has proven very useful for the broad range of matrix sizes, polymer molecular weights, and agent types examined herein, even though it was originally developed for lidocane release from 45 kDa PLGA microspheres,[1] (Figure **8**B, Table 1). The diffusivity coefficients ranging from 10^{-14} to 10^{-16} m^2/s calculated in prior models also support this finding[98,100]. Our regression-free predictions (Figure 10–12) help to confirm that this power expression will relate D to matrix size for many different polymers with an acid-based, autocatalytic, first-order rate expressions, including both polyesters[124] and polyanhydrides[118].

Even though the mathematical framework presented herein provides broader applicability than prior models,[4,95,97-101] it still requires several assumptions. Specifically, the model considers a water soluble agent that dissolves rapidly, relative to the duration of release, and that is loaded discretely in a bulk eroding, biodegradable polymer matrix. Efforts are currently under way to relax these assumptions in order to describe more complicated systems. For instance, we speculate that systems exhibiting slower kinetics during the initial burst may be subject to dissolution effects. Other efforts will focus on replacing the correlation of D to R_p with a physically relevant degradation rate expression that inherently accounts for size dependent autocatalysis to provide greater accuracy when examining matrices with extreme sizes (<100 nm or >1 mm). Furthermore, simple diffusion reaction equations can be added to the current model framework, extending its predictive capabilities to slowly hydrating or surface eroding systems, such as large polyanhydride implants. However, even prior to these additions, the model still predicts published data on agent egress from bulk eroding biodegradable matrices (Figure 10–12), which can provide a range of release profiles (Figure 12).

Finally, having confirmed the model's predictive capabilities, the range of release behaviors that can potentially be attained from bulk eroding matrices were explored. Predictions for such matrices cover a continuum of behaviors ranging from abrupt burst–lag–burst profiles to sustained linear release (Figure **12**). These profiles satisfy the dosing schedules for numerous therapeutic applications, such as the constant delivery of a chemotherapy agent or the replication of multiple vaccine doses with a single injection[11,125]. Along with (1) the model's applicability to a wide array of agents and (2) its use of physically relevant parameters, its ability to capture a broad range of release behaviors (3) completes the set of three specifications required for any framework that supports a rational design methodology.

3.5 CONCLUSIONS

A simple, deterministic model was developed for the prediction of release for hydrophilic, agents encapsulated in bulk eroding biodegradable polymer matrices. Model development required application of diffusion-reaction mathematics and the development of two new correlations in order to extend predictive capabilities to the broad range of agents investigated. Further, regression-free predictions from this model provide strong support for the alternative explanations developed to account for the magnitude of the initial burst and the duration of the lag phase. The current diffusion-reaction-correlation framework can also be expanded to cover poorly-soluble drugs, polymer types, and device geometries, including centimeter scale matrix implants, which are all affected by matrix hydration.

4.0 MATHEMATICS FOR HYDRATION LIMITED SYSTEMS

4.1 INTRODUCTION

The bulk eroding polymer systems discussed in Chapter 3.0 do not typically deliver drug at a constant rate, the release behavior required for the safe delivery of most prescription medications. For this reason, scientists developed surface eroding drug delivery matrices whose degradation and erosion behavior naturally produce sustained release. Surface eroding systems, as their name suggests, erode preferentially from the surface inward. This behavior is a function of polymer hydrolysis rate, which is much higher than in bulk eroding systems, and their millimeter/centimeter scale sizing. The rapid consumption of water by hydrolysis and the large volume of water required to fill the matrix (mm^3 vs μm^3) work to keep water out of the bulk of the polymer matrix. This limits the processes of drug dissolution and pore formation, which mediate diffusive release, to the surface of the polymer matrix.

The gradual formation of pores in or erosion of the matrix surface is thought to be the rate limiting step in release from systems, such as polyanhydride implants. Theoretical descriptions of this process are found in most models of surface eroding systems.[15-17] Of note is work by Gopferich et al on the development of a stochastic model of surface erosion that has been featured in several articles examining controlled release of different small molecules.[15, 18-21] Similar models of surface erosion have also been developed using non-stochastic approaches,

although these models have only been tested on select sets of mass loss or small molecule release data.[16, 17]

Recent data by Burkersroda et al reveals that systems which begin drug release under surface erosion most likely transition to a bulk eroding mechanism as mass is lost from the surface and the matrix size shrinks (i.e. the characteristic length scale of diffusion decreases) [22]. The matrix size at this transition from surface to bulk erosion has been dubbed the "critical length". Conversely, this critical length can also be viewed as the distance water can penetrate into a matrix before it is entirely consumed by hydrolysis. Calculations using an average degradation rate and initial molecular weight placed this length at 75μm for polyanhydrides[22], which suggests that many implants made from these polymers will undergo a transition from surface to bulk erosion while release is still occurring.

This chapter describes the first model suitable for predicting a broad array of release behaviors from surface eroding matrices that transition from surface erosion to bulk erosion during the course of their lifespans. This work was summarized in a manuscript by Rothstein et al. that was published by the journal Biomaterials in 2009[126]. This model builds off of the model in Chapter 3.0 that focused on predicting release for a wide array of agents from bulk eroding systems[12]. Specifically, the current model combines diffusion/reaction equations, which account for the system's hydration kinetics, along with sequential descriptions of dissolution and pore formation to compute drug release. Further, all parameters required to solve these equations can be obtained prior to controlled release experiments, allowing predictions to be made without regression. In support of prior work reporting empirically obtained critical lengths [22], the diffusion/reaction equations employed by the current model are used to compute this characteristic parameter from rate expressions[23]. To test the model's accuracy, regression-free

predictions were compared with published controlled release data from several different polyanhydride and poly(ortho-ester) implants.

4.2 METHODS

4.2.1 Release Paradigm

Consider a hydrolysable polymer matrix loaded with a finite amount of release agent or drug. This agent is randomly dispersed throughout the matrix in a powdered or crystalline form. Further the agent is loaded discretely (below its percolation threshold), occupying either small granules or larger occlusions, as dictated by the matrix fabrication method. These occlusions or granules are distributed randomly throughout the polymer matrix, such that the probability of finding drug at any point in the polymer matrix is constant at all positions within the matrix.[12]

At time zero, water or buffer begins to hydrate the matrix. Specifically, water diffuses into the matrix and is simultaneously consumed through the hydrolysis of the polymer matrix [22]. Hence, a larger matrix with a faster hydrolysis rate, such as a polyanhydride implant, will have a sharper concentration gradient of water than a smaller matrix (microsphere) or one with a less labile polymer, such as a poly(lactic-co-glycolic) acid.

Following the hydration of a region of matrix, release of drug can be limited by its solubility or dissolution kinetics. The dissolution rate expression for this process depends upon the agent's solubility and concentration[15] as well as the concentration of solvent. If an agent is highly soluble in water, dissolution may happen on a time scale that is much shorter than the

duration of release. In systems where hydrophobic molecules have been encapsulated, however, dissolution can occur over a considerable amount of time, dramatically affecting the release profile.[15, 24]

After an agent has dissolved, its diffusive egress may be further restricted by the encapsulating matrix. In this case, the matrix needs to degrade to the point where a network of pores is formed, permitting egress of encapsulated agent[12, 25]. This degradation is assumed to happen randomly and heterogeneously throughout hydrated regions of the matrix. Further, the degradation of the matrix occurs in tandem with the dissolution of the agent, and both are dependent upon the hydration kinetics of the system. The interplay between these factors can be translated into a framework of coupled equations for describing release.

4.2.2 Model Development

The time and space-dependent concentration profile of water within a hydrolysable polymer matrix of initial molecular weight (Mw_o) can be calculated from competing diffusion-reaction equations. As water diffuses into a matrix, a process described by Fick's second law, it is also consumed in hydrolysis of the polymer matrix, (written below as a second order reaction, which applies to polyesters and polyanhydrides[8, 26]). Hence, equation 1 below describes the presence of water within the polymer matrix.

$$\frac{\partial C_w}{\partial t} = \nabla \cdot D_w \nabla C_w - k C_w Mw \qquad (1)$$

Where C_W is the time and space dependent concentration of water, D_W is the diffusivity of water in the polymer matrix (found to be on the order of 10^{-12} m^2/s for a broad array of systems [22]), k is the degradation rate constant, and Mw is the polymer molecular weight.

As part of the hydrolysis reaction, polymer bonds are also broken leading to a decrease in the molecular weight of the polymer matrix. The kinetics of this process can be described by the standard second order rate expression commonly used for both polyesters and polyanhydrides.[8, 26] (Equation 2)

$$\frac{\partial Mw}{\partial t} = -kC_w Mw \qquad (2)$$

It is assumed that components of the polymer matrix (e.g. initially high molecular weight polymer degradation products) do not diffuse considerably before the onset of erosion (Mw ≈ 4 kDa), by which time the release of most types of agents will have commenced. In line with previous models, a "degradation front" can be defined at a point in the polymer matrix where the gradient of the polymer molecular weight (dMw/dr vs. r) is at a minimum[19, 27]. This minimum is defined as the inflection point of the continuous function, $Mw(r)$, such that the initial average molecular weight at this front is ½ Mw_o, provided that the core of polymer matrix is still at its initial molecular weight.

With the hydration kinetics defined, the dissolution of the drug can be calculated, which is normally done with a second order rate expression.[28] Unlike the standard systems used to derive this second order expression, the solvent concentration of the present system varies with position and time, and hence must be considered as well. The standard expression is also written in terms of the solute surface area and mass transfer coefficient which have been translated into equivalent, readily measurable parameters.(Equation 3)

$$\frac{\partial C_S}{\partial t} = -k_{dis} C_{Sn} C_{An} C_{Wn} \qquad (3)$$

where k_{dis} is the intrinsic dissolution rate constant, C_{Sn}, is the normalized concentration of solid drug in the polymer matrix, C_{An} is the difference between the aqueous agent concentration and its maximum solubility (C_{Amx}), normalized by C_{Amx}, and C_{Wn} is the normalized concentration of water. Boolean expressions were used to ensure that $C_{Sn,}$ $C_{An,}$ and $C_{\backslash Wn}$ were bounded by 0 to 1, ensuring a physically relevant model solution. Next, the position-(r) and time- (t) dependent concentration of dissolved agent in a polymer matrix can be calculated from Fick's second law and the dissolution rate expression. (Equation 4)

$$\frac{\partial C_A}{\partial t} = \nabla \cdot D_{eff} \nabla C_A + k_{dis} C_{Sn} C_{An} C_{Wn} \qquad (4)$$

where D_{eff} is an effective diffusivity term. Integrating the total normalized concentration of agent in the matrix over all space yields the cumulative fraction of agent remaining in the matrix at each point in time (Equation 5)

$$P(t) = V^{-1} \int \frac{C_S + C_A}{C_{So}} dV \qquad (5)$$

$$P(t) = \int \frac{C_S + C_A}{C_{So}} \cdot \frac{2 \cdot r}{L \cdot R_P{}^2} dr \text{ (For a rod or disc)}$$

And the cumulative fraction of agent release ($R(t)$) is: (Equation 6)

$$\mathrm{R(t)} = 1 - P(t) \qquad (6)$$

As in Chapter 3.0 the D_{eff} term in Equation 4 is dependent on the matrix porosity (ε) and the diffusivity of the agent through the porous matrix (D_A). However, in the hydration-limited systems covered by this model, porosity is time- and space-dependent and is therefore based

directly on the molecular weight of the polymer instead of degradation time as done in Chapter 3.0 . (Equation 7)

$$\varepsilon = 1 - \frac{1}{2}\left[erf\left(\frac{Mw - Mw_r}{\sqrt{2\sigma^2}} \right) + 1 \right] \qquad (7)$$

This means that the molecular weight of the polymer matrix during release (Mw_r) is used directly in the porosity expression. Changes are also made in the calculation of agent diffusivity (D_A), which correlated directly to matrix size for bulk eroding systems. For a surface eroding matrix, autocatalytic degradation only occurs in the region of matrix that is hydrated, thus the system's critical length is used to determine the diffusivity from the correlation in Figure **8**.

The boundary conditions for the polymer phase, as well as the aqueous and solid release agent phases, match those defined in a prior model for bulk eroding matrices[12]. Briefly, symmetry conditions ($dC_n/dr = 0$) are defined at the matrix center and perfect sink conditions ($C_n = 0$) are set at the matrix surface (at radius R_p and length L in a cylinder or disk). For water concentration, the same internal symmetry conditions still apply, but the concentration of water at the matrix surface is set to match that of an infinite reservoir, with a concentration of Cw_o calculated as the density of water over its molecular weight. Further, when the encapsulated agent is gathered in large occlusions or pockets (relative to the size of the entire matrix), such as would be found in a double emulsion fabricated microsphere, the matrix should be represented with two sub-domains, as demonstrated previously,[12] to account for the resulting initial burst.

4.2.2.1 Limiting Cases

Depending on the nature of the encapsulated agent, it may be possible to simplify the mathematical description of release. If an agent possesses a high aqueous solubility and

dissolves rapidly, such that the rate of dissolution is at least 2 orders of magnitude faster than the rate of diffusion, the timescale of dissolution is negligible. When modeling such cases,[30-32] the drug was assumed to dissolve instantaneously in water. Hence, Equation 3 can be neglected entirely and Equation 4 can be simplified to the following form. (Equation 8)

$$\frac{\partial C_A}{\partial t} = \nabla \cdot D_{eff} \nabla C_A \qquad (8)$$

where C_{Ao} becomes the initial concentration of agent. In total, these simplifications reduced the model to three sets of diffusion-reaction equations instead of four and eliminated three input parameters (C_{So}, k_{dis}, and C_{Amx}).

Alternatively if an agent has a $Mw_r > Mw_o$, by definition, it can diffuse freely through the newly hydrated polymer matrix and does not require degradation of the matrix for egress. Specifically, the agent is small enough to pass freely through the matrix and, as such, pores formed during degradation are no longer needed to provide a pathway for diffusive egress; hence $D_{eff} = D_A$. In this case the expression for matrix porosity (Equation 7) can be neglected.

4.2.3 Model Implementation

By adopting the proven approach to calculating release as detailed in section 3.2.5, existing correlations[12] can be used along with the model to generate regression-free predictions. To calculate such predictions, the model was coded in Matlab® (Mathworks, r2007a) and computed using the finite element method on Comsol® (v3.1). Meshing was successively refined, until

node-density independent results were observed. Otherwise, default solver settings were maintained.

4.2.3.1 Critical length

To investigate the effects of polymer molecular weight (Mw_o) and degradation rate (k) on the transition from surface to bulk erosion, only equations 1 and 2 were considered. This transition occurs at a set matrix size, dubbed the critical length.[22] Burkersroda et al originally defined the critical length as the distance water can travel through a matrix before the rate of diffusion equals the rate of degradation, such that in a surface eroding system, the rate of degradation surpasses the rate of diffusion.[22] However, when mathematically accounting for these two rates with Fick's second law and a second order rate expression (applicable to autocatalytic hydrolysable polymers) this original definition becomes physically untenable because the C_w term in the hydrolysis rate expression prevents the reaction rate from ever surpassing the diffusion rate. Thus, in order to determine the erosion mechanism of the matrices examined herein, we defined critical length as the matrix size where the polymer residing in the degradation front hydrolyzes at its most rapid rate, as noted by a minimum in $\partial Mw_f/\partial t$ vs. t. In other words, during surface erosion, this front moves progressively inward, slowing its traverse only as the matrix begins to uniformly hydrate. With the onset of bulk erosion, the hydrolysis reaction taking place throughout the matrix can no longer consume the water before it penetrates to the matrix core. This leads to a matrix where the water concentration is at a maximum and the polymer molecular weight has not significantly decreased from its initial value. Together, these conditions maximize the degradation rate ($-kC_wMw$), resulting in the fastest possible drop in the average polymer molecular weight. Hence, it can be said that the matrix size, where degradation proceeds (on

average) at its fastest average rate, denotes the end of surface erosion and the onset of bulk erosion, and therefore can be defined as the critical length.

Using this definition, the critical length was calculated for a variety of polymers, including PLA, PLGA, PFAD:SA, and PSA, at initial molecular weights ranging from 5kDa to 130kDa. The results of these calculations were used to determine if published release data [1, 30, 32] was generated by surface eroding, bulk eroding, or transitioning phenomena. Specific calculations were also performed to check the erosion mechanism of matrices used in other modeling literature.[20, 31]

4.2.4 Release Predictions

The simplified forms of the model described in section 4.2.2.1 were validated against release data from matrices that could be represented in 2-dimensions using axial symmetry. Values for common model parameters R_p, L (for a cylinder), Mw_o, Mw_A, C_{Wo}, C_{So}, C_{Amx}, k, D_w, and k_{dis} were specified directly from, or calculated using parameters specified in, the materials and methods sections of published literature [30-33]. The correlations developed in Chapter 3.0 were used to calculate values for D_A and Mw_r.

It is important to note that the poly(ortho-ester) matrices investigated herein are unique in the field of controlled release because they contain a small molecule anhydride excipient. This is proposed to alter the degradation mechanism of the polymer by increasing the rate of autocatalysis in the system.[34] Fortunately, data on the hydrolysis of this anhydride excipient was published for these matrices and was used to enhance model caculations.[31] Specifically, this

data was used to calculate the amount of water diverted from polymer degradation into anhydride hydrolysis as a function of time. The newly calculated rate expression was amended to the hydrolysis reactions to adjust for the additional consumption of water by the excipient.

4.3 RESULTS

4.3.1 Matrix degradation kinetics

Solutions to equations 1 and 2 generate hydration and degradation profiles for a specified polymer matrix. Figure 13 shows degradation profiles (Mw/Mw_o as a function of r and t) for matrices composed of a single polymer where the dominate erosion mechanism has clearly been predetermined by carefully selecting the matrix size. In a system undergoing surface erosion, the degradation-erosion front will move inward toward the center of the matrix as both degradation and erosion are confined to the periphery (Figure 13A). In bulk eroding systems, in which degradation occurs randomly throughout the matrix, the matrix size remains constant as its average molecular weight decreases (Figure 13C). This change in average molecular weight begins at the most rapid rate possible, with water concentration and polymer initial molecular weight both being at maximal values, and decreases as the number of hydrolysable bonds is depleted. Hence, average degradation rate in the polymer matrix should be at a maximum with the onset of bulk erosion (or in other words, during a transition from surface to bulk erosion) (Figure 14A). In turn, the critical length is calculated as the matrix size (marked at the center of the degradation front) when this transition occurs. Increasing the polymer degradation rate,

indicating a more labile hydrolysable bond type, correspondingly decreases the critical length, indicating more dominate surface eroding behavior. Likewise, increasing the polymer initial molecular weight also decreases the critical length (Figure **14**B).

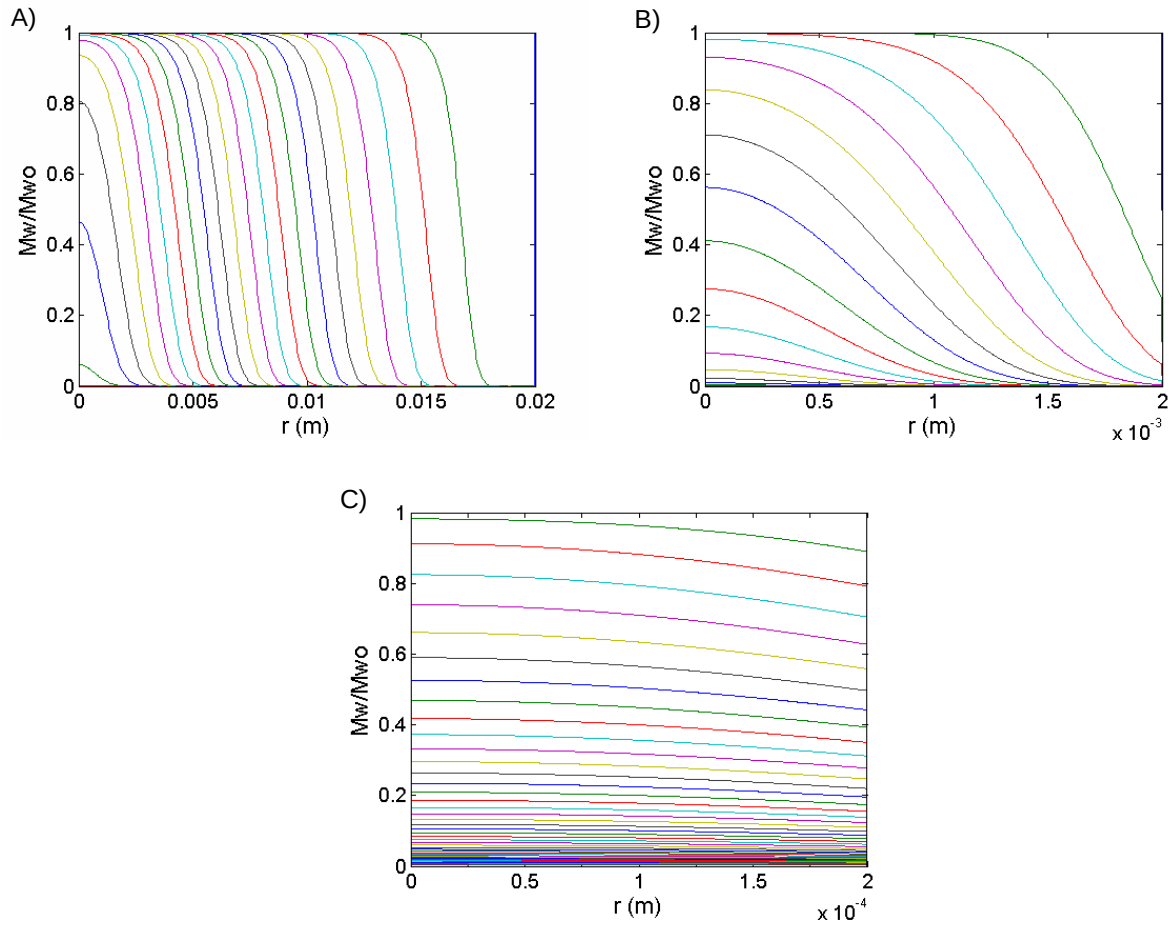

Figure 13: Degradation profiles (*Mw* relative to Mw_o as a function of distance and time) for various spherical matrices of 10kDa PSA.

Matrix size is varied (X axis) to explore the various erosion schemes: A) surface erosion, B) a transition from surface to bulk erosion and C) bulk erosion. The lifetime of each matrix changes with its size, such that each line in A) represents 1 month, B) represents 1 day and C) represents 2 hours. In each figure, the line furthest to the right and top indicates the earliest time point.

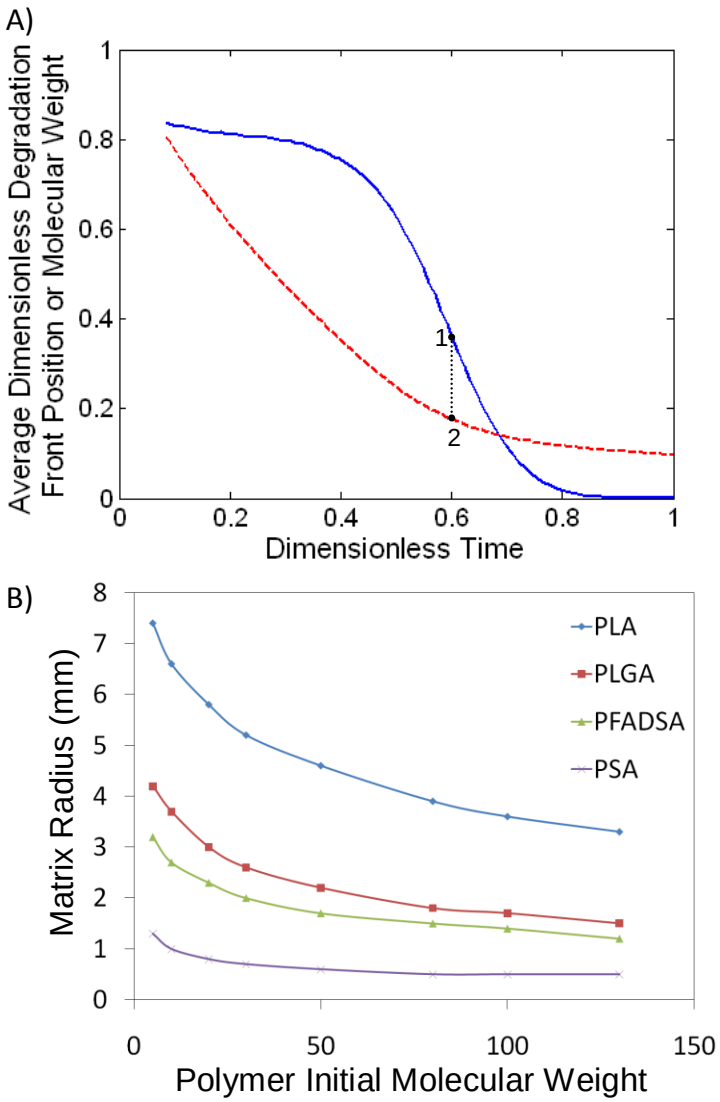

Figure 14: Calculation of critical length

Calculations used a 2nd order rate expression as a function of both the initial molecular weight of polymer and hydrolysis rate constant. A) Critical length (point 2) was calculated as the matrix size (dashed line) in which the average molecular weight of polymer at the degradation front (solid line) decreases most rapidly (point 1), indicating the onset of bulk erosion. B) Values for critical length as a function of initial molecular weight for a variety of polymer matrices: PLA (diamond), 50:50 PLGA (square), 50:50 PFAD:SA (triangle) and PSA (circle). Linear interpolations have been added between data points of the same set to aid in interpretation

Having determined the matrix specifications required to maintain surface erosion, the model's ability to predict controlled release from matrices with a variety of different erosion mechanisms was examined. Further, systems with different hypothesized, release rate-limiting steps were also examined. The tested systems range from bupivacaine release from FAD:SA polyanhydride disks (dissolution limited, bulk eroding), to gentamicin release from FAD:SA polyanhydride rods (degradation limited, surface eroding), to amaranth release from POE disks (degradation limited, surface and bulk eroding).[30-32]

4.3.2 Dissolution controlled release

Work by Park et al.[30] examines the release of a small molecule, bupivacaine, from a 50:50 FAD:SA polyanhydride disk with a 4 mm radius and 1 mm thickness sized at slightly below the calculated critical length for this system (~1.7mm). This suggests that the system would exhibit bulk eroding behavior and, as such, model predictions made with and without taking into account the hydration kinetics should both match the bupivacaine release data with comparable accuracy (**Figure 15**). In line with this result, both predictions follow the trend set by the *in vitro* data with the prediction from the surface erosion model producing a slightly more accurate result than the simplified version of the model that neglected hydration kinetics. As error in the measurement of *in vitro* release is cumulative greater deviation between model predictions and experimental data is expected at later time points. It was also hypothesized that dissolution kinetics were an important factor in determining the release rate of bupivacaine and failing to consider them increased the SSE by a factor of 25 (SSE = 4.9004, data not shown).

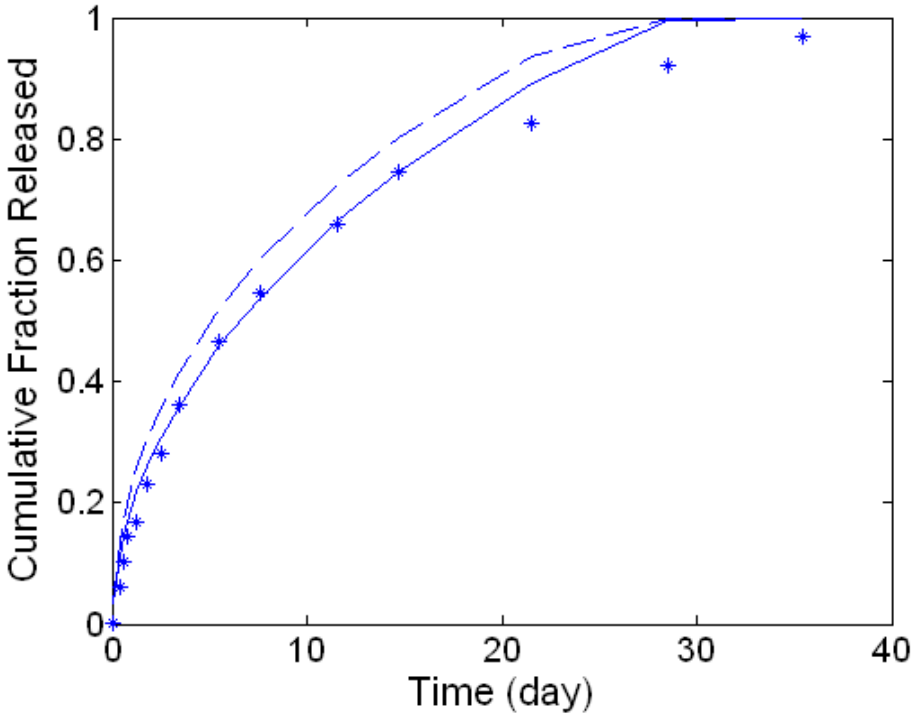

Figure 15: Predictions of dissolution-controlled, release of drug.

The experimental data (asterisks) was generated from polyanhydride disks releasing the sparingly soluble agent, bupivacaine. [30] Model predictions were generated without regression while considering surface erosion (solid, SSE = 0.0204), and assuming bulk erosion (dashed, SSE = 0.0691). To make these regression-free predictions, system-specific parameters were set as follows: R_p = 4mm, L = 1mm, Mw_o = 50kDa, C_{So} = 288.42mol/m^3 and C_{Amx} = 2.184mol/m^3 k_{dis} = 0.046mol/m^{3}s. D was calculated as 4.61x10^{-12}m^2/s from a correlation published previously.[12] Model solutions were computed at times corresponding to each experimental data point.

4.3.3 Degradation controlled release

Stephens et al [32] documented gentamicin release from a 35.8kDa Mw_o 50:50 FAD:SA polyanhydride bead with a 4mm diameter and a 12mm length, a matrix on the same order of magnitude as, but still slightly larger than the calculated critical length of 1.9mm. Based on the calculations of critical length presented in Figure **14**B and the those made by Burkersroda et al.,[22] this system should exhibit surface eroding behavior, and any attempt to accurately model it should account for hydration kinetics.[22] If a prediction for release is made without accounting for hydration kinetics, as detailed in[12], a relatively poor fit to the data is observed (SSE = 0.4350). However, when accounting for hydration kinetics, using equations 1 and 2, the model's prediction improved dramatically (as expected), resulting in an SSE of 0.0657 (Figure **16**).

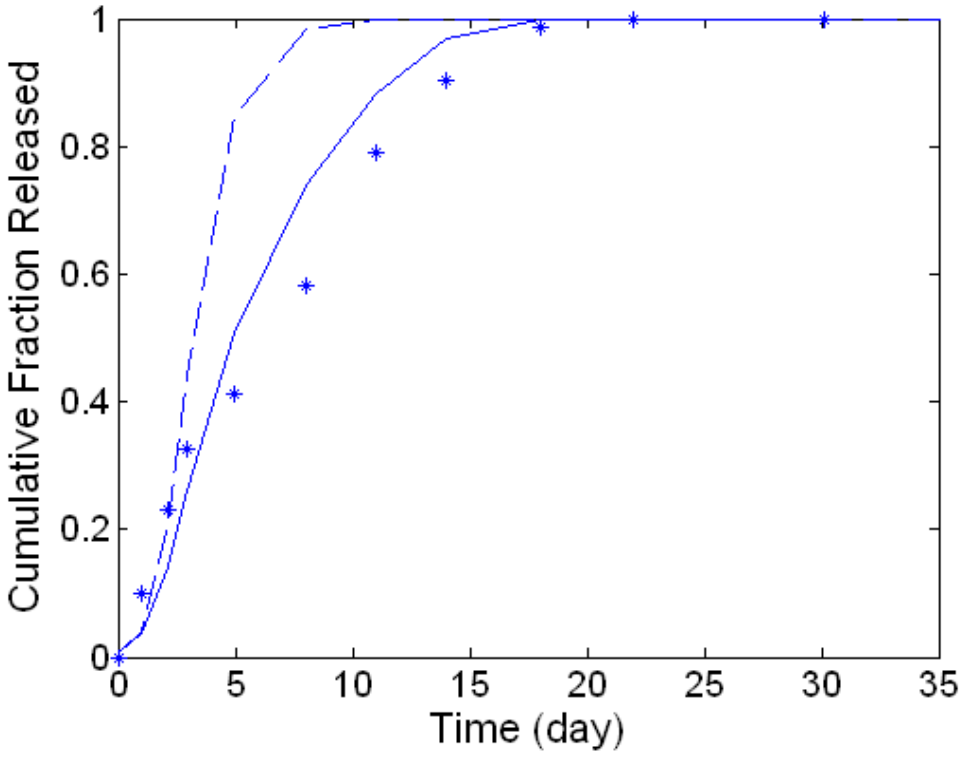

Figure 16: Predictions for degradation-controlled release of drug.

The experimental data (asterisks) charts gentamicin release from FAD:SA matrix rods.[32] Model predictions were generated without regression while considering surface erosion (solid, SSE = 0.0657) and assuming bulk erosion (dashed, SSE = 0.4350). To generate these regression-free predictions, the following values were used: Rp = 2mm, L = 12mm, Mw_o = 35.8kDa, Mw_r = 13.3kDa, D_A = 5.94x10-12m^2/s. Model solutions were computed at times corresponding to each experimental data point and linearly interpolated.

Work by Joshi et al examined amaranth dye release from POE disks (10mm diameter, 1.4mm thick), which had their erosion mechanism controlled by the addition of phthalic anhydride. When a low amount of anhydride (0.25w/w%) was present in the disk, a bulk eroding mechanism was postulated to dominate, a point confirmed by our own critical length calculations (data not shown). In contrast, with the addition of just 1% anhydride excipient, the critical length dropped to 684μm, a value slightly below the shortest matrix dimension, suggesting that surface erosion should dominate (at least at early times).[31] Predictions of drug release from both of these systems take into account both the increase degradation rate from and the consumption of water by the anhydride excipient. Because these predictions were only computed at experimentally measured time points and linearly interpolated, abrupt changes in the rate of release seem to occur. Predictions made without considering the presence of anhydride increased error is observed in the predictions (data not shown). Accounting for these effects significantly improved prediction for both the 0.25% anhydride matrix, reducing error by a factor of 4, and the 1% anhydride matrix, reducing error by a factor of 6, when compared to previously published results.[31]

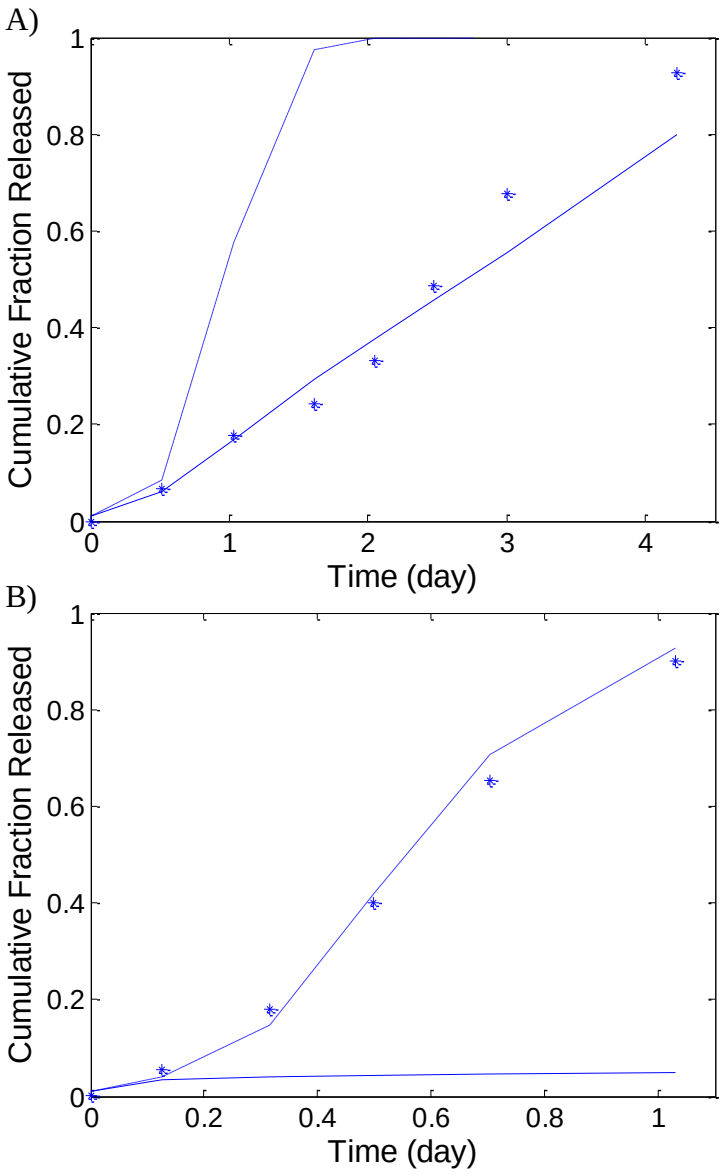

Figure 17: Predictions of release from (A) bulk eroding and (B) surface eroding POE matrices.

Predictions have been made for the experimental data for dye release (astricks), while accounting for the hydrolysis of the anhydride excipient, with the complete model (solid line, (A) SSE = 0.0237 and (B) SSE = 1.1539) and the simplified version which assumes bulk erosion (dashed line, (A) SSE = 1.0077 and (B) SSE = 0.0061). For calculations in both A and B, the following parameters were used: Mw_o = 28.2kDa, Mw_r = 10.2kDa, Rp = 5mm, and L = 1.4mm. Based on their differing anhydride contents, values of D_A were unique to A and B, with $D_A = 1.44 \times 10^{-12}$ m^2/s in A and $D_A = 9.75 \times 10^{-12}$ m^2/s in B.

4.4 DISCUSSION

Biodegradable matrices for controlled release have been traditionally classified as either surface or bulk eroding and mathematical models of drug delivery from these systems have often reflected this classification in their assumptions.[7-10] Recent data suggests that many surface eroding systems actually transition to a bulk eroding mechanism while drug release is occurring.[22] With this in mind, a new model was developed to predict drug release from matrices undergoing multiple different erosion schemes, the first of its kind to describe the release of a wide array of agents without regression. This model uses diffusion-reaction equations to describe the hydration kinetics, drug dissolution and degradation controlled release. Using the equations governing matrix hydration, a mechanistically accurate method for calculating a system's critical length was developed, and then applied to a range of common systems. Regression-free predictions (which use parameters that can be obtained prior to release experimentation) were made including and (for validation purposes) ignoring the effects of matrix hydration in both smaller and larger than their respective critical lengths. Specifically, the model has been used here to predict bupivacaine release from polyanhydride disks[30] and gentamicin release from polyanhydride cylinders[32] as well as amaranth red release from poly(ortho-ester) disks[31]. The model's applicability is not, as shown previously, limited to small molecules and should apply with comparable accuracy to systems that encapsulate and release macromolecules.[12]

Several of the fundamental concepts from the current model's paradigm have been separately employed in prior models.[12-17] However, the equations used to translate these concepts into mathematical predictions for drug release have, however, been altered in some way

from their previous forms. For example, a dissolution rate expression has been used in prior published work.[15] Unlike this previously published expression[15], the form in equations 3 and 4 include a term for the dimensionless concentration of water that accounts for potential solubility limitations associated with partially hydrated systems. Another example comes from the porosity expression, which has been translated from a time-dependent form that assumes a uniform degradation rate [12] to a version with broader applicability, based on the local molecular weight of the polymer matrix. Finally, the concept of using diffusion/reaction equations to create a model that uniformly captures different erosion schemes has also been investigated before. One prior model based on species-dependent, diffusion/reaction equations was successfully developed and applied to data for dye release from POE disks (Figure **17**). This model made predictions using system-specific parameters that could not be directly measured. In contrast the model derived in this Chapter uses a far simpler diffusion-reaction description of release that still provides comparable predictive power. This is confirmed by regression-free predictions of the amaranth red release data made with a greater degree accuracy (i.e. lower error in the prediction of data) that with prior models.[31]

An examination of hydration and degradation profiles based on Equations 1 and 2 show that the model derived in this Chapter can produce profiles that resemble surface erosion, bulk erosion and the transition between the two based on a careful selection of matrix size. Further, these degradation profiles (Figure **13**A, B) provide a direct means for calculating a theoretical critical length (i.e. where a given polymer transitions from surface to bulk erosion) (Figure **14**). In contrast to the original calculations of critical length, which used an Erlang distribution to represent the degradation rate,[22] this new calculation relies on a second order rate expression that can directly account for radial gradients in polymer molecular weight within the matrix. When

accounting for the different degradation rates used in these two expressions, both sets of calculated values for critical length agree within order of magnitude for all systems tested.

Comparison of predictions from the model to experimental data from biodegradable matrices serves to validate elements of its release paradigm. The bupivacaine-loaded disks modeled in **Figure 15** showcase the importance of the dissolution and hydration rate expressions in generating accurate (SSE = 0.0172) predictions for the release of a sparingly soluble agent from a polyanhydride matrix.[30] (**Figure 15**) Attempting to predict the release of bupivacaine without considering its slow dissolution produced inaccurate predictions. Conversely, predictions made without considering the system's hydration kinetics show only a slight decrease in model accuracy. *Prima facie,* it may be surprising that a slight drop in accuracy is observed with this system which, being a bulk eroding system, is most often characterized by rapid, uniform hydration.[11] However, prior work indicates that, while bulk eroding systems in the micron size-range hydrate in minutes, bulk eroding implants (as defined by diffusion rate > degradation rate) on the order of millimeters can take days to become uniformly hydrated.[13] When such an implant only delivers drug over several days or weeks, this longer hydration time can significantly delay release, even though the system can be technically considered "bulk eroding".

Regression-free predictions for the POE matrix (Figure **17**A) provide a different view for the importance of accounting for various mechanisms of matrix dynamics and physical agent egress. Like the bupivacaine-loaded matrix featured in **Figure 15**, predictions for this system were also significantly better when hydration kinetics were accounted for by the model. This provides additional support for the conclusion that hydration kinetics can significantly influence the rate of drug release from bulk eroding implants. Unlike dissolution-limited release of

bupivacaine, though, the readily-soluble amaranth red being released from this system is thought to only be restricted by the POE matrix. This system contained an anhydride excipient which had to be accounted for in the model's description of matrix degradation. [31] Attempting to predict release from this system without accounting for the diversion of water into the hydrolysis of the anhydride led to increased error during day 1 to 3, when the anhydride excipient is postulated to be hydrolyzing.[31] (data not shown) Even with this increased error, predictions from the current model still offer an improvement in accuracy (lower SSE) over prior modeling work.[31]

The implants examined in Figure **16** are slightly larger than the calculated critical length, and gentamicin is large enough to be readily restricted by the polymer matrix, making this a prime example of how release occurs in a system that transitions from surface to bulk erosion.[32] Support of the model paradigm for release from a transitioning system is found in the accurate regression-free prediction (SSE = 0.0821) data from this system[32] (Figure **16**). Failing to consider matrix hydration kinetics greatly (8-fold) decreases the accuracy of this prediction, as would be expected for a system that begins under surface erosion. This change is much more dramatic than the one observed for comparable bulk eroding systems (e.g. **Figure 15**), which provides a perspective on the crucial that role hydration kinetics play in systems that transition from surface to bulk erosion.

With respects to the POE controlled release data in Figure **17**, it is apparent that the simplified form of the model, assuming bulk erosion, generates a more accurate prediction of the amaranth red release data from the disk with 1% anhydride content than the full version of the model, even though the matrix should theoretically begin release under a surface eroding mechanism. However it is important to note that published empirical evidence, from time-lapse

images of matrix cross-sections, clearly shows a distinct change in internal morphology, between 5 and 8 hours of incubation, that suggests water has already perfused into the matrix core.[35] This hydration appears to occur much more rapidly than is predicted by equations 1 and 2 (data not shown). During the time period between 5 and 8 hours, the initially rapid, average hydrolysis rate also transitions to a near zero value[31], which is inconsistent with published predictions based on random chain scission theory.[31] Taken together, this evidence suggests that another process, beyond the diffusion/reaction kinetics considered herein, causes water to perfuse the matrix earlier than expected by simple diffusion and hydrolysis for this system. It is possible that the unaccounted driving force could come from an increase in matrix osmotic pressure, brought about by the 1w/w% of anhydride excipient.[36] Regardless, this data serves an example of how actual phenomena can create situations with dynamics that extend beyond model assumptions. However, once the correct physical phenomenon has been determined (using cross sectional analysis here), the model will accurately predict release if constrained accordingly.

Together, the validations performed on published release data sets (Figures 16-18) confirm that the regression-free predictions appear accurate when the systems in question conform to the model's fundamental assumptions. System attributes, such as high loading (above the percolation threshold) or the presence of excipients, can cause the experimental data to deviate from model predictions. Future work could further expand the applicability of the model developed herein with addition of equations accounting for such phenomenon such as system osmotic pressure or drug percolation.

4.5 CONCLUSIONS

A new model for predicting release from surface eroding biodegradable matrices has been developed. This model attributes egress to matrix hydration, agent dissolution, and polymer degradation instead of relying on the traditional assumption that release is solely erosion controlled. Further, accounting for matrix hydration with diffusion/reaction equations captures the transition from surface to bulk erosion in common polymer systems. Strong agreement with multiple published data sets supports future use of the model as a design tool, allowing researchers to rapidly acquire the matrix specifications that will yield a desired release profile.

5.0 IMPACT OF PREDICTIVE MATHEMATICAL MODELS ON *IN VITRO* CONTROLLED RELEASE ASSAYS

5.1 INTRODUCTION

One direct application of the models developed in Chapters 3.0 and 4.0 is to collection and interpretation of *in vitro* release data. This drug release data is generated by simply suspending and incubating microparticles in buffer at body temperature over time. Ideally this data provides a cost-effective means of gauging if a formulation's release kinetics will be suitable for a given application. However, interpreting in vitro data or, moreover, designing a study to efficiently capture unambiguous data can be non-trivial. As discussed in prior Chapters, a formulation's rate of drug release can fluctuate dramatically over the course of an assay (Figure 2), often in ways that are difficult to intuit. Incorrectly timing the collection of release data can mask key fluctuations in release rate or even make it appear that release is in fact complete when it is not.

The challenges faced in gathering and interpreting the data generated by *in vitro* release assays are similar to those encountered in analysis of pharmacokinetic (PK) data. Like *in vitro* release assays, the data collected in PK studies provides evidence of drug concentration only at discrete points in time. However, in PK studies today, it is now standard to employ proven mathematical models that allow researchers to accurately interpolate and extrapolate upon collected data[127]. This type of analysis is essential for the accurate computation of important PK

processes adsorption, distribution, metabolism and excretion[33]. If comparable model-driven analysis were regularly applied to *in vitro* release data as well, then key performance parameters such as the rate and duration of release could be determined for incomplete or sparse data sets. Further, model predictions could permit sample points to be optimally timed in subsequent *in vitro* or *in vivo* assays if these parameters need to be validated more fully. Such analysis would be particularly valuable when designing formulations of PLGA, whose patterns of release drug are often difficult to anticipate[95].

Accordingly, this chapter will demonstrate how a mathematical model can be used to retrospectively evaluate existing sets of release data in order to generate additional insight into the formulations' release behaviors. Specifically, data sets for evaluation were selected to illustrate common issues, like lack of closure or widely spaced sampling times, that make their results difficult to definitively interpret. The mathematical model from Chapter 3.0 will be used for this evaluation because its validated covered system similar to those considered herein[126,128]. When appropriate, additional *in vitro* release assays were also carried-out to validate sets of interpolative and extrapolative model predictions. Overall, these mathematical evaluations of *in vitro* release data have the potential to yield useful information about formulation performance and insight that can guide the design of futures studies. The contents of this chapter have been summarized in an article title "A Retrospective Mathematical Analysis of Controlled Release Design and Experimentation" accepted for publication in Molecular Pharmaceutics.

5.2 MATERIALS AND METHODS

5.2.1 Materials

Poly(lactic-co-glycolic)acid (PLGA) RG502 ($Mw_o \approx 9kDa$) was purchased from Boehringer Ingelheim (Ingelheim, Germany). Enfuvirtide (T-20) was obtained through the AIDS Research and Reference Reagent Program, Division of AIDS, NIAID, NIH from Roche. Nitro oleic acid (NO_2-OA) was composed by an equal mixture of 10-NO_2-octadec-9-enoic acid and 9-NO_2-octadec-10-enoic acid and synthesized as previously described[129]. Solvents, assay reagents, and other chemicals were purchased from Thermo Fisher Scientific (Waltham, MA).

5.2.2 Microparticle fabrication

Microparticles were prepared using the emulsion processing technique as described[52]. Briefly, 200 mg RG502 PLGA was dissolved in 4 ml dichloromethane (oil phase). One hundred µl of an agent stock solution (either 2mg/ml enfuvitide in 2.4mg/ml sodium carbonate solution or 1mM NO_2-OA in methanol) was added to oil phase, which was then mixed for 10s using a probe sonicator (Sonics and Materials Inc., Danbury, CT). This mixture was then homogenized at 2,300 rpm for 1 minute in 60ml of 2% PVA (MW ~ 25,000, 98% hydrolyzed) solution, using a homogenizer (Silverson L4RT-A). This emulsion was immediately poured into 80 ml of 1% PVA solution, and dichloromethane was allowed to evaporate. After 3 hours, the particles were centrifuged (1500g, 10 min, 4°C) and washed x4 in deionized water. Microparticles were then

re-suspended in 5 ml of deionized water, frozen on dry ice and lyophilized (Virtis Benchtop K freeze dryer, Gardiner, NY; operating at 60mTorr).

5.2.3 Microparticle characterization

Microparticles were sized using the volume impedance method with a minimum of 10,000 measurements on a Beckman Coulter Counter (Multisizer 3). Microparticle surface morphology and shape were examined using a scanning electron microscope (JEOL JSM-6330F, Peabody, MA). The loading of the enfuvirtide microparticles was measured by dissolving 5mg of microparticles in 250 ul dimethylsulfoxide (DMSO). Peptide was then extracted with the addition of 1 ml of 0.05M NaOH / 5% sodium dodecyl sulfate (SDS) and measured using the microBCA assay. The loading of NO_2-OA could not be measured by this method as the presence of SDS interfered with the detection of this agent.

5.2.4 *In vitro* release assay

Release data was measured accumulatively, as done previously[52]. A known amount of microparticles was suspended in 500ul of phosphate buffered saline (DPBS, pH 7.4, GIBCO, Invitrogen) and placed on an end-to-end rotator at 37^{o}C. At regular intervals the microparticle suspensions were centrifuged, allowing the supernatant to be collected and particles to be resuspended in an equal volume of DPBS.

Enfuvirtide concentration in the supernatant was detected either by microBCA or high pressure liquid chromatography (HPLC). The microBCA assay was carried out using

Spectramax M5 microplate spectrophotometer (Molecular Devices, Sunnyvale, CA) as detailed in the manufacturer's protocol (Pierce, Thermo Fischer). For HPLC, detection was carried out as done previously[130]. A Dionex Ultimate 3000 HPLC system (Thermo Fisher Scientific, Waltham, MA) was used with a XTerra RP18 5µm 3.0x15mm column (Waters Corporation, Milford, MA) and enfuvirtide was detected on a Dionex RF2000 fluorescence detector (ex = 280nm, em = 350nm). Solvents and gradients were kept consistent with previous work, yielding peaks for enfuvirtide at 4.86min and insulin (internal standard) at 2.6min.

NO_2-OA concentration was quantified using high-performance liquid chromatography-electrospray ionization mass spectrometry (HPLC-ESI MS/MS) as previously reported[129,131]. Briefly, the released NO_2-OA was chromatographically resolved using a 20 × 2-mm cartridge column (Mercury MS Gemini 3µm C18, 110 Å, Phenomenex, Torrance, CA) with a flow rate of 0.75 ml/min using a water (A)/acetonitrile (B) solvent system containing 0.1 % acetic acid. A linear gradient of B from 11 to 100% was developed in 3.5 min and used to separate the ions, followed by their detection on a triple quadrupole mass spectrometer (API 5000, Applied Biosystems/MDS Sciex, Framingham, MA) using the specific 326.3/46 and 344.3/46 transitions for NO_2-OA and $^{13}C_{18}$-NO_2-OA respectively. For quantification, peak areas of NO_2-OA and $^{13}C_{18}$-NO_2-OA were calculated using Analyst 1.4.2 quantification software (Applied Biosystems/MDS Sciex, Thornhill, Ontario, Canada), and the ratio of analyte to internal standard was calculated to determine the concentration.

5.2.5 Collection of published release data

Published data was collected from the figures of manuscripts using Plot Digitizer software (v. 2.4.1), as done previously[126,128]. Release profiles in these figures were enlarged to a size of 600 by 400 pixels allowing accurate measurement of the scales on their axes. Data points were then manually targeted, yielding a numerical coordinate for each point. All sets of published release data collected were assayed accumulatively, by measuring the concentration of drug or protein released into the media.

5.2.6 Model predictions

All mathematical predictions of controlled release were made using the model developed by Rothstein et al., as done previously[128]. This model was coded in MATLAB(v7.12) and solved using the finite element method with COMSOL(v3.5a). To initialize solutions, values for the drug's molecular weight (Mw_A), the polymer's initial molecular weight (Mw_o) and the microparticle radius (R_P) were assigned based on the published materials and methods of each system considered. The value for occlusion size (R_{occ}) was calculated from SEM images of the microparticle internal morphology, when available, and otherwise was back-calculated from the average magnitude of the given system's initial burst as derived previously[128]. As R_{occ} only contributes to the prediction of initial burst magnitude, this back-calculation does not interfere with the model's predictions regarding the timing or rate of the secondary burst, which are of primary focus in this work. The polymer degradation rate (kC_w) was held constant for each copolymer ratio as follows: 50:50 PLGA, $kC_w = 0.08636 day^{-1}$; 75:25 PLGA, $kC_w = 0.0342 day^{-1}$;

and PLA, kC_w = 0.0169day^{-1}. With these input parameters, the model could then predict the given system's release profile. The results were then plotted against the respective set of experimental data for statistical analysis.

As the mathematical model used currently does not account for kinetics of the initial burst (only the magnitude[128]), data points within the first 72 hours of release were omitted from this statistical analysis. The accuracy of mathematical predictions was quantified by the normalized residual squared error (nRSS = residual sum of squares divided by the number of data points compared) and used as a metric of prediction accuracy instead. For the results section on widely spaced data points, equivalent calculations were made to quantify the prediction's deviation from linearity with a specified gap between two data points (nRSSi). Both of these metrics, unlike the r^2, do not unduly weight values near the mean.

5.3 RESULTS

Evaluation of published data reveals two major areas of opportunity where *in silico* predictions may be able to better inform the design and validation of degradable controlled release formulations. First, if data is collected infrequently enough to produce a jump in cumulative release, the duration and kinetics of release can be difficult to resolve and an *in silico* prediction can help interpolate between widely spaced data points. Second, release studies may also (for any number of reasons) be terminated prior to the completion of release, leaving subsequent kinetics undocumented and perhaps even leaving the impression that the partially documented profile is complete. In this case, *in silico* predictions can be used to extrapolate upon the existing

release data. Both of these areas of opportunity are illustrated in more detail with the following examples:

5.3.1 Interpolation of release data sets with widely spaced sample points

A number of data sets include intervals in sampling that result in low resolution of the release profile. This can occur for a number of reasons, including an expectation that release will follow a different pattern, unavailability of the researcher for empirical sampling, or concern that more closely spaced intervals would not allow for enough drug release to permit detection. However, when data sampling is too infrequent, important changes in the rate of drug delivery may be difficult to identify. This was the case when enfuvirtide release was measured from PLGA microparticles at 10 day intervals (Figure **18**A). The low sampling rate was selected to ensure detection of enfuvirtide, a therapeutic peptide, by the micro BCA (μBCA) protein assay, which had a detection limit of 980 ng/ml. The resulting gaps in data accounting for 33 and 44% of drug release leave open many interpratations (broken lines, Figure **18**A), which can be clarified by the model's prediction (solid lines, Figure **18**A). Subsequently, release from these microparticles was measured using high pressure liquid chromatography (HPLC) which has a detection limit below 39.1ng/ml for enfuvirtide, despite being less cost and time efficient. This detection method allowed enfuvirtide release to be measured every 1 to 2 days, filling in the gaps left by the prior study (Figure **18**B) in order to validate any conclusions made through model predictions. The resulting HPLC-detected release profile closely follows the profile predicted by the earlier mathematical analysis, providing strong evidence that the interpolation based on model predictions accurately describes the actual enfuvirtide release behavior.

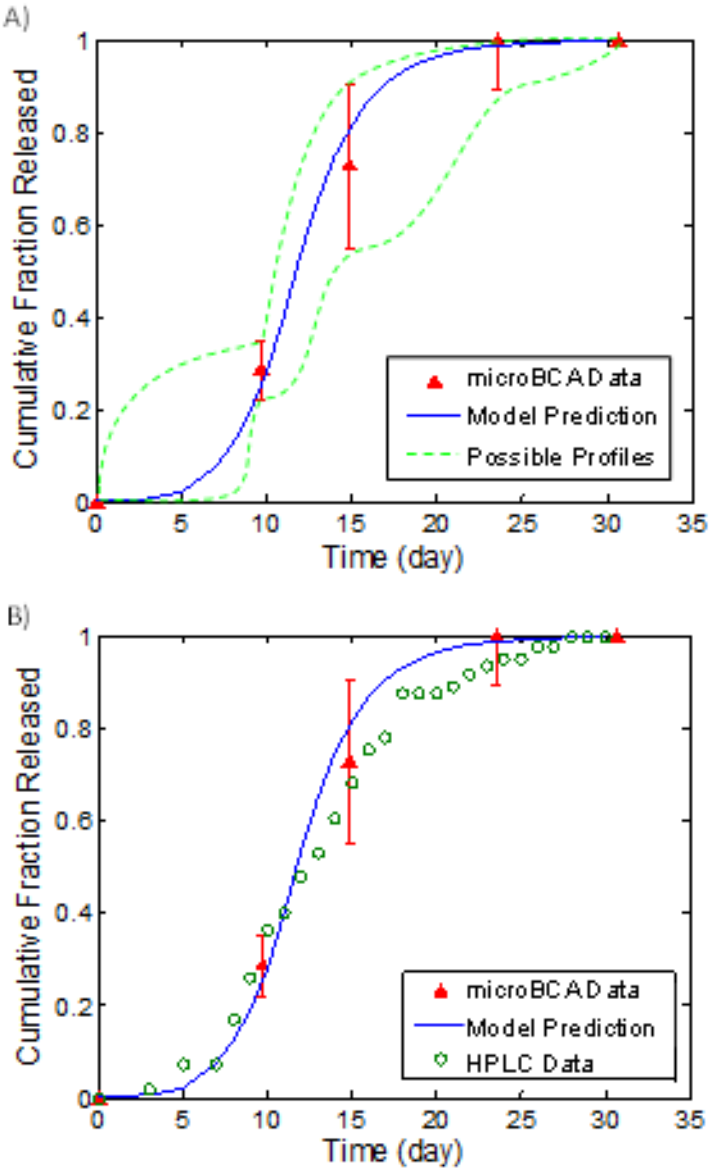

Figure 18: Testing model predictions for the interpolation of *in vitro* release data from enfuvirtide loaded 9kDa 50:50 PLGA, 20µm particles.

A) Initial release measurements using the µBCA assay with widely spaced intervals (triangles). Broken lines are provided to illustrate the range of possible alternate interpretations that could be made for the release profile based on the standard error. An interpolative prediction was made using the mathematical model which would suggest that actual release profile (solid line). B) Release measurements made by highly sensitive HPLC experiments at short intervals confirms the accuracy of the interpolative prediction (circles). (nRSS = 0.0030)

As with our data, the literature includes a number of release data with significant gaps between sample points. For instance, in one assay of lysozyme release, over 40% of the drug is delivered during a 28 day window where no data was collected (Figure **19**A)[43]. As a result, the timing of the transition from first burst to second burst is unclear and could follow any number of patterns within the range marked by green curves. In this specific case, mathematical analysis of this data suggests that release is predicted to continue in a sustained manner between data points without a more prominent burst of drug with possible upper and lower bounds at 30 (or alternatively) 50 days (Figure **19**B). Importantly, the variation between this prediction and ideal linearity (a point-to-point interpolation in the gap; nRSSi = 3.0E-4) is similar to what is calculated as the overall model deviation from all other experimental data points (nRSS = 3.8E-4). In another study, superoxide dismutase release was measured at 6 points over 60 days (Figure **20**A)[77]. Because these sample points were spaced unevenly, significant gaps occur from days 3 to 29 and days 38 to 50, accounting for 15% and 40% of release, respectively. This leaves the data open to a range of interpretations (indicated by green shading) including the possibility that release proceeds linearly over the 60 days (Figure **20**A, broken line). However, in this specific case, the model prediction suggests that release is not sustained for the duration of 60 days. In contrast, a lag-burst pattern is predicted through the first gap where little release is occurs between days 3 and 20, followed by rapid release from day 20 onward(Figure **20**B). During this window (days 3 to 29), the prediction's deviation from point-by-point linear interpolation ($nRSSi_1$ = 1.27E-2) far exceeds the error inherent in the model's prediction (nRSS = 4.7E-3; nRSSi1 > nRSS), suggesting that the predicted deviation from linearity in the gap is indeed statistically much greater than the collective deviation from other data points. In the second gap (days 38 to 50), the prediction's deviation from linearity ($nRSSi_2$ = 4.9E-3) is

actually comparable to the error inherent in the model's prediction ($nRSSi_2 \approx nRSS$), suggesting that no significant change in release rate is expected to occur during this gap.

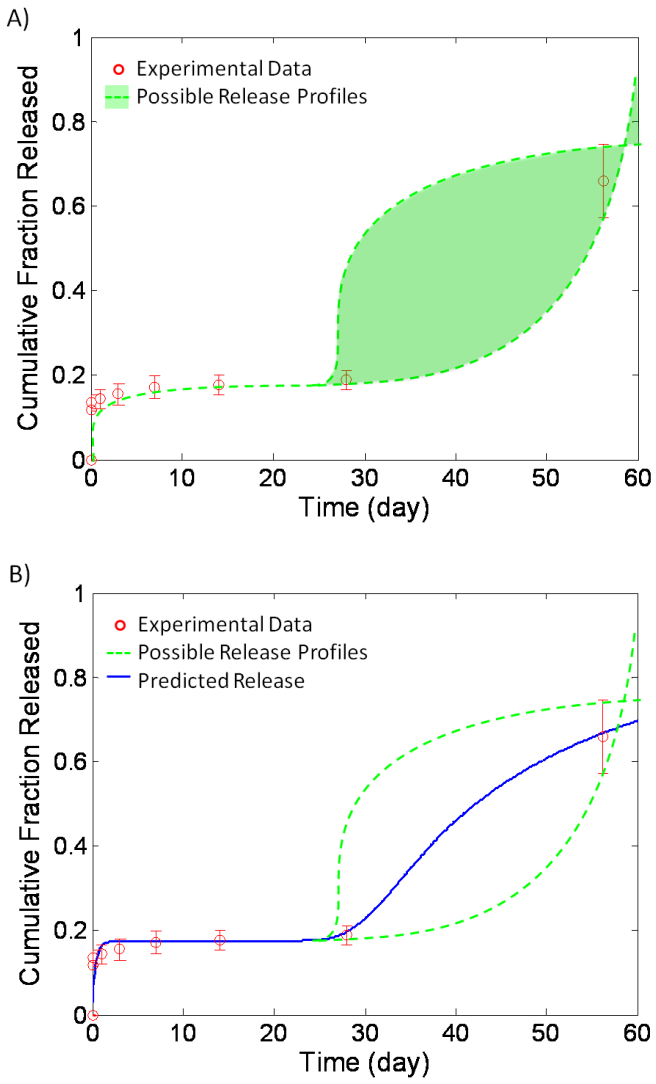

Figure 19: Evaluations of *in vitro* data for lysozyme encapsulated in 12kDa 50:50 PLGA[17].

A) *In vitro* release data points (*circles*) jump from 18% at day 28 to 66% by day 56, leaving a range of potential interpretations as to the formulation's release kinetics (*shaded area*). B) Mathematical results predict a specific a release profile for this formulation (*line*).

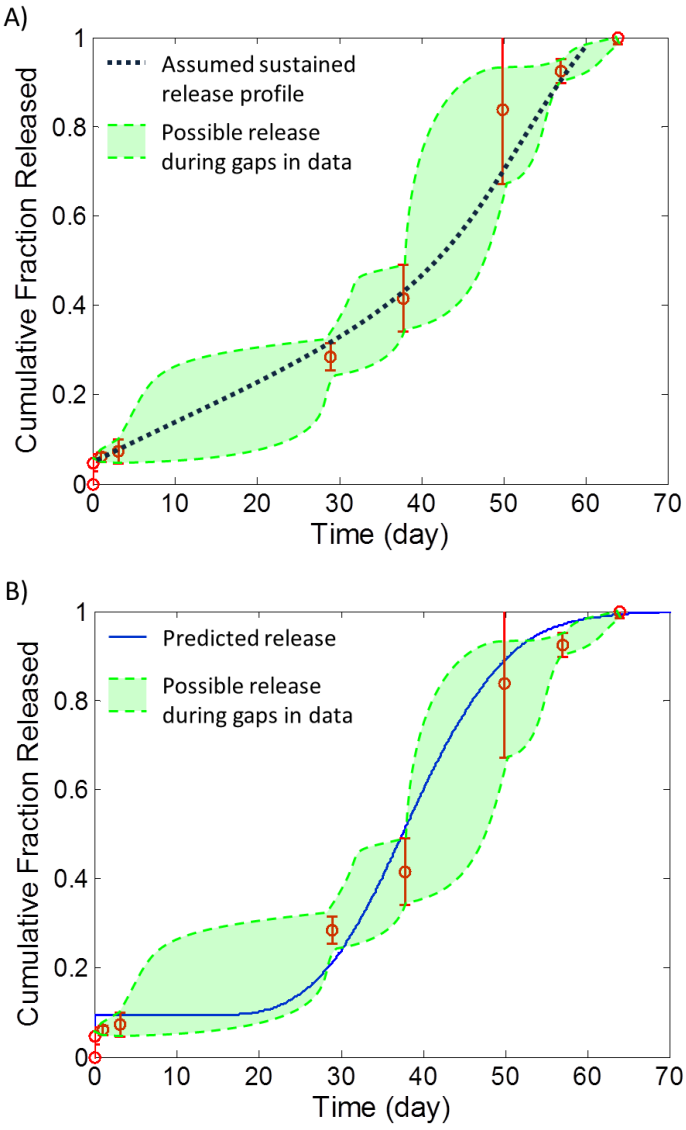

Figure 20: Evaluations of *in vitro* data for superoxide dismutase (SOD)

SOD was encapsulated in 40-70kDa 50:50 PLGA microparticles (14μm)[18]. A) Gaps in this data (*circles*) suggest that SOD release could proceed in a sustained, linear fashion (*dotted line*) following the initial burst. B) Mathematical results indicate a non-linear release profile for this formulation (*line*).

Significant gaps also appear in release data from PLGA microparticles loaded with model enzymes[43], hormone antagonists[70,132], and anti-inflammatory agents[133], among others[39,68] (release behavior not shown, but summary statistics are included in Table **2**). In some cases, retrospective analysis predicts that release will not deviate from a sustained or linear manner during the gap between data points[39,132,133] (Table **2**, nRSSi < nRSS or nRSSi ≈ nRSS)[70,133]. However, in other cases significant changes in release rate occur during gaps (Table 1, nRSSi > nRSS)[43,68,70].

Table 2: Interpolative Predictions

Encapsulated Agent	**R_p (μm)**	**R_{occ} (μm)**	**Mw_o (kDa)**	**kC_w (day^{-1})**	**Mw_A (Da)**	**Gap Size (Day, %)**		**Overall Error (nRSS)**	**Linear Error (nRSSi)**	**Ref**
Carbonic anhydrase	0.533	0.205	12	0.08636	68900	28	45	0.0020	0.0246	[17]
Leuprolide	20	1.8	10	0.08636	1210	7	43	0.0014	0.0021	[19a]
Octreotide	10.5	0.525	28	0.08636	1020	7	45	0.0025	0.0029	[19b]
Dexamethasone	5.5	2.86	70	0.08636	392	13	37	0.0061	0.0061	[20]
Gentamicin	276	69	36.2	0.08636	477	8	45	0.0012	0.0030	[21a]
Butorphanol	200	40	29.7	0.3278	327	1	44	0.0062	0.0035	[21b]

5.3.2 Extrapolation of release data sets that terminate prior to completion

Many sets of release data document only one burst when additional release would be expected[42,95,128]. This is not surprising given that the additional release, often in the form of a secondary burst, may only occur after weeks, months or years, while of the most functional assays or animal models using these formulations require just days or weeks to complete. Indeed, our studies on the novel anti-inflammatory agent, NO_2-OA, began with a single batch of particles and 1 week release assay to confirm that this novel agent could be encapsulated and delivered intact from microparticles (Figure 21A). Specifications for this formulation, including size, polymer molecular weight, and internal matrix morphology were measured, and used to initialize a model prediction that extrapolates beyond the range of the preliminary data (Figure 21B). In order to test the accuracy of this prediction, the preliminary formulation was reproduced and assayed in triplicate for the full predicted duration of its release profile, with a sampling frequency selected to capture key changes in the rate of release This second assay confirmed that the formulation's release profile closely follows the model prediction (Figure 21C). Notably, our initial release curve only captured less than 25% of the total release behavior, which was captured by the model prediction.

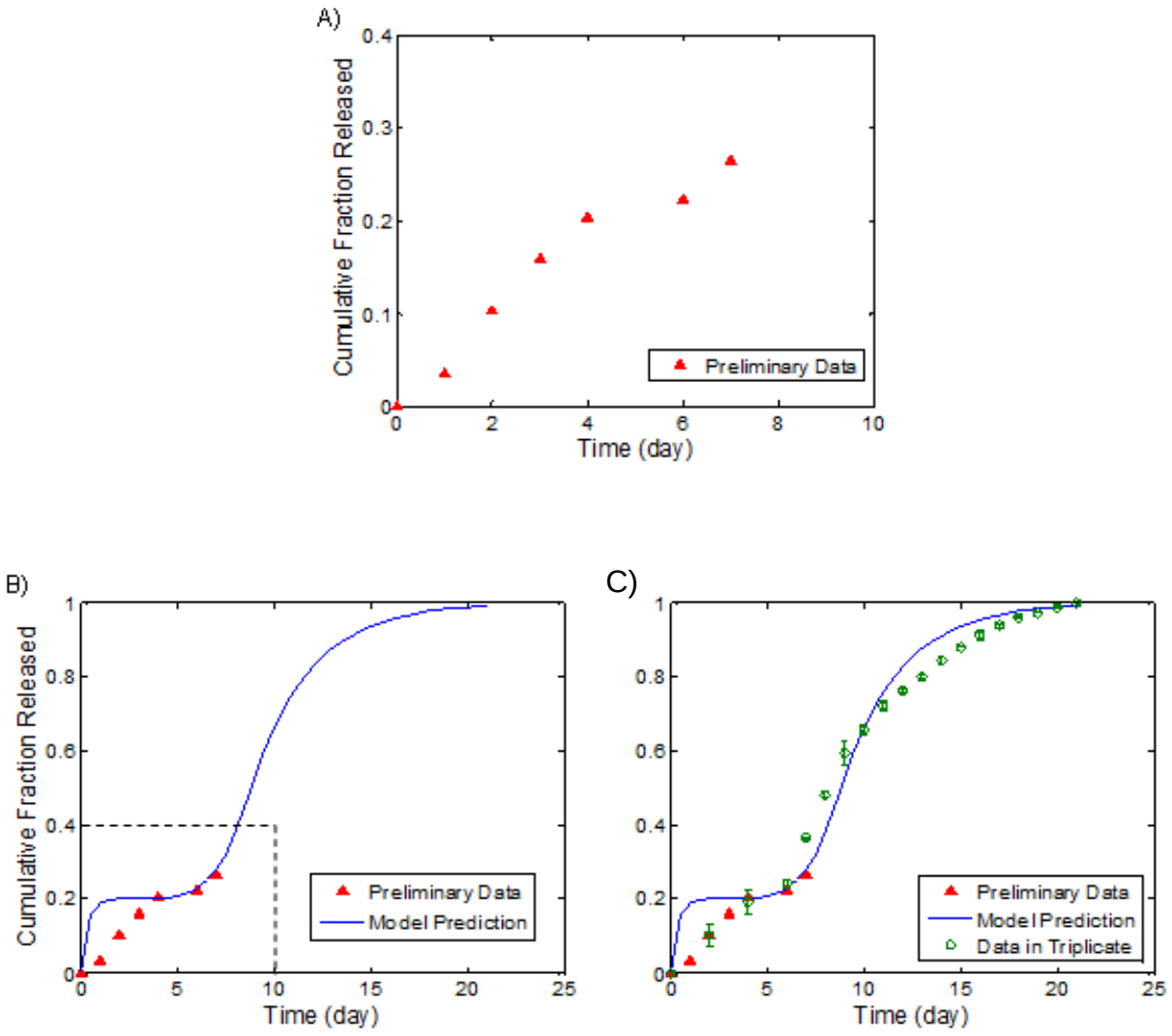

Figure 21*:* Testing an extrapolative prediction

A) Data from preliminary *in vitro* assay of NO_2-OA release from 9kDa 50:50 PLGA 20µm particles. B) Predicted release behavior for the same formulation. C) Release from formulations produced in triplicate closely followed the model prediction. (nSSR = 0.0020)

Like this prior example, the literature includes a number of examples where release assays are, for whatever reason, terminated prior to closure. Indeed, one set of PLA microparticles loaded with the protein superoxide dismutase (SOD) was assayed for 50 days without showing additional release beyond the initial burst. However, predictions indicate that SOD release will only reach completion in an additional 200 days (Figure 22)[77]. Importantly, this will result in

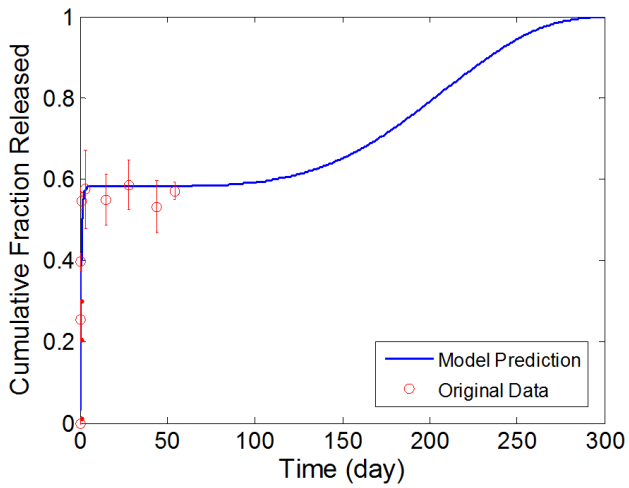

Figure 22: Extrapolated SOD release from 106kDa poly(lactide) microparticles.

In vitro data (circles) only documents 60% of release[18]. The 40% of encapsulated protein remaining is predicted to release between days 150 and 250.

release of 40% of the encapsulated drug following day 150 if this formulation were placed *in vivo* and not removed before this time. In another study, recombinant human Growth Hormone (rhGH) release was measured for 28 days, recording delivery of 78% of the anticipated payload[134]. Mathematical predictions show that release, which appears to asymptote, actually began a secondary burst on day 20 (Figure 23). This burst continues until day 40, whereas no additional information is provided past day 30 by the assay. Predictions were also evaluated for data sets from PLA and PLGA formulations loaded with many other proteins, peptides and small molecules[72,84,90,135-138] (Table 3). For a number of these systems, the release is predicted to continue for more than 2 months beyond the end of *in vitro* data collection[90,137,138].

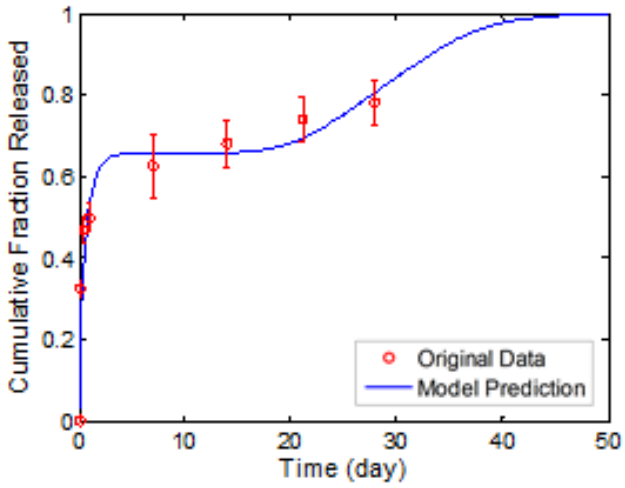

Figure 23: Release of rhGH from 45kDa 50:50 PLGA microparticles.

In vitro data (circles) was only collected for 28 days[22]. *In silico* predictions (line) shows a second burst of release starting at day 20 and continuing until day 45.

Table 3: Extrapolative Predictions

Agent	R_p (μm)	R_{occ} (μm)	Mw_o (kDa)	kC_w (day^{-1})	Mw_A (Da)	Assay End (Day, %)		End of Release (Day)	Error (nRSS)	Ref
VEGF	2.55	1.84	34	0.0864	21000	28	74	87	2.30E-04	[3a]
BSA	22.5	5.85	18.9	0.0864	66500	34	26	74	2.20E-04	[23a]
GM-CSF	25	1.23	40.4	0.0864	22000	7	5	91	2.66E-05	[23b]
VEGF	2.2	1.05	110	0.0634	21000	30	51	113	9.64E-05	[23c]
BSA	17.5	5.25	130	0.0864	66500	25	33	66	3.06E-04	[23d]
Levofloxacin	1180	802.4	80	0.0169	361	46	69	91	7.39E-05	[23e]
Paclitaxel	25	6.75	100	0.0169	854	30	27	340	1.70E-04	[23f]

5.4 DISCUSSION

Retrospective analysis of *in vitro* release is the use of modern technology and understanding of release phenomena towards the interpolation and exploration of prior studies to gain further information on a formulation's performance in the absence of additional experimental data. For instance, published release assays can terminate before drug release is complete or contain widely-spaced intervals of time between data points, complicating interpretation of a formulation's drug delivery kinetics. While such data may be suitable for planning initial functional assays that evaluate a formulation's activity, a more detailed understanding of a formulation's release kinetics would be useful when refining a formulation design or planning

animal studies, like those for long-term dosing or evaluating disease outcome. Further, when translating formulations to human use, a full understanding of how a biodegradable polymer matrix releases an encapsulated agent is extremely important. To most efficiently plan such studies or possibly even make the best decision as to whether or not the studies would be fruitful, prior information is needed on: a) how the expected rate of release varies between data points, and/or b) if or when additional release can be expected beyond the release assay's termination. One possibility to obtain this information would be to iteratively conduct a series of long-term release assays. However, mathematical analysis of existing release data may offer a tremendous time- and cost savings in obtaining this useful information.

In order to be useful for retrospective analysis, a mathematical model must effectively describe or predict a formulation's release kinetics, particularly in the regions where data are sparse or non-existent. The model used herein has an extensive record of validation that encompasses PLGA microparticles loaded with a wide variety of drugs (Section 3.3). Importantly for this study, the model has demonstrated consistent and accurate predictions of both the timing and rate of secondary burst release for small molecule-, peptide- and protein-loaded microparticulate systems. These predictive capabilities are essential for handling analysis of data sets that lack information about the second burst and therefore require extrapolation. Other models would be more suitable for retrospective analysis of the kinetics of the initial burst, poorly soluble agents, or matrix implants, hydrogels, and novel controlled release systems[42,96,139].

The model-aided analysis used herein can help determine if a formulation actually provides an acceptable rate of drug delivery when widely spaced data points leave uncertainly as to its release kinetics. One outcome of this analysis is the ability to use more cost-effective,

rapid detection techniques, which would otherwise be eliminated from consideration due to their poor sensitivity. For instance, in the evaluation of enfuvirtide release, mathematical predictions can confirm the utility of a microBCA assay in the detection of release over a more expensive and lengthier HPLC protocol (Figure **18**). Without supporting model predictions, the 10 day sampling interval necessitated by the microBCA assay's poor detection limit could result in missing key changes in release behavior, potentially leading researchers to misinterpret the formulation's variable release rate as "sustained" or "linear". This misinterpretation could be extremely costly especially since true, sustained or linear release is the most critical desirable aspect of many modern release formulations.

Indeed, the "linear release" design criterion applies to any formulation intending to produce constant serum concentration, encompassing well over 50% of the top 200 best-selling drugs on the market today[8]. For example, Figures 2 and 3 contain data sets with gaps of at least 20 days and more than 40% release that could be assumed to span intervals of sustained release. Indeed in the case of lysozyme release, mathematical predictions suggest that release is actually sustained from day 30 onward using the described formulation (Figure **19**). This predicted profile is consistent with those documented in other sets of release data from lysozyme-loaded PLGA microparticles of comparable chemistry and molecular weight[140,141]. In evaluating release of superoxide dismutase, however, predictions suggest that SOD release follows a burst-lag-burst pattern, instead of a constant, sustained one, which would have been desirable for an antioxidant (Figure **20**). Similar behaviors are reported for a number of other protein loaded PLGA microparticles[42]. Having the ability to evaluate protein release data as sustained or pulsatile, without frequent sampling, should become increasingly valuable as work on the controlled release of costly cytokines, chemokines, growth factors and other biomolecules continues to

expand[142-144]. In the absence of plots, statistical metrics comparing a linear interpolation to the model prediction, such as the normalized residual sum of squares (nRSSi), can indicate if changes in the rate of release are indeed occurring between data points. When assumed point-to-point interpolation differs significantly from a model prediction, but the data points do not, changes in the rate of release are occurring during between sampling points.

Mathematical analysis can also aid in the understanding of release kinetics when an experiment does not reach completion because it is (for whatever reason) terminated after just the initial burst phase of release. Recording only this initial release data is often useful when exploring formulations for an entirely new drug candidate or when planning preliminary studies with cell functional assays which last for just days or weeks. However, the presence or absence of delayed release of drug could be extremely important when refining a formulation design or planning extended animals studies. A case study is provided by a controlled release formulation of nitro-fatty acid, a novel anti-inflammatory lipid whose stability in the acidic microclimate of degrading PLGA microparticles remains unknown. Accordingly, a short, 2 week release assay, revealed both NO_2-OA's stability and its initial rate of release. However, this assay documented less than 30% of drug delivery. Clues to the duration of release can come from data on erosion, which are responsible for governing release in many hydrolysable polymer systems[42]. Similar polymer microparticles erode most significantly between days 8 and 30[6,41], defining a window when pore formation and erosion-mediated release may occur. Model predictions during this time period have the potential to provide further detail into the actual release behavior. For instance, model predictions suggest that this formulation exhibits release continuing in a sustained manner through day 28, which is an appropriate delivery schedule for the eventual

clinical application of this active agent. A subsequent release assay conducted in triplicate confirmed the accuracy of the model prediction, lending support for this type of analysis.

For formulations without sustained release profiles, extrapolative predictions can also aid in setting the dosing frequency for subsequent animal studies and the duration of sampling in future release assays. An example of how predictions can aid in setting dosing schedules is represented by the analysis illustrated in Figure 22. The *in vitro* release data from this formulation shows 60% of superoxide dismutase SOD being delivered over 8 days, implying that a once-weekly dosing schedule would seem logical based on the experimental data. Yet, mathematical predictions suggest a secondary burst of SOD is imminent at 30 days following the start of release. Based on this information alone, the results may warn a user that repetitive administration at 1 week intervals could lead to unexpected release of drug that is over 5 times the desired dosing of SOD beginning at day 60. Retrospective analysis suggests (alternatively) that adjusting the dosing interval to once every 8 weeks and repeating the release experiments could potentially minimize the simultaneous delivery of SOD from repeat administration while still producing the desired effect. An example of how predictions can aid in setting release assay duration is represented by the analysis in Figure 23. This *in vitro* data set could suggest that the rate of release slows from day 15 until the assay's close at day 30. In contrast, model predictions suggest that release may actually accelerate between days 20 and 30 instead of decelerating. This behavior would warrant collection of data until day 40 when closure is predicted, if it was necessary to experimentally determine this formulation's maximal rate or duration of release. These information-loss examples are representative of release assays conducted on a number of other protein and peptide formulations. This suggests that extrapolative mathematical prediction may prove extremely useful when developing

formulations for a wide variety of applications and in particular for the delivery biologics or poorly soluble molecules, which are noted for often having lengthy release profiles[126,128].

However, it is important to note some limitations of the current model for this type of analysis. For instance, the model equations (Section 3.2.2) do not provide a way to predict the rate (as opposed to the magnitude) of the initial burst, which is correspondingly over-predicted in 10 of 19 simulations herein. Existing mathematics[145,146] (or future work on the current model construct) describing dissolution limitations or electrostatic interactions with polymer matrix may serve to account for any systematic, over-predicted release in these cases. Cumulative release was also over-predicted during the last 10-20% of drug delivery in 6 out of the 10 simulations that include data is this region. This systemic deviation might be due to the model's approximation of pore formation as a cumulative normal distribution[128]. A comparison to experimental data reveals that this function begins to overestimate the rate of erosion (mass loss from the polymer matrix, responsible for pore formation) when just 20% of original mass remains[41]. A more physically accurate description of erosion, perhaps accounting for crystallinity among oligomers, might correct this systemic overestimation of final release[93].

Regardless, this retrospective analysis (producing *in silico* data for 20 real-world *in vitro* release assays) is, to our knowledge, the first instance of such use of mathematical modeling technology for biodegradable matricesThere are similarities to this kind of analysis to previous nascent methods to compute specific pharmacokinetic drug properties (e.g. bioavailability and clearance route) in the 1960s[127]. Since then, pharmacokinetic analysis has grown substantially both in the scope of its mathematics and impact of its results. PK modeling analysis now regularly makes predictions for the processes of adsorption, metabolism, distribution, and excretion (ADME). It is also now an essential component of the US regulatory approval

process[33]. Furthermore, PK modeling has most recently grown to encompass molecular simulations of drug-protein binding in order to predict ADME processes during drug discovery[147]. In contrast, the role of predictive and data modeling has significant room for expansion in controlled release formulation development. Indeed, since Higuchi first demonstrated the utility of mathematics for describing solubility limited drug release from a matrix system, models have been developed for a number of specific biodegradable polymer-based drug delivery systems[139,148]. In practice though, the systematic or statistical design of experiments (DoE) is still considered state of the art and is significantly faster than the trial-and-error approaches used in past decades[20]. Augmenting DoE with existing models of release would be a simple, inexpensive, and rapid way to achieve greater efficiency in the formulation development process. In the future, even further gains could be derived from harnessing molecular scale simulations, as done in drug discovery, to predict drug-polymer interactions thought to influence release[24]. We are currently exploring such methods to add power of prediction at some expense to the generalizability of the results produced.

5.5 CONCLUSION

Predictive modeling is of extreme potential value for the analysis of *in vitro* release data in much the same way that modeling is now considered an integral part PK studies. The *in vitro* and *in silico* data presented herein demonstrate predictive modeling as a key for interpreting *in vitro* release assays and planning subsequent studies, either *in vitro* or *in vivo*. By interpolating and extrapolating with predictions, the necessary duration of an assay can be determined, the timing

of sample points can be set and the suitability of different detection techniques can be evaluated. These benefits are not only of interest during formulation design, but also during the establishment of quality by design (QbD) manufacturing routines, when connections between a formulation's attributes and performance are established.

6.0 CASE STUDY: DELAYED RELEASE VACCINE PLATFORM

6.1 INTRODUCTION

Vaccines have arguably had the greatest impact on public health of any known medical intervention [149]. Successful inoculation with several doses of "dead" or disabled pathogen produces long-term immunity from highly virulent diseases, some of which have no cure once they reach the point of mature pathogenesis [11]. Unfortunately, citizens of many developing countries frequently do not receive the 2nd or 3rd vaccine doses needed to establish immunity. In fact, the World Health Organization (WHO) estimates that four to five million deaths could be prevented annually with complete vaccination [150] ("complete" in that patients receive all subsequent booster shots[11]). Over half of these deaths are children under age five [150]. These preventable deaths occur in spite of a long-standing global immunization program (GAVI) supported by a partnership between international organizations, national governments, industrial concerns and private donors [24]. A platform for delayed release vaccination could improve effectiveness by ideally allowing a single injection at birth to autonomously provide all requisite doses at the correct times. Because this at-birth approach would target individuals when they are most likely to be at a medical facility, it would provide savings not only from reduction in number of injections needed but also from reduced reduce administrative costs for record keeping and logistics.

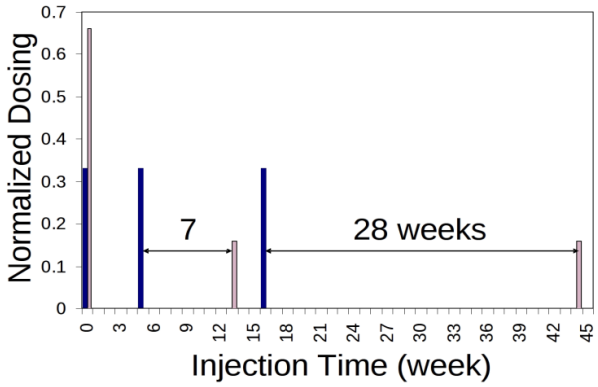

Figure 24: Comparison of dosing schedules

Control injections (dark) and heuristically designed DRV(light) from Men et al. The timing of the 2nd & 3rd doses from the best formulation dramatically differs from the optimal delivery times. Dose magnitudes assume an equal distribution of agent between all microspheres.

The design of a single shot vaccine has remained a challenge for over 25 years because of the complexities of how controlled release formulations provoke an immune response. Early studies revealed that simply prolonging antigen delivery did not promote immunity, but rather tolerance [151,152]. This promoted development of formulations that mimic the dosing of proven vaccines autonomously releasing multiple bursts of antigen over time [152]. Researchers have produced single injection vaccines that deliver multiple bursts of antigens such as tetanus toxin, diphtheria and hepatitis B. [11,153]. However difficulty arose in replicating the multi-dose administration schedules for these real-world antigens because of the trial-and-error methods used to tune the performance of the polymer carrier that controlled release [154]. As evidence, one of the most well thought out formulation design studies to date mimicked the immunization

schedule currently used for tetanus toxoid by combining particle sets that burst at different times. Out of 5 attempts, the timing of burst release from the best result was over 6 months later than suggested by the CDC immunization schedule (Figure 24)[155]. Such a delay not only altered the immune response, but also complicated implementation of the assays needed to measure it. Many more studies have used simpler controlled release formulations, examining antibody titres elicited from single polymer microparticles documented to provide burst-lag-burst profiles *in vitro*. However antibody titres are not a direct enough measurement of immune response to correlate *in vitro* release results to *in vivo* antigen release and in many cases such measurements were not extended much beyond the controlled release formulation's lifespan[11,153]. Interestingly, one of the few studies to extend titre measurements well beyond the duration of antigen delivery concluded that repeat administration 12 months after the original inoculation would be necessary to sustain protective immunity[156]. Fortunately, this research prompted further immunological exploration of microparticle vaccines by raising questions about the adjuvancy of microparticles and the impact of antigen stability.

To compensate for a lack of long term immunity researchers have enhanced immune response by making use of a microparticle's biomimetic adjuvant potential. Specifically, particles that resemble bacteria in size are taken up by dendritic cells and macrophages at the site of injection and then transported to the lymph nodes[52]. Injection of small (1-5μm) particles has been documented to produce strong immune responses to ovalbumin, diphtheria toxoid, tetanus toxoid,GP120 (HIV) and many other antigens[157]. (Particles larger than 5-10μm are not readily phagocytized and show much less potential as adjuvants[52].) The immediate adaptive immune response to a single injection of small particles was in most cases comparable to that of complete Freud's adjuvant or multiple does of protein-alum complex with strong type 1 and type 2

responses[11]. Studies have also documented that the elevation of antibody titres provoked by these vaccines extends beyond 1 year, although the role of isotype is not investigated. From this body of work, it is clear that single injection of antigen loaded microparticles can promote a very strong immune response, much stronger than can be achieved with conventional FDA approved adjuvants and antigens[11,158].

Extensive research has also focused on the stability of antigens delivered by microparticle vaccines with the view that it might be a major barrier to their clinical application. During microparticle production, storage and administration protein antigens are subject to conditions that can cause them to denature or aggregate. These conditions include high shear and organic solvents during production, lyophilization for storage, as well as elevated temperatures and acidic conditions following administration[11]. Accordingly studies have focused on methods of protecting protein antigens from these conditions. Success has been achieved with unique antigen-excipients combination such as tetanus toxoid paired with bovine serum albumin and trehalose or ovalbumin paired with polyethylene glycol, which have been correlated to higher antibody titres[159-161]. The possibility of encapsulating and releasing intentionally aggregated antigen, such as a protein-alum complex, has yet to be investigated.

When moving forward with proof-of-concept development of a new delayed release vaccine, the findings of prior research must be taken into account. First, if a "boost" is desired, microparticles must be able to hide at least some portion of antigen from the body until predetermined times. Proven immunization schedules encompass a number of dosing times between 0 and 18 months of life[154]. Second, the antigen delivered by the microparticles must be in a stable and intact form. Ensuring antigen stability will prevent alterations in the formulation's release kinetics due to unintended aggregation or binding with the polymer matrix

as well as loss of antigenicity due to degradation by poly(lactic-co-glycolic) acid oligomers[11]. Third, the microparticles must be sized larger than 10μm in diameter, but still be small enough to be injected with standard syringes. This will prevent uptake by antigen presenting cells, which not only alters the rate of antigen release, but also causes a prompt and potentially harmful adaptive immune response[158].

This chapters details the model-aided development and testing of delayed release vaccine microparticles. Polymer stock materials were selected for the microparticles based on simulations and successful production of DRV microparticles was confirmed by microscopy. The in vitro release behavior of DRVs was subsequently measured and compared to model predictions. *In vivo*, the DRVs were tested for the capacity to delay antigen release with the ovalbumin-specific type II T cell (OT-II) proliferation assay. The type of immune response generated by DRV microparticle depots was further measured with the lysis of SIINFEKL pulsed spleenocytes and analysis of serum IgG response by ELISA.

6.2 MATERIALS AND METHODS

6.2.1 Materials

Poly(lactic-co-glycolic)acid (PLGA) copolymers were purchased from Evonik Industries AG (Essen, Germany). Specific types were as follows: RG502 (9kDa), and RG504 (30kDa). Grade V ovalbumin was purchased from Sigma Aldrich (St. Louis, MO). Alhydrolgel (alum), solvents,

assay reagents, and other chemicals were purchased from Thermo Fisher Scientific (Waltham, MA).

6.2.2 Polymer Selection

In vitro release profiles were predicted for the stock 50:50 PLGA and 75:25 PLGA copolymers available with acylated chain ends from Evonik Industries. For these initial predictions, it was assumed that average occlusion size was significantly smaller than polymer size (*Rocc* << *Rp*). (Acylated chain ends minimize the fraction of surface-associated occlusions and minimal the initial burst[142].) These potential release profiles were then compared to target windows for delayed release: days 7-12, days 14-19, and days 28-33. Polymers with the least sum-squared error between their predicted release profiles and the targets windows for the DRV were selected for use in microparticle fabrication.

Table 4: Production Conditions

	Sonication		**Homogenization**	
	Power	*Time (s)*	*Rate (RPM)*	*Time (s)*
DRV	30%	30	1000	60
SRF	30%	10	3200	60

6.2.3 Formulation Production

Ovalbumin was adsorbed to alum, as done previously [162]. Under sterile conditions, 10mg of OVA dissolved in 4.5ml of 0.01DPBS and mixed with 1ml of alum for 30 minutes. OVA-alum was then collected by centrifugation at 10,000 RCF for 1 minute. The concentration of OVA in the aspirated supernatant was measured by microBCA assay and used to calculate the loading of the OVA-alum.

Microparticles were prepared by the double emulsion process detailed in Section 5.2.2. Dichloromethane and the dissolved polymer were added directly to the OVA-alum. To help ensure encapsulation of the OVA-alum, the volume and mass of the polymer/DCM phase was doubled. Dispersion of the high viscosity OVA-alum required a sonication time of 30s at 30% amplitude instead of 10s at 20% required a more homogeneous primary emulsion. Homogenization speed was also decreased to 1000 RPM to increase particles size, which was thought to reduce phagocytosis and the initial burst release of OVA-alum. After preparation microparticles were washed for an additional 48 hours to further reduce the burst release of OVA-alum and stored at -80^{o}C until use.

6.2.4 Formulation Characterization

Microparticles were sized using the volume impedance method with a minimum of 10,000 measurements on a Beckman Coulter Counter (Multisizer 3). Microparticle surface morphology and shape were examined using a scanning electron microscope (JEOL JSM-6330F).

Formulations doped with OVA-Texas Red were examined with confocal microscopy to determine the occlusion size and distribution of active agent within the particles. The loading of antigen was measured by dissolving 5mg of microparticles in 250 ul dimethylsulfoxide (DMSO). Antigen was then extracted with the addition of 1 ml of 0.05M NaOH / 5% sodium dodecyl sulfate (SDS) and its concentration was measured using the microBCA assay.

6.2.5 *In vitro* Release Assay

Release data was measured accumulatively, as done previously13. Briefly, a known amount of microparticles was suspended in 500ul of phosphate buffered saline (DPBS, pH 7.4, GIBCO, Invitrogen) and placed on an end-to-end rotator at 37^{o}C. At regular intervals the microparticle suspensions were centrifuged, allowing the supernatant to be collected and particles to be resuspended in an equal volume of DPBS. OVA concentration in the supernatant was measured on a Spectramax M5 microplate spectrophotometer (Molecular Devices) using the microBCA assay as detailed in the manufacturer's protocol (Pierce, Thermo Fischer).

6.2.6 Mice

Female C57BL/6 and B6.SJL-PtprcaPepcb/BoyJ (CD45.1+) mice were used at 6–12 weeks of age (Jackson Laboratory, Bar Harbor, ME) for immunization. OVA-specific type 2 T cells were harvested from C57BL/6 mice for the proliferation study. Spleenocytes for the CTL lysis study were harvested from C57BL/6 mice. All animals were maintained under standard animal house conditions in accordance with Department of Laboratory Animal Research.

6.2.6.1 Immunization protocols

*For the OVA-specific CTL lysis and OT-II proliferation assays***:** CD45.2 mice were injected in the footpads with 2 week delay microparticles containing 20µg of OVA at 4 or 22 days prior to the harvest of OT-II cells and spleenocytes. Positive control mice were injected with OVA-alum 4 days prior to harvest of OT-II cells and spleenocytes.

For IgG titre assays: C57BL/6 mice were injected intradermally with a 1:1 mixture of 2 and 4 week delay microparticles containing a total of 40µg/300ul OVA-alum (50µl/footpad and 200µl/abdomen). As a positive control naïve B6 mice were inoculated with 20µg/150ul OVA-alum (25µl/footpad and 100µl/abdomen) at days 14 and 28.

6.2.6.2 OT-II Proliferation Assay

CD4 T cells were harvested from the lymph nodes (LN) of OTII mice and were purified using anti-CD4 MACS microbeads (Miltenyi Biotec Ltd., Bisley, U.K.). Five x 10^6 T cells were labeled with 5 µM CFSE for 8 minutes then washed immediately 20ml HBSS (serum-free) 3 times and resuspended 2.5 x 10^7 for injection (i.v., s.c., and footpad) into recipients. Popliteal and inguinal lymph nodes harvested 96 hours after transfer and dispersed into cells through a cell strainer. Harvested cells were labeled with Anti-CD45.1-PE (A20) and CD4-PerCP-Cy5.5 (RM4-5) and analyzed for reduction CFSE concentration in CD4+ and CD45.1+ cells by flow cytometry on a BD LSRII with CellQuest software (BD Biosciences). Final analysis and graphical output were performed using FlowJo software (Treestar, Costa Mesa, CA).

6.2.6.3 Measurement of ova-specific CTL lysis

Spleens were collected from naïve B6 mice and cells were collected in sterile PBS through a cell strainer. Spleenocytes were isolated with red blood cell lysis buffer and washed 3x with PBS. Naive syngeneic spleenocytes were resuspended in RPMI and split into two equal populations. One set was pulsed with 100 µg/ml SIINFEKL for 1 hour at 37^{o}C and labeled with 5µM Horizon V450 ($V450_{hi}$). The other set was incubated for 1 hour without SIINFEKL and labeled with either 0.5µM V450 ($v450_{lo}$) (Molecular Probes, Eugene, OR, USA). Labeled and pulsed cells were subsequently mixed at a 1:1 ratio and approximately 10^7 cells were injected intravenously into immunized mice. After 12h, mice were killed and spleenocytes were collected as done in Section 6.2.6.2. Spleenocytes were then fixed and analyzed for the disappearance of V450 by flow cytometry on a BD LSRII with CellQuest software (BD Biosciences). The percentage of OVA-specific lysis was calculated as follows: % specific lysis = (1 - ((ratio of $V450_{lo}/V450_{hi}$ in naive mice)/(ratio of $V450_{lo}/V450_{hi}$ in immunized mice))) x 100.

6.2.6.4 Titre measurement of IgG1a and IgG2c

Two weeks after the completion of vaccination, serum concentrations of ova specific immunoglobulin was measured by ELISA as done previously[163]. Blood was collected from each mouse by cardiac puncture and centrifuged to isolate serum. For the ELISA, OVA coated plates were washed (1:2200 tween), blocked with 10% FBS (1hr) and washed again prior to a 2hr incubation with serum samples. Plates were washed and secondary antibodies for IgG1 and IgG2c (1:20,000 dilutions, 10% FBS) were added for a 1hr incubation. Plates were washed and incubated with avidin-horseradish peroxidase conjugate (HRP, 1:1000 in 10% FBS) for 45min. Plates were washed and then developed with alternate exposure to TMB and 0.01M sulfuric acid.

Titres were determined by calculating the dilution required to achieve a cut-off o.d. reading of 0.2, and were expressed as the reciprocal of that dilution.

6.3 RESULTS

Literature includes a wealth of articles documenting the development of microparticle vaccines via experimental methods[11,152,155,161,164-173]. These articles often include tables listing varied manufacturing parameters or material properties and figures documenting each variant's *in vitro* release behavior. In this chapter formulation development began with *in silico* predictions to calculate which materials would be best for production of the required delayed release formulations. Each DRV was then produced and tested *in vitro* for its release profile. *In vivo* studies were then performed to determine how the immune response compared to controls including manual administration of unencapsulated antigen and adjuvant at specified times.

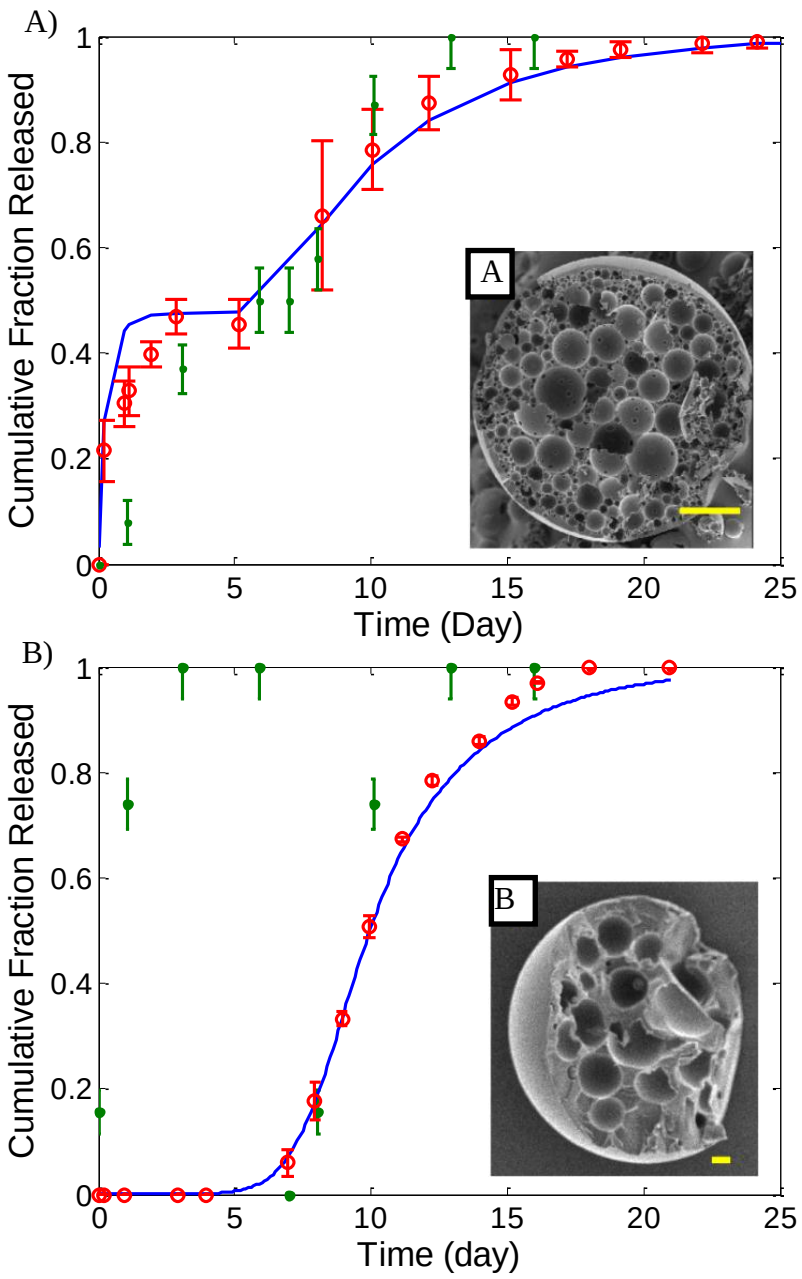

Figure 25: *In vitro* release of OVA from delayed release microparticles measured by spectraphotometry.

Model predictions appear as blue lines, dissolution of OVA-alum is shown with green dots and release from microparticles is shown with red circles. Microparticles of A) RG502H displayed a significantly burst B) RG502. SEM inserts show internal morphology of each microparticle set.

6.3.1 Formulation Designs and *In vitro* Release

Simulations were performed to determine the best materials for the DRV applications. Computations were initialized based on the rate of OVA dissolution from OVA-alum and a delay of 1, 2, or 4 weeks. Calculations identified 50:50 PLGA copolymers with molecular weights of 12kDa, 21kDa, and 53kDa as the most suitable materials production of the DRVs. Acylated and acid end capped versions of the 12kDa polymers both tested for their effect on release (Figure 25). Results were also compared both to dissolution data from OVA-alum and model predictions. Because the acylated polymer yielded a lower initial burst than the acid end capped, this type chemistry was used for the 21kDa and 53kDa polymers as well. In vitro release assays confirmed that formulations produced from these model-identified materials yielded release profiles in line with both model predictions (Figure 26).

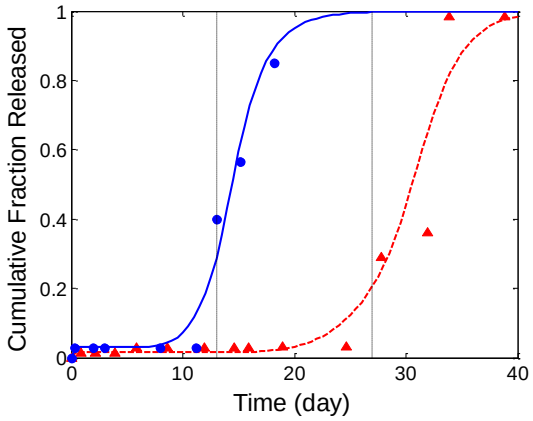

Figure 26: Microparticle formulations tailored for 2 and 4 week lag phases.

Vertical dotted lines indicate the start of weeks 2 and 4. *In vitro* release data appears as points and corresponding *in silico* predictions appear as lines. The loading 2 week (*blue*) and 4 week (*red*) formulations were measured at 19.2µg/mg and 26.0µg/mg, respectively.

6.3.2 Formulations Properties

The DRV microparticles were produced by double emulsion and analyzed by SEM. Microparticles lyophilized immediately following fabrication were found to have a rough surface morphology that became significantly smoother following the 48hours of washing used to remove the initial burst (Figure 27). Confocal microscopy across microparticles' widest plane of focus shows that the majority of OVA-alum is encapsulated within the DRV in discrete occlusions (Figure 28). This internal distribution of antigen is similar to the pattern discrete occlusions surrounded by dense a polymer matrix imaged via SEM (Figure 25B, insert). Sizing by the volume impedance method yielded volume-averaged diameters of 25.4±7.8µm and 19.2±7.4 for DRV and SRF particles respectively (Figure 29). This ensures that 99.6% of the DRV particles are greater than 5µm in diameter.

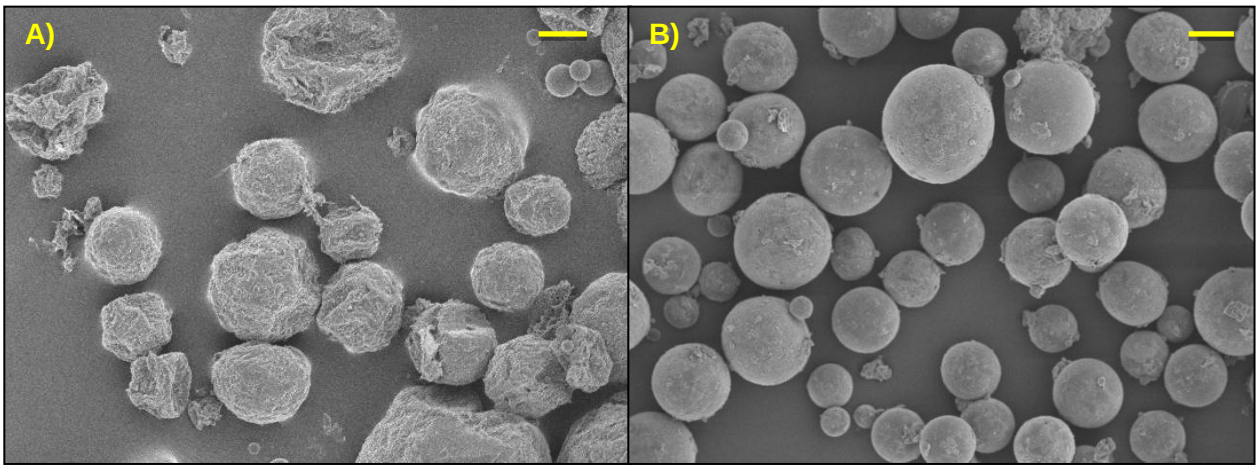

Figure 27: Comparison of OVA-alum microparticles A) pre- and B) post- wash.

A) Post fabrication lyophilized microparticles display a rough morphology. B) After washing in PBS for 48 hours, microparticle morphology becomes significantly smoother. Scale bars are 10μm.

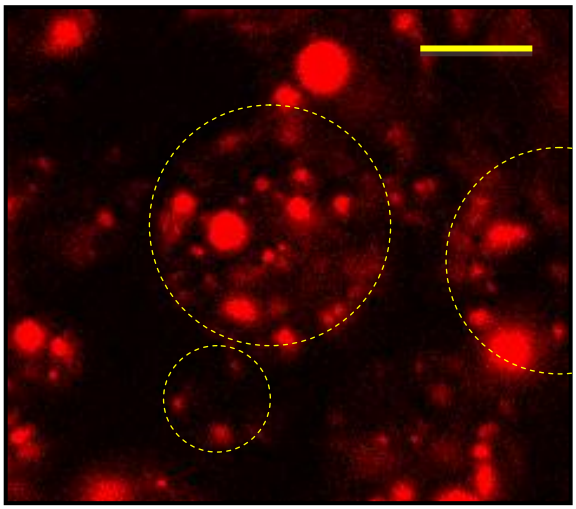

Figure 28: Confocal microscopy analysis of 4 week DRV formulation.

Doping of particles with OVA-alexa fluor 647 conjugate shows antigen grouped in well-defined occlusions and scattered on the particle surface. Select microparticles in the plane of focus have been ringed with dashed yellow lines under higher contrast to highlight their boundaries. Scale bar is 10μm.

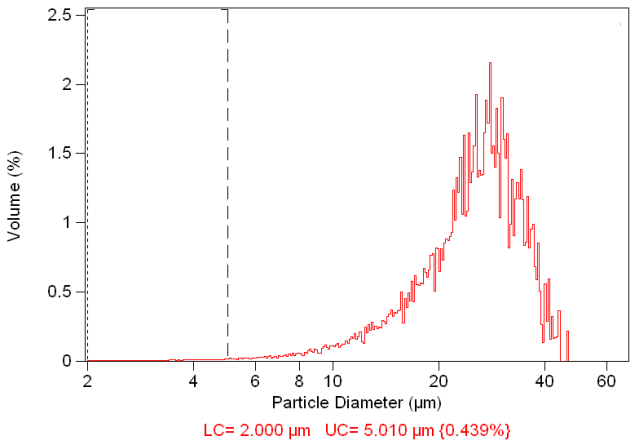

Figure 29: **Sample sizing result from DRV particles.**

Almost all of the antigen (99.5%) is found in particles that are too large to phagocytose (> 5um diameter).

6.3.3 *In vivo* testing of the DRV

The alum adjuvant used in the DRV formulation is noted for promoting an Th2 immune response, but phagocytized microparticles are noted for promoting a strong CTL immune response. Assays of both Th2 and CTL responses to antigen presentation throughout the duration of antigen release will be needed to assess how model-designed microparticles perform *in vivo*. An attempt was also made to isolate and evaluate dendritic cells for the uptake of fluorescently labeled OVA. However, this cell population proved too scarce to provide a sensitive measure of antigen presentation. (Data not shown)

6.3.3.1 OT-II proliferation

The day 4 and 22 sample points used in the OT-II proliferation assay capture both periods of lag and periods of active antigen release from the DRV microparticles shown in Figure 26. The OT-II response to the DRV microparticles at day 4 was significantly lower than the positive OVA-alum control or microparticles, post-burst at day 18 ($p<0.001$). OT-II proliferation at the later time points rivaled the maximal response to an equal injection of OVA-alum, reported to occur four to six days post immunization (Figure 30).

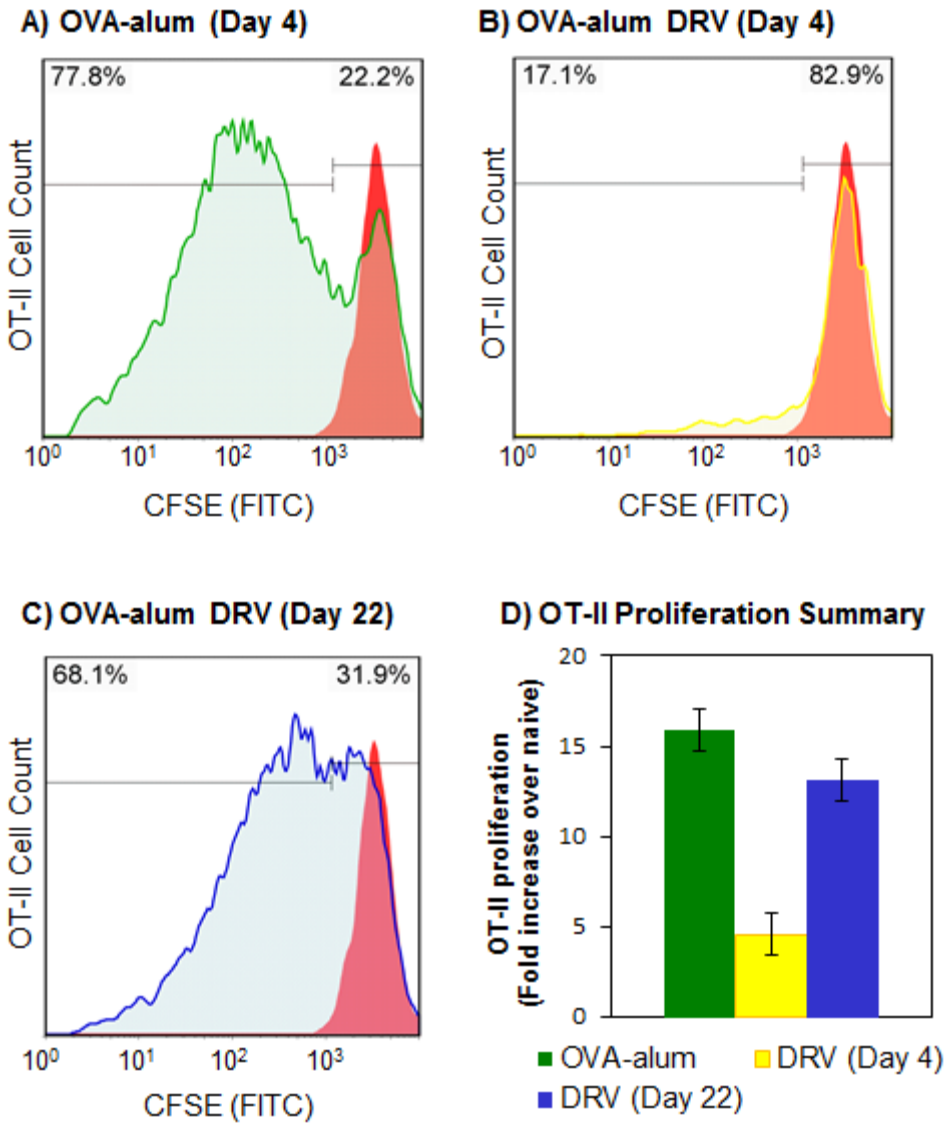

Figure 30: Comparison of OT-II cell proliferation from DRV microparticles and control vaccines

Proliferation of OT-II cells was charted by reduction in CFSE concentration and gates were drawn based on naïve mice. Typical OT-II proliferation results for A) OVA-alum 4 days post injection, B) DRV microparticles 4 days post injection and C) DRV microparticles 22 days post injection appear as *shaded lines*. In each histogram (A, B, C) proliferation results for a characteristic naïve mouse appear as a *solid red peak*. B) Fold increase in proliferation results from the DRV microparticles at day 22 and OVA-alum group are significantly higher the DRV microparticle at day 4 ($p < 10^{-5}$, n=3).

6.3.3.2 OVA-specific CTL lysis

Protein alum vaccines are not typically associated with strong cellular immunity. However, microparticle phagocytosis can generate a prompt CTL response. Two injections of OVA-alum (days 0 & 7) only reduced SIINFEKL-pulsed spleenocyte populations by as much as 18.4±3.1%. An equivalent two dose ovalbumin microparticle vaccine (one injection, Figure 25A) produced comparably low killing of pulsed spleenocytes (max = 20.6±5.4, Figure 31). In contrast, this CTL activity assay produce killing of more than 90% for a single dose gene-gun vaccine.

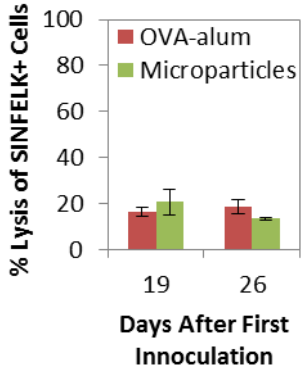

Figure 31: OVA-specific CTL lysis

The two injection ova-alum vaccine and two dose microparticles generate CTL responses at 19 and 26 days post inoculation that are not statistically different at $p < 0.15$.

6.3.3.3 IgG1 and IgG2c titre

Antibody titres are not as immediate (or sensitive) a measurement of immune response as CTL lysis or OT-II proliferation. However, they do offer a means of determining if the overall isotype of a delayed release vaccine differs from that of a matching OVA-alum vaccine. This chapter compared IgG responses from an ova alum vaccine with doses at day 0 and day 14 (positive control) to a DRV that release OVA-alum at two and four weeks post injection (Figure 26). For both vaccines IgG1 titres were 3-5 times higher than the IgG2c titres (Figure 32). Also the titres generated by the OVA-alum and delayed release vaccines are indistinguishable at alphas up to 0.5 or higher. ELISA titres measured 8 weeks after inoculation were negligible in all groups (data not shown).

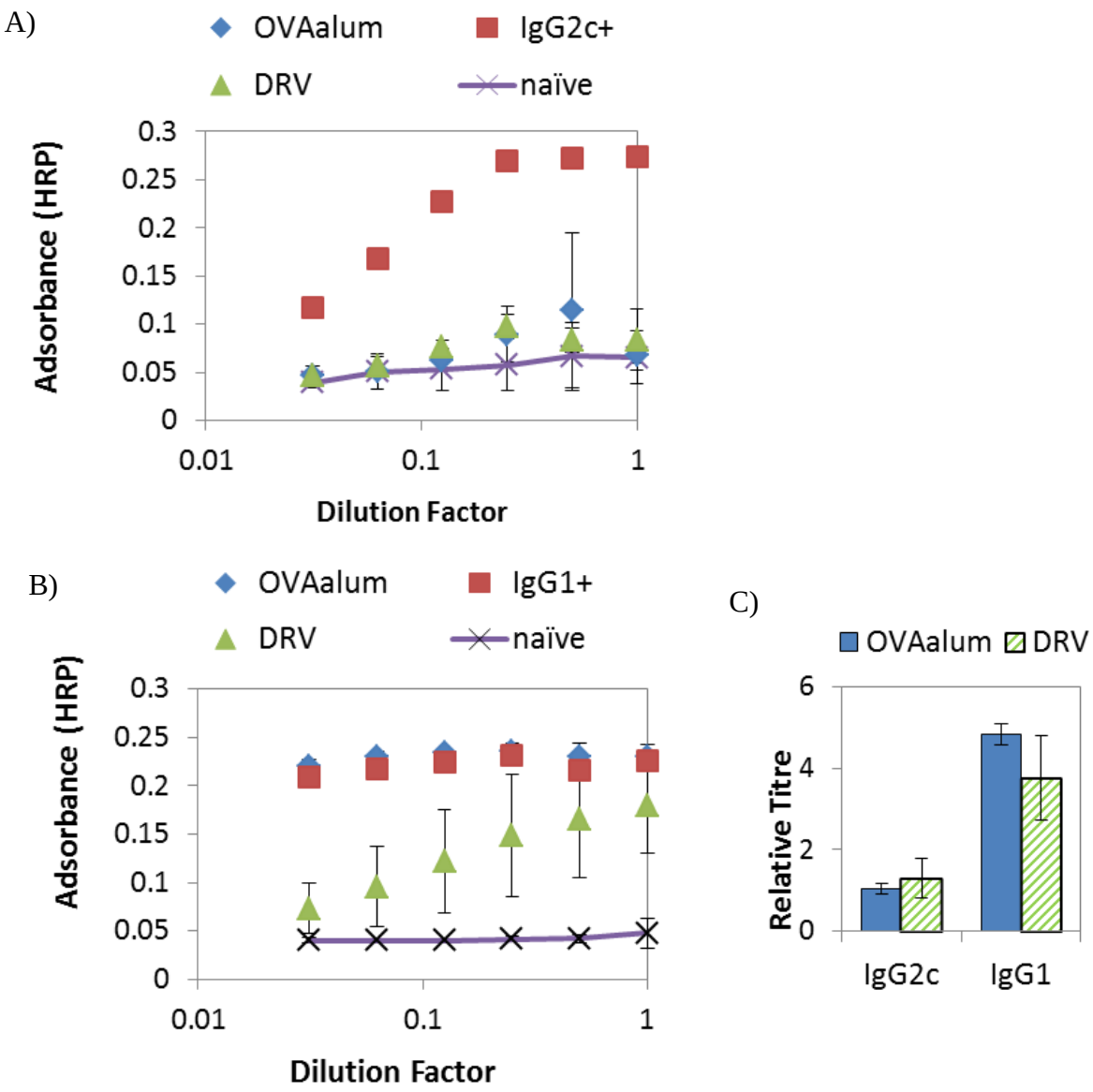

Figure 32: **Titres of OVA-specific IgG2c and IgG1 antibodies.**

Serial dilutions of serum samples were performed to ensure detection of A) IgG2c and B) IgG1. Serum from mice immunized with OVA adsorbed to 1-5µm iron beads (IgG+) was used as an internal control to confirm successful completion of the assay. Based on the dilution data, the 1x groups were selected for further evaluation. C) OVA-alum and DRV produced comparable fold increase in antibody titres over naïve. As expected for alum adjuvant, IgG1 titres were significantly higher than IgG2c for both groups. ($p < 0.006$)

6.3.4 Results Summary

Microparticles engineered for delayed antigen delivery displayed in vitro release profiles that match model predictions. *In vivo* these particles elicit a strong OT-II response following antigen release, but not before it. Antibody titres and CTL lysis results also show that the microparticles do not skew the response to the OVA alum antigen. These results are comparable to unencapsulated OVA-alum, which generates immunity where the humoral (type 2) response is characteristically stronger than the cellular (type 1) response.

6.4 DISCUSSION

Testing of the delayed release vaccine (DRV) platform from this chapter demonstrates that antigen can be masked from the adaptive immune system by microparticle carriers and then revealed at set times to provoke a specific immune response. Generating this proof-of-concept data required new microparticles designed specifically to suppress the initial burst and provide a set lag or delay prior to antigen release. These particles delivered ovalbumin antigen co-encapsulated with alum, a common vaccine adjuvant known to promote a strong type II immune response. Because microparticles can prompt a type I response, this DRV design allowed changes in vaccine adjuvancy to be documented clearly though T cell activity studies and antibody titres. These studies add new information on how formulations can be custom-designed to tune the timing of vaccine delivery without changing the type of the immune response.

All four DRV formulations (burst-lag-burst in Figure 24A, 1 week delay in Figure 24B, 2 week delay in Figure 25, and 4 week delay in Figure 25) designed in this chapter produced *in vitro* release profiles conforming to model predictions, a prerequisite for animal studies. Early work on microparticle vaccines produced designs with burst-lag-bursts or continuous release profiles, but yielded no clear metric for controlling *in vitro* antigen release and the need for delivery systems whose release kinetics can be precisely tuned continues to be cited today[157,174]. When evaluated for specifically timed, delayed antigen release, the 30 year body of literature on controlled release vaccines includes numerous examples where the timing antigen release has been altered or the initial antigen release suppressed, but none where both features are found together[157,169,174]. As evidence, researchers developing depot formulations with timed bursts of antigen release typically tested 7 designs in order to discover the one or two where the duration of release was suitable for animal study[155,156,164,170,172,175]. Similarly, in one of the few studies to demonstrate delayed release (less than 7% initial burst) the five different designs tested all released Hepatitis B antigen between days 40 and 50[161]. More recent work has shifted from the design of specific antigen release profiles and towards the enhancement of vaccine adjuvancy with microparticles that are designed to be taken up by the antigen presenting cells (APCs)[174,176-182]. In the low pH environments of APCs lysozomal compartments microparticles rapidly degrade instead of producing burst-lag-burst or delayed release profiles[38,52]. In contrast, larger microparticles (>5μm diameter), like the DRV formulations tested in this chapter, establish depots once injected and can be engineered deliver multiple, delayed antigen doses, autonomously replicating the administration schedules for vaccines such as DPT, Hep. B, Rotavirus, Hib, and inactivated Polio. However, the success of this depot-based immunization

strategy depends, not only the microparticle vaccine's release profile, but also its ability to deliver antigen and adjuvant intact.

Many reviews on microparticle vaccines cite antigen stability as a major hurdle to establishing protective immunity with a single injection and the strategies adopted for increasing antigen stability are diverse[11,152,157,174]. Researcher have co-encapsulated sugars, synthesized novel materials, and even produced formulations with surface-bound, instead of encapsulated, antigens[11]. These approaches, however, are not easy to integrate into a delayed release vaccine. Both novel materials, such as polyethylene glycol copolymers, and surface adsorption strategies, would alter the antigen's release profile from the desired lag-burst pattern[183,184]. Similarly small molecule excipients, like mannitol, release from formulations much more rapidly than proteins and show correspondingly less protection at late points in time, specifically when a DRV delivers antigen[77,185,186]. Instead of taking one of these approaches, the strategy adopted for stabilizing antigen in this chapter comes from a non-vaccine protein controlled release formulation. Nutropin® Depot, the only protein-loaded PLGA microparticles ever to achieve FDA approval, stabilized human growth hormone in complexes with zinc salts[74,187,188]. This payload bears resemblance to protein-alum complexes found in diphtheria, tetanus toxoid and other vaccines[149]. Accordingly the present work microencapsulated OVA-alum using a double emulsions process similar to the one used in the production of Nutropin® Depot and demonstrated immunogenicity.

An immunologically successful DRV design was defined as one that would match the strong type II immune responses generated by OVA-alum, without also generating the measureable type I cell mediated immune attributed to the phagocytosis of microparticles[11,189,190]. In the present work, OVA-specific Th2 proliferation and IgG1 ELISA

assays detect measureable type II immune responses from the DRV microparticles following antigen release. Prior use of the OT-II proliferation assay on OVA-alum vaccines has generated comparable proliferation responses to the unencapsulated OVA-alum positive control used in this chapter[189]. Other microparticle vaccines have also been tested with the OT-II cell proliferation assays, but these formulations were not designed to mask antigen as done in the present Chapter[168,181]. Instead, this prior work documents a strong immediate response to < 5μm microparticles that act as adjuvants by passively targeting antigen presenting cells[168,181]. These adjuvant-sized particles have also been documented generate a strong type 1 immune response through the lysis of SIINFEKL-pulsed spleenocytes and levels IgG2c titres, the two metrics used in this Chapter[11]. Because no Type-I response was anticipated from OVA-alum, or indeed detected, gene gun and OVA adsorbed to iron beads were used as also positive controls in addition to OVA-alum. Results from these controls are consistent with well-functioning CTL-lysis and ELISA assays of other gene gun and particle vaccines[190,191]. These studies of type I response, along with the positive OT-II and IgG1 results confirm that the DRV formulations tested do not alter alum's intrinsically Type 2 adjuvancy.

While the ability to autonomously deliver antigen is essential, the issue of payload size must be considered as well if moving forward with the development of the delayed release vaccine platform. In the OVA mouse model, doses of at least 10μg OVA (with alum)/50μl/hind-footpad are required to generate significant T cell proliferation, which is among the most sensitive metrics immune responses[189]. This dosing level of approaches the upper concentration limit for the delivery of microparticles via a 25G needle (25mg of particles per mL). Doses more than 7 times higher than this level are used in assays that test protective immunity[190]. Clinical vaccines offer more leeway with doses as low as 10μg of antigen per ml for the

Hepatitis B vaccine, but significant improvements to loading or administration are still required for further testing in the OVA mouse model. This may be achieved with a different microencapsulation process where a core of lyophilized antigen-adjuvant is coated with biodegradable polymer[192].

6.5 CONCLUSIONS

The aim of the chapter was to design PLGA microspheres that would mask the injection of antigen for a specific period of time without otherwise skewing the immune response. Insights from the mathematical model developed in Chapter 3.0 guided the selection of polymers that would delay release of antigen release for 1, 2 or 4 weeks. Testing of these DRV microparticles in the OVA mouse model strongly suggests that microparticles do indeed hide antigen. Results also show that the depot-sized microparticles do not skew the type II response provoked by the alum adjuvant towards a type I response, which would be indicative of microparticle phagocytosis. This DRV platform, if successful in disease relevant animal models, may provide a template for autonomously delivering common vaccines through a single injection at birth.

7.0 CASE STUDY: A SUSTAINED RELEASE FORMULATION

7.1 INTRODUCTION

Developing a platform that sustains a constant rate of drug release over weeks or months without a permanent implants has continued to challenge controlled release engineers since the early 1980s[193]. Successes achieved thus far typically involve large synthetic drugs with wide therapeutic windows[194]. The one exception, Nutropin® Depot, had its FDA approval withdrawn in 2004 for financial reasons. A study of the literature on macromolecule formulations reveals that peptide and protein release from PLGA microparticles typically begins with a significant initial burst (>20%) and often includes a lag before any subsequent release [5,6,30,43,68,70,72,73,80,100,104,108,109,195]. Methods of altering this naturally triphasic release profile abound (as reviewed in Chapter 2.0), but all still require extensive experimental work to initialize mathematical models or otherwise precisely tune release.

Beyond PLGAs a number of other biodegradable and bioresobable polymers have been developed specifically for controlled release. A case example is polyanhydrides, which were designed to degrade much faster than their polyester counterparts. The rapid degradation of polyanhydrides was postulated to cause erosion preferentially from the surface inward, thereby releasing drug at a much more constant rate than bulk eroding PLGA microparticles[53,196,197]. Experiments on the release of hydrophobic drugs from large polyanhydride matrix implants did

confirm their ability to sustain release. Recent mathematical models, including our own in Chapter 4.0 , show that this linear or sustained release behavior is not maintained for smaller matrices or very hydrophilic, small molecule drugs[41,126]. Even without this limitation, the design of polyanhydride matrices has remained limited by the absence of a predictive model. The same is true for new biodegradable polymers designed specifically for even better sustained release, the stabilization of protein cargos, or ease of injection. Hydrogels of polyethene glycol or polyaminoacids, polyphosphoazines, cross-linked dextrans and drug-polymer conjugates all must be tuned through iterative experiments and in many cases require modification of the materials' chemistry to achieve the desired release behavior[187,198]. Further, the library of data on these newer polymers is not yet complete enough to support the development and validation of a predictive mathematical model. Simply put, literature does not include any case of *ab initio* mathematically engineering a formulation that sustains a constant rate of release over weeks or months.

As demonstrated in Chapter 6.0 , the math model developed in Chapter 3.0 can be used to predict the release profiles of theoretical polymer matrices. Data in Figure **12** even suggests that a combination of PLGA polymers can be used to sustain release. Testing of the sustained release concept could focus on development of formulation that delivers a water-soluble macromolecule for as little as one month. This goal would provide a proof of concept challenge on par with the develop of nutropin depot[199]. Macromolecules therapeutics also provide a very clinically relevant scenario for testing the benefits of controlled release because they are not noted for naturally releasing at a constant rate and their delivery currently requires frequent injections, which makes them A) painful to administer and B) a high non-adherence risk[12,42,200].

When considering pharmaceutically relevant macromolecules for a case study, the peptide drug enfuvirtide (T20) is of the utmost interest. The drug is currently delivered in two daily 90mg bolus injections which sustain a 2.94 mg/L serum concentration in highly infirmed patients[201]. This administration schedule makes adherence to enfuvirtide prescriptions challenging[202]. In the body, enfuvirtide is rapidly metabolized by proteases that consume nearly 90% of each injection [201]. Encapsulation in PLGA microparticles may protect this peptide from degradation and lower treatment costs by using the peptide more efficiently. Finally, as one of the only approved HIV fusion inhibitors, which prevents viral entry into T cells, a sustained release formulation of enfuvirtide could be used to treat HIV prophylactically and may prove more successful than oral prophylactics, which have been significantly hampered by poor adherence in clinical trials[203].

To the best of our knowledge, a FDA-approved, controlled release formulation of enfuvirtide has yet to be realized. Recent efforts by the pharmaceutical company Trimeris Inc. have focused on developing controlled release versions of similar anti-HIV peptides in their product pipeline (TRI-1144 and TRI-999), using novel technologies, such as entrapment in an organic salt complex or *in situ* forming gel[204]. At its best, the organic salt formulation maintained near-constant rate of drug delivery over two weeks following a distinct initial burst (Figure 33). However, noticeable fluctuations also occurred in the *in vitro* release rate before the assay was terminated on day 16, with just 50% of drug being released. Results from the gel formulation showed even more variability in release data (*data not shown*)[204]. Although both of these formulations offer improvements over the rapidly metabolized peptide solution delivered by bolus injection, resorting to these novel technologies has not necessarily brought researchers significantly closer to obtaining desirable release profiles with a formulation that will swiftly

progress through US regulatory mechanisms. In PLGA formulations, enfuvirtide sustained release has only been documented for 72 hours before ceasing [205]. However, longer, more linear release of this drug holds the potential to improve patient quality of life both through less-burdensome administration and reduced treatment cost.

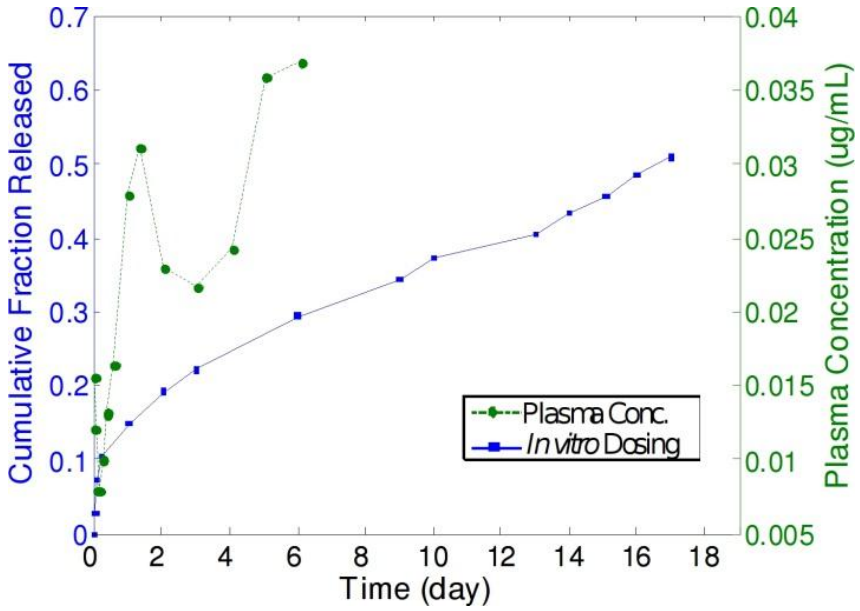

Figure 33: In vitro and in vivo enfuvirtide delivery profiles from a controlled release formulation.[78]

The novel peptide-organic salt complex formulation fails to maintain constant plasma concentrations of the anti-HIV peptide or provide a constant rate of drug delivery.

In this chapter, we develop a sustained release formulation engineered for the month-long delivery of enfuvirtide and other macromolecules. The model from Chapter 3.0 was employed to identify a suitable combination of polymers for this application. The resulting formulation contained three microparticle components whose *in vitro* release profiles were assayed with either a dextran Texas Red conjugate or enfuvirtide. The enfuvirtide formulations that performed in accordance with model predictions of in vitro release were tested for activity using a cell-based HIV infectivity assay.

7.2 MATERIALS AND METHODS

7.2.1 Materials

Acylated poly(lactic-co-glycolic) acid (PLGA) copolymers RG502 ($Mw_o \approx 9kDa$) and RG504 ($Mw_o \approx 30kDa$) were purchased from Boehringer Ingelheim (Ingelheim, Germany). Acid end-capped 50:50 poly(lactic-co-glycolic) acid (4.6kDa) was purchased from Lakeshore Biomaterials (Surmodics, Inc.). Enfuvirtide (T-20) was obtained through the AIDS Research and Reference Reagent Program, Division of AIDS, NIAID, NIH from Roche. Solvents, assay reagents, and other chemicals were purchased from Thermo Fisher Scientific (Waltham, MA).

7.2.2 Microparticle Production

Microparticles were produced by the double emulsion process as done in Section 5.2.2 (Table 4). Enfuvirtide was dissolved at 2mg/ml in a solution of 22.55 mg/ml of mannitol and 2.39 mg/ml of sodium carbonate. 200ul of enfuvirtide solution was sonicated in 4ml of dichloromethane with 200mg of PLGA. This mixture was homogenized in 2% PVA and the

dichloromethane was allowed evaporate over 4 hours before microparticles were collected by centrifugation.

7.2.3 Microparticle Characterization

Microparticles were characterized by size, loading, surface morphology and internal morphology as done in Section 6.2.4. Microparticle size distribution was measured by the volume impedance method. The loading of enfuvirtide was measured by dissolution in DMSO and extraction in 50mM NaOH / 5% SDS. Scanning electron microscopy was used to evaluate particle surface morphology and laser confocal microscopy was used to determine the internal distribution of drug within the microparticles.

7.2.4 HPLC detection

High pressure liquid chromatography (HPLC) was used to measure the concentration and stability of T20 released from microparticles as done in Section 5.2.4. Samples of releaste from T20 microparticles were diluted 1:20 with 35:65 ACN:H_2O containing 175µg/ml porcine insulin. Standards of T20 (serial dilutions: 20-0.04µg/ml) were assayed at a 1:20 dilution with 35:65 ACN:H_2O as well. A standard curve was calculated from the ratio blanked peak areas for the two T20 peaks and one peak for insulin.

7.2.5 Enfuvirtide (T20) Stability Calculations

Unencapsulated enfuvirtide possessed two HPLC peaks that changed magnitude following encapsulation and release. To calculate stability, the heights of these two peaks were set relative to a 100% scale for both the released (post-encapsulation) and unencapsulated enfuvirtide. The percent stability was then calculated based on the ratio of the pre- and post- encapsulation peaks for "active" enfuvirtide.

7.2.6 T20 Activity Testing

The activity of enfuvirtide was tested using a single replication cycle infectvivty assay as done previously[206]. Briefly, TZM cells cultured in DMEM (90%), 10% FBS, 100 units of Penicillin and 0.1 mg/ml of Streptomycin, were plated in 96 well tissue culture plates at 2.5 x 10^3 cells/well. Five-fold dilutions of releaste from t20 loaded or 3 fold dilutions of releasate from blank microparticles were added plated cells. Standard curves were prepared with serial dilutions of T20 spanning 10,000 to 0.01ng/ml. All groups described above were prepared and tested in duplicate. Following a 24 hour incubation, virus stock (at 50%ID, as determined previously [207]) was added to all wells and 37°C incubation was continued for 2 days. Then cells were lysed and analyzed with a luciferase assay (Promega). As a control, standard curves of T20 (10,000 to 0.01ng/ml and 0ng/ml) were incubated with plated cells (no virus), which were lysed after 72hours and measured luciferase baseline and cell health (via MTS assay).

7.3 RESULTS

The performance goal for the design of the sustained release formulation (SRF) platform is the month long delivery of a peptide of protein. Based on this goal, predictions made using the model in Chapter 3.0 identified a mixture of three microparticles types that sustain release of T20 for one month (Table 5). Because detection T20 release required implementation of a new HPLC protocol, a preliminary formulation was created using 3kDa dextran-Texas Red (dexTR) conjugate, which was predicted to have the same release kinetics as T20. Imaging of these particles by SEM revealed these particles to have uniformly smooth surfaces and a spherical shape (Figure 34A). A similar morphology was observed for T20 loaded microparticles as well (data not shown). Confocal microscopy of the dexTR microparticles revealed drug occluded in small pockets scattered randomly throughout the polymer matrix (Figure 34B). This microscopy data is indicative of a formulation that supplies little initial burst release as detailed in Section 3.2.1, Figure 7.

Table 5: Composition of 50:50 PLGA Mixture

Mw (kDa)	*Amount (%)*
5.8 ± 1.5	20.1
10.2 ± 1.4	31.8
31.8 ± 2.3	48.1

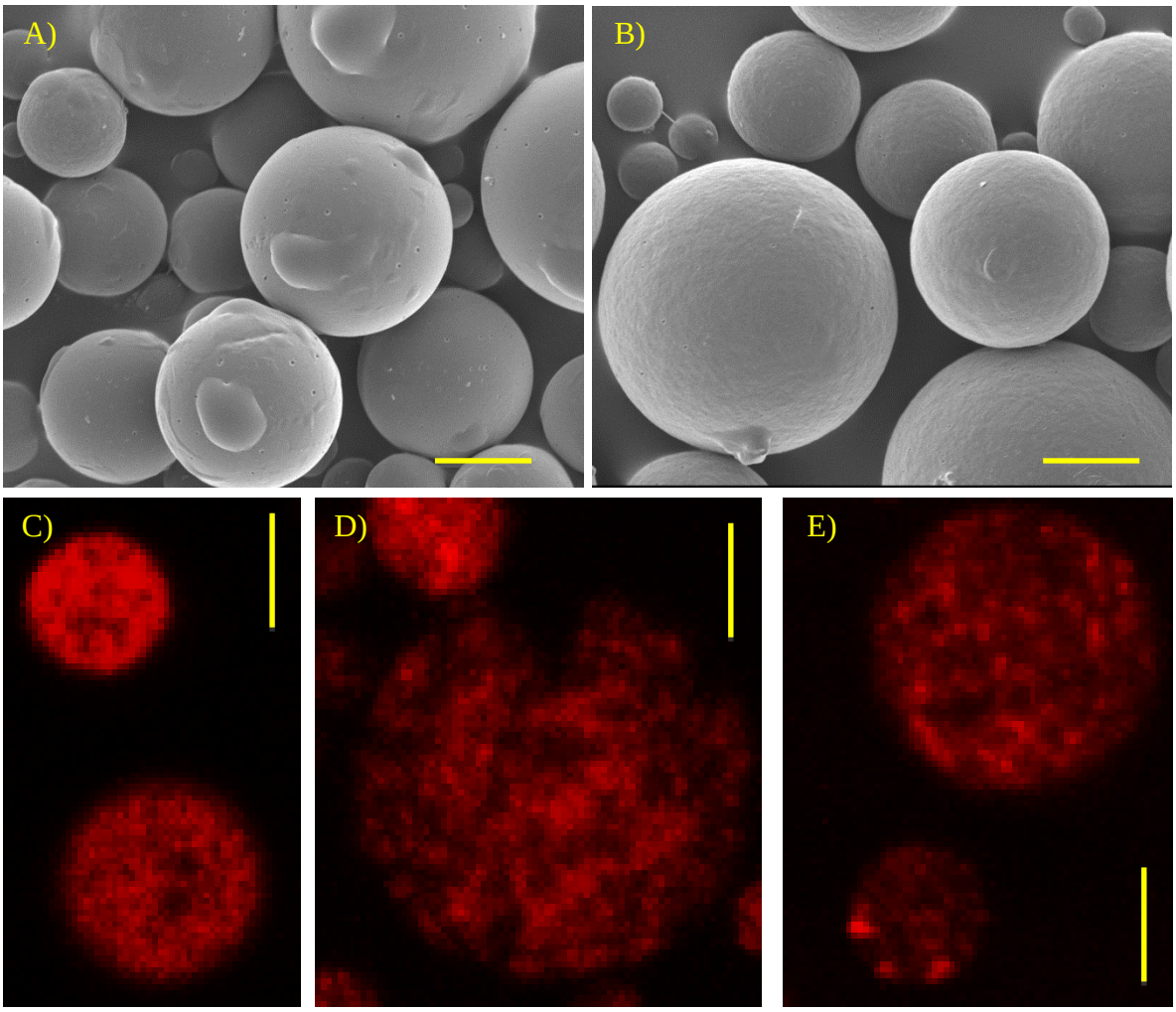

Figure 34: Scanning electron and confocal microscopy images of particles from SRF formulation.

SEM images of A) RG502 and B) RG504 particles show uniform shape and smooth surface morphology. Confocal images of C) DLG1A, D) RG502 and E) RG504 microparticles show Dex-TR (representative of T20) dispersed throughout the matrix. (Scale bars are 10µm)

In vitro release testing from the dexTR loaded formulation confirmed that each component microparticle of the formulation released according to model predictions and, in combination, produced a linear release profile (Figure 35). Comparable results were achieved with particles mixed in model prescribed ratio prior to *in vitro* testing (Figure 36). This successful validation of the formulation design with dexTR provided grounds for testing the design with the therapeutic peptide enfuvirtide.

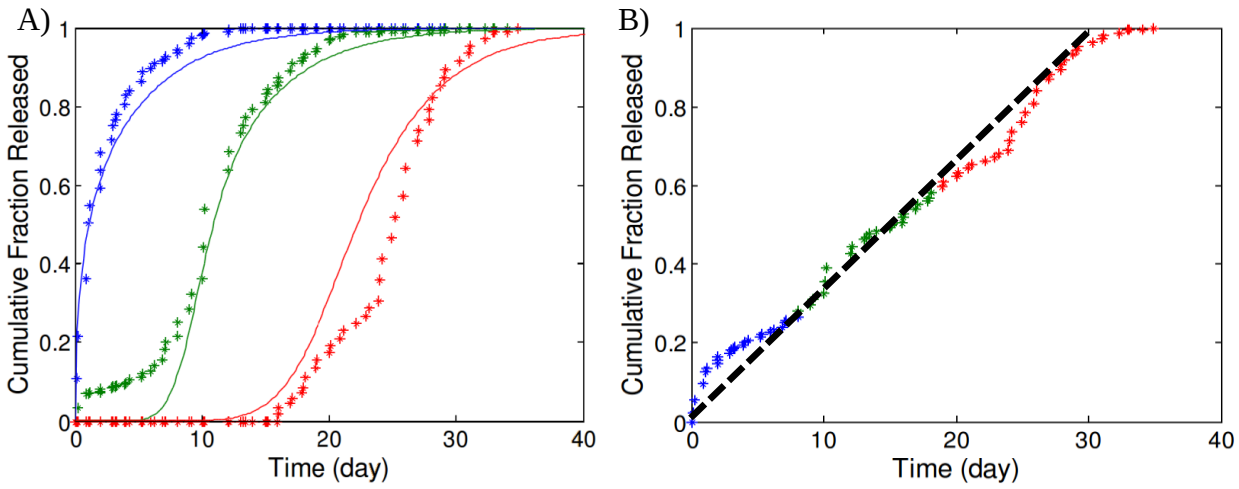

Figure 35: *In vitro* release of DexTR from SRF microparticles.

A) *In vitro* release (*dots*) follows model prediction (*line*) release for each formulation. B) When combined at the model-defined ratio these individual release profiles continue at a near-constant rate for 30 days.

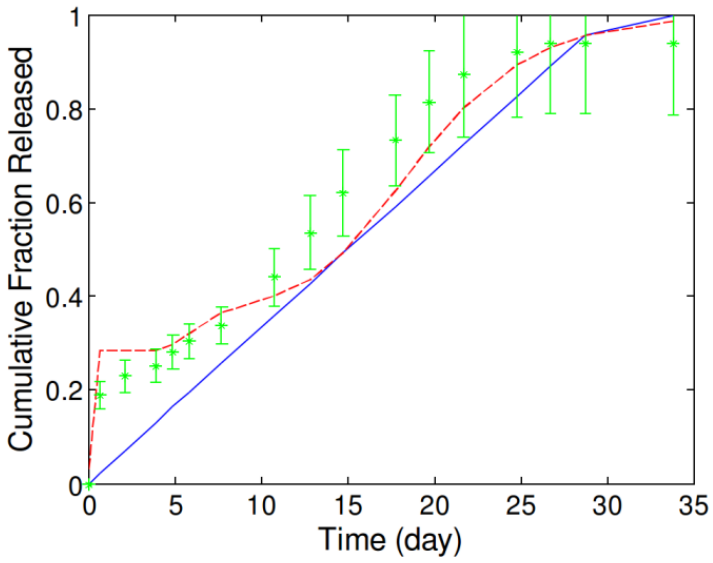

Figure 36: *In vitro* release from the model defined mixture of DexTR microparticles.

Experimental data is shown with green dots. Predicted release for the microparticle mixture appears as a dashed red line. Model solutions were computed at times corresponding to each experimental data point and linearly interpolated. The target rate of release is indicated with a solid blue line.

Because enfuvirtide lacked the fluorescent label of dexTR, measurement of its *in vitro* release was slightly more complicated. Implementation of the HPLC protocol for detecting T20 in serum described in Section 7.2.4, yielded a standard curve that followed a power expression from 0.04µg/ml to 20.00µg/ml (Figure 38). This detection range allowed the successful detection of T20's *in vitro* release (Figure 37). A comparison of the predicted and *in vitro* release profiles yielded mixed results. Both the 9kDa and 30kDa formulation performed in accordance with model predictions. However, release from the 4.6kDa polymer matrix was significantly slower than predicted. In fact, the measured *in vitro* release profile more closely mimicked the predicted behavior of larger macromolecule, such as a protein, rather than that of

the 4.5kDa peptide, T20. Because 4.6kDa polymer was the only one with acid-terminated chain ends, matrix charge may play a role in the observed deviation. This speculation aside, the *in vitro* release data from the T20 formulation confirms that 2 of the 3 component microparticles tested do indeed follow model predictions, making them suitable for activity testing.

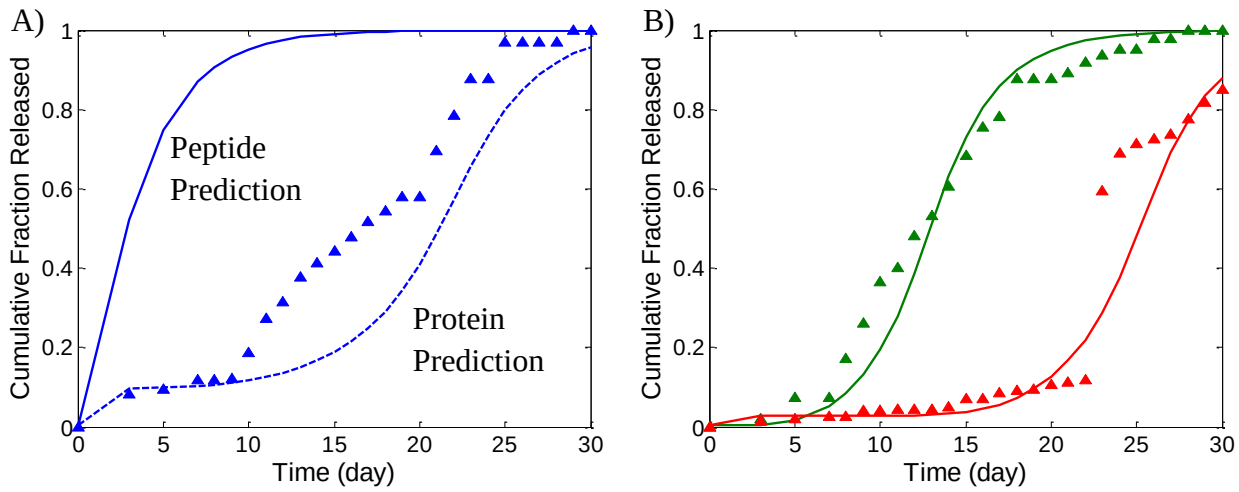

Figure 37: *In vitro* release of T20 from three model-defined component microparticles of SRF

Experimental data measured by HPLC are shown as triangles and predictions are shown with lines. A) T20 release from DLG1A polymer microparticles more closely followed behavior anticipated for protein (*dashed line*) than for the 4.5kDa peptide, enfuvirtide (*solid line*). B) Data from RG502 (*green*) and RG504 (*red*) polymer microparticle closely matched model predictions.

7.3.1 Enfuvirtide Activity Results

Microparticles of PLGA produce an acidic microclime as they hydrolyze, which can denature or degrade sensitive peptide and protein cargos. If these changes occur, the rate of active agent release can be altered from model predictions. Because of this, released enfuvirtide was assayed both for stability and activity.

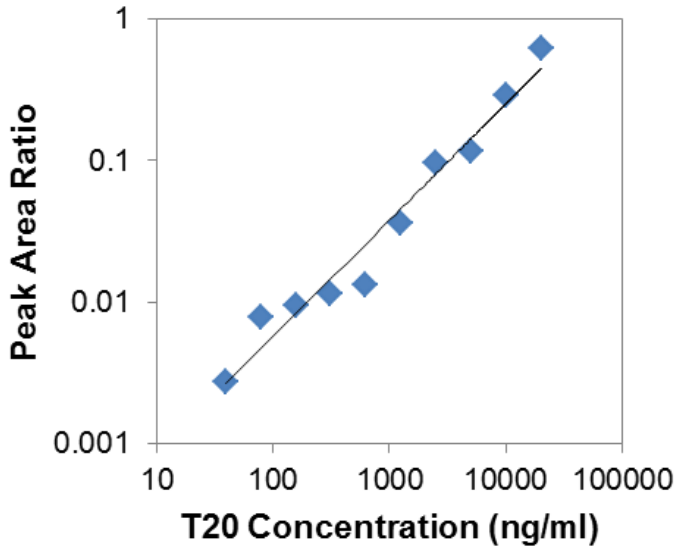

Figure 38: Detection of T20 by HPLC.

Area of T20 peak was zeroed against blank and then normalized by an insulin internal standard. The trend line is $y = 0.0191x^{0.8700}$; $r^2 = 0.944$. Data point size is indicative of error (n = 3).

7.3.1.1 Measurement of T20 stability

When a peptide is degraded, in a complex with the polymer or aggregated, it exhibits a shift in retention time that can be detected with HPLC. Prior to encapsulation, T20 exhibited two minor peaks accounting for 5% and 0.5% of the overall composition. At lower T20 concentrations (more likely to be found in releasate) the smallest peak was undetectable. Further, the main and minor peaks accounted for 90±7% and 10±7% of T20 respectively due to the sensitivity of HPLC measurements. Following encapsulation and release, peptide stability was largely maintained for each of the component formulations in the SRF. Table 6 lists the % of peptide remaining intact for each formulation during periods of measurable release (i.e. when release was consistently above the detection limit).

Table 6: T20 Stability via Analysis of HPLC Peak Areas

Formulation	**A (4.6kDa)**	**B (9.0kDa)**	**C (30kDa)**
Window (day)	10-19	8-18	23-30
T20 Intact (%)	83 ± 4%	83 ± 19%	72 ± 23%

7.3.1.2 Measurement of T20 inhibition of viral replication

When examining the potential of using the sustained release formulation of T20 for HIV prophylaxis depends on both release kinetics and the activity of the released drug. Assessment the T20 releasate's ability of prevent HIV infection was made using the TZM cell functional assay. Sensitivity was documented over a range of 0.027ng/ml to 330ng/ml below which <5% of cells were uninfected and above which >95% of cells were uninfected (Figure 39). A sigmoidal fit to this data, yields IC-50 and IC-90 values of 11.1ng/ml and 139ng/mL, respectively. An MTS assay conducted on TZM cells exposed to microparticle releasate or stock enfuvirtide showed no significant change from naïve cells, confirming that the infectivity assay results are not an artifact of diminishing cell health (data not shown).

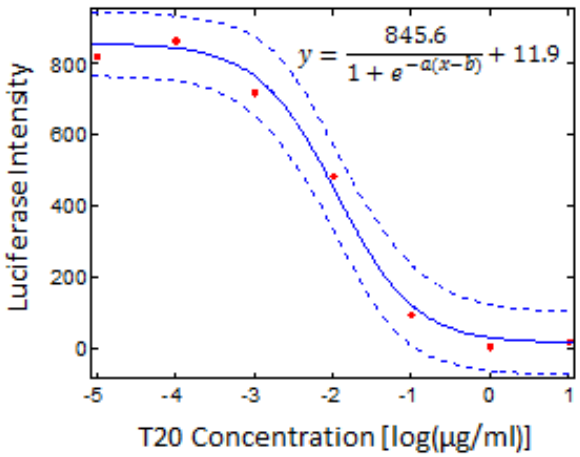

Figure 39: Luciferase expression of TZM cells exposed to HIV in the presence of T20.

Infectivity data (red dots) were fit by a sigmoid function (*solid blue line*) scaled to average max and min luc expression, as shown on graph. Least squares optimization yielded a = 2.0±0.7 and b = -1.7±0.2 (bounds of a 95% confidence interval, *dotted blue lines*). Goodness of fit: SSE = 5955 and r^2 = 0.993. (Prior to analysis, data was normalized by the baseline expression of luc, 528.5 data not shown.)

With the sigmoidal fit standard curve, the concentration of active enfuvirtide in releasate samples was back calculated. The cumulative release of active T20, as measured by the TZM assay, closely follows overall T20 release as measured by HPLC for formulations B and C (Figure 40). Formulation A was not tested for activity because its release kinetics did not follow model predictions.

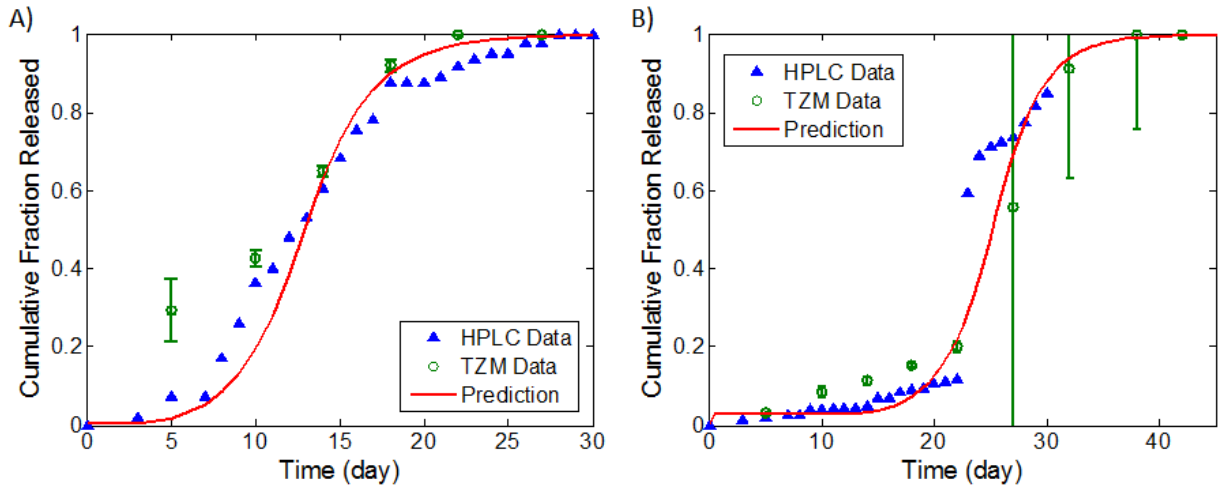

Figure 40: The rate of active T20 release (green circles) follows model predictions (red lines).

Active and stable (HPLC, blue triangles) T20 also release at the comparable rates. The cumulative release of active T20 (green circles) was calculated from infectivity assay results and standard curve in Figure 39. Loss of T20 activity at later times (lower concentration) may lead to higher than predicted initial release in A.

7.3.2 Results Summary

The model-guided development of a platform for sustained macromolecule release produced a unique formulation composed of three microparticle components. When tested with a model agent, dexTR, all three of these component matrices performed as predicted. However, when T20 was supplemented for dexTR, only 2 of the 3 formulation performed as predicted. These two successful designs were tested for activity, which was found to vary little over the duration or release.

7.4 DISCUSSION

The design of a platform for the sustained delivery of macromolecules could improve patient adherence by as much as 85%. This chapter generated proof-of-concept data for its sustained release formulation on the delivery of enfuvirtide for 1 month. Polymers were selected for this formulation based on predictions from the model in Chapter 3.0 as opposed to a variation-of-parameters, experimental approach that is the current state of the art[19,20]. With the exception of the 4.6kDa acid end-capped polymer, release profiles were comparable for enfuvirtide and a texas-red labeled dextran "peptide" surrogate. An addition to the current model quantifying how changes to polymer chemistry affect release might resolve this exception. However, the accurate performance of acylated (ester end-capped) polymer microparticles still provides opportunity for the activity analysis of released enfuvirtide with viral infectivity assay. This single replication

cycle infectivity assay confirmed that the delivery of active enfuvirtide was consistent with the overall rate of enfuvirtide release.

The sustained release formulation bypasses the natural tendency of PLGA copolymers to provide triphasic release profiles (as described in Section 2.1) by using three such copolymers in combinations. Interestingly a similar strategy was adopted in a recent article where two of piroxicam loaded microspheres were combined to extend release, although creation of a linear release profile was hampered by limited control over the release behaviors of the building blocks[208]. Sustained release has also been achieved by polymer blends or reduced drying rates, which served to broaden PLGA's polydisperisty[68,209]. However, these have proven difficult to control and adapt to new manufacturing or performance requirements. In contrast, the three build-blocks used herein work together in unison to sustain macromolecule release. Further, the extensive validation model conducted in Section 3.3.1 suggests that modeling results should apply equally well to many other water-soluble peptides or macromolecules in the 3-5kDa range. However, one of the three T20 formulations tested deviated from model predictions and requires additional discussion.

The only formulation whose release deviated from predictions during *in vitro* release testing suggests that an additional factor or factors might affect drug release under specific conditions. The most likely explanation is that release of the enfuvirtide peptide (T20) was slowed by interacts with the 4.6kDa polymer used in matrix, not accounted for in the initial prediction. In environments of pH < 4.1 enfuvirtide become positively charged, which would allow it to interact electrostatically with the carboxylic acid chain ends of the encapsulating polymer matrix. This is supported by the fact that 4.6kDa polymer matrix, which had by far the highest concentration of acidic chain ends of all T20 formulations produced, was the only one to

show deviation. If T20 is bound irreversibly to the polymer matrix, it might behave like a large protein complex that is predicted to release when the polymer matrix degrades into soluble oligomer. However, T20's release rate falls in between the predictions for the bound and unbound systems (Figure 37A). This behavior is not presently covered by model from chapter 3. Retrospective analysis of the model's correlation between D and R_p points to two outliers, SPF66 (isoelectric point at pH = 4.8) and leuprolide (isoelectric point at pH = 9.9), that may be affected similar interactions. Further study of peptides with isoelectric points at pH of 4 or greater should provide the data needed to better understand how reversible electrostatic interactions effect drug release.

The activity of enfuvirtide, an HIV fusion inhibitor, was quantified in terms of its stability and ability to block viral infection. The present work assesses the stability of the peptide through analysis of HPLC peaks. As enfuvirtide degrades, new peaks appear in the HPLC chromatograph preceding the original peptide peak and grow in proportion to the concentration of each new form of the peptide. Prior work on the detection of enfuvirtide by HPLC has identified two truncated forms of enfuvirtide, which also appear in the our data[210]. The fact that these peaks only grow by 10-30% following encapsulation and release is surprising for such a large peptide. In literature, peptides and proteins ranging from octreotide acetate to stromal-derived factor-1 alpha are typically denature, degraded or otherwise inactivated by the double emulsion encapsulation process or by the prolonged incubation within the microparticles before release[76,94,132,159]. For example, the stability of octreotide peptide was reduced to 59% and 34% of the original following its release from 10kDa and 30kDa 50:50 PLGA microparticles, respectively [132]. Enfuvirtide's comparative stability of 83% in the 4.6kDa and 9.0kDa PLGA microparticles may arise from its insolubility under the acidic conditions that arise as these

polymers degrade[211,212]. (For the less acidic 33kDa microparticles, a stability of 72% was measured upon release.) Similarly strong stability data have been achieved with solid-in-oil-in-water (S/O/W) emulsions, where peptides or proteins were encapsulated as dry powders[94,213]. However, release from these S/O/W systems is dominated by large initial burst (>60%) because the dry powders are difficult to mix uniformly during production and remain near the particle surface[94]. In contrast, the enfuvirtide microparticles developed herein delivered less than 10% their payloads in the initial burst because the enfuvirtide was encapsulated in a soluble form and is thought to only solidify as the microparticles degrade and become acidic. These details on enfuvirtide stability, however, are only an indicator of activity or the drug's ability to prevent HIV from entering CD4+ cells, which itself can be tested in cell-based assays.

The single replication cycle cell infectivity assays offer a convenient and sensitive way to quantify enfuvirtide activity as well as many other potentially prophylactic drugs that can prevent a virus from integrating its DNA into a host chromosome. The present work used this type of assay to measure the infectivity of HIV in the presence of releasate from enfuvirtide loaded microparticles and known concentrations of unencapsulated enfuvirtide, which served as a control. Both sample and control groups were pre-incubated with the target TZM cells (HeLa cells that expresses CD4, CXCR4 and CCR5 and contains Tat-inducible luciferase reporter) to simulate the prophylactic use of enfuvirtide. A comparable prophylactic assay setup has not been previously attempted, but co-incubation of enfuvirtide and HIV-1 isolates with TZM cells in prior studies yielded IC-50 ranges of 0.45-22.5ng/ml and IC-90 ranges of 2.25-802ng/ml from an assortment of HIV-1 isolates[214]. The enfuvirtide standards of present work were assayed with mixed HIV-1 isolates instead of single isolates. The resulting IC-50 (11.1 ng/ml) and IC-90 (139ng/ml) values from this mixture are comparable to the average IC-50 (7.2±8.1ng/ml) and IC-

90 (312±346ng/ml) of the single isolates tested previously[214]. This result is also consistent with data from other HELA cell-based HIV infectivity assays, which establish enfuvirtide IC-50 and IC-90 ranges at 4-31.2ng/ml and 67-342ng/ml, respectively, [215,216].

To the best of our knowledge, the present work represents the first instance of a cell-based assay being used assess the activity of enfuvirtide released from a drug formulation *in vitro* or *in vivo*. Prior work on enfuvirtide formulations typically moves directly from *in vitro* release testing to *in vivo* pharmacokinetic studies where enfuvirtide concentration in serum is measured by HPLC[204,205]. This measurement of intact or stable enfuvirtide is not necessarily the same as concentration of active enfuvirtide. The present work uses the TZM cell assay to measure the rate of active enfuvirtide release and confirms that it closely follows its *in vitro* release rate as measured by HPLC. This suggests that the enfuvirtide activity also remains constant for the duration of release. However, to conclusively determine if stable enfuvirtide is active, an infectivity assay (TZM cell or other) would need to be used on enfuvirtide isolated by chromatography of *in vitro* releasate or *in vivo* serum samples.

7.5 CONCLUSIONS

Using enfuvirtide as a representative peptide drug, the sustained release formulation developed herein has been evaluated as a platform for the month-long delivery of active agent. The design of the formulation was aided by predictions from the model developed in Chapter 3.0 that identified commercially available PLGA polymers which would provide acceptable rates and durations of release. The building-block solution to sustained release by this approach affords

flexibility in compensating for the stability of drug in each polymer microparticle component of the formulation. Cell culture testing of enfuvirtide's ability to prevent infection also confirmed the rate of active agent release. As this result may be due to enfuvirtide's insolubility in acidic environments, further investigations of agent activity would be warranted if this formulation were used with other peptides or proteins.

8.0 FUTURE WORK

The studies reported in Chapters 3.0 - 7.0 establish that mathematical models can predict the *in vitro* performance of long-acting controlled release and even be used to expedite their design. The utility of this finding is limited by the availability of system-specific predictive models and, in the case of formulation design, sensibly defined algorithms that return physically relevant critical quality attributes and process parameters. To this end, significant work remains to be done. The predictive models derived in Chapters 3.0 and 4.0 do not include mathematics for describing hydrophobicity or electrostatic interactions. For instance, the data in Figure 37 suggests that peptide charge alters release from select polymer matrices. This effect might be difficult to document because the acid environment that arises as microparticles degrade may alter the charge of agents with sufficiently high pKa(s). Mathematics accounting both for microparticle acidification and the impact of electrostatic interactions on agent diffusion would be needed to predict the release behavior of affected systems. Another limitation comes from matrix size, the lower limit of which has yet to be fully explored. At nano-scale sizes, the linear correlation used to handle autocatalysis may breakdown due to quenching the autocatalytic acidic microclime by buffer salts. When widely accepted and consistent methods of nanoparticle manufacture and characterization are developed, it should be possible to conduct mathematical validations of their *in vitro* release behavior and extend existing correlations to cover these

systems. Alternately, it might become practical to integrate expressions describing role of acidic catalysts in the degradation of the microparticles. This would allow changes in particle size and agent charge (a function of pH) to be accurately accounted for in future predictions of *in vitro* release and extend the gains in efficiency realized with the current models to a much broader range of pharmaceuticals scenarios.

Certain pharmaceutical scenarios are not effectively represented by in vitro release data. Cases that do not involve water-soluble agents being delivered locally (as done in Chapters 6.0 and 7.0) fall into this category. These cases include the large majority of drugs not presently delivered by injection and many sparingly or even highly insoluble drugs as well. Designing useful formulations for such drugs requires predictions of systemic drug concentrations in serum (i.e. *in vivo* pharmacokinetic data). Making accurate *in vivo* predictions would require a model with an extensive record of validation against pharmacokinetic data from controlled release formulations. In developing the models in Chapters 3.0 and 4.0 , nearly 50 data sets from a library of over 300 research articles were ultimately used in validation testing. Building an accurate "*in vivo*" model would also likely require increased knowledge of how the physiological environment affects drug release and transport or distribution from depot medications. Live animal imaging (LAI) techniques, such as magnetic resonance imaging, may offer a means of monitoring how a dynamic physiological environment spatially and temporally impacts drug release. A model developed based on insights from LAI studies could be validated against published sets of *in vitro* and *in vivo* release data to confirm the accuracy of its predictions.

Beyond design, predictions of *in vitro* behavior are useful for the Quality by Design manufacturing of controlled release formulations. Documentation of how manufacturing conditions affect *in vitro* release can help engineers determine if a formulation will be safe to

use. For application to QbD, the system properties used by predictive mathematical models must be correlated to the performance of specific manufacturing technologies or facilities. This may prove complicated because tuning occlusion size, matrix geometry and other system properties requires experience with specific manufacturing equipment and protocols. It may also prove that multiple aspects of the manufacturing process affect the system properties computed by the predictive model. This is likely the case for polymer molecular weight, which may be altered by shear during emulsification or slow drying during lyophilization. Establishing correlations between system properties now computed and the process parameters that affect them will be an essential next step in the application of current predictive models to QbD. This quasi-empirical, model-driven approach should prove significantly more efficient than the entirely empirical, design of experiments approach now used to generate quality assessments of formulations.

Beyond the derivation, implementation and application of a model of release for hydrolysable polymer matrices, this thesis serves to highlight how a math model can provide new ways of addressing challenges in drug delivery. The increasingly complex scenarios presented by environmentally responsive materials, zero-dimensional nanotubes and others as well as by new treatment goals may be better resolved by a similarly math model-rich approach. Models may prove essential for a number of applications requiring precise temporo-spatial control, including the delivery of growth factors for regenerative medicine and the delivery of cytokines or chemokines for immunotherapy. Furthermore, to better incorporate controlled release behavior into new therapeutics, models will also be needed for predicting *in vivo* performance of hydrolysable polymer matrices. Fortunately new techniques, such as live animal imaging, may make it easier to measure and compare *in vivo* release kinetics, helping researchers understand how *in vitro* design tools might be applied to precisely control the concentration of

drug in a specific physiological compartment over time. With continued advances to the design "tool-box", future scientists and engineers may someday tailor controlled release formulations to provide specific dosing kinetics to any given physiological compartment by simply selecting correct materials and processing methods. This would pave the way not only to the broad-scale production of custom release systems for any application, but perhaps even to patient-specific, or "individualized", controlled release systems that can accompany individualized medicine in the future.

APPENDIX

GLOSSARY OF ABBREVIATIONS

A.1 MODEL VAIRABLES

C_A	Concentration of dissolved agent in the polymer matrix
C_{Amax}	Maximum concentration of dissolved agent (solubility limit)
C_{Ao}	Initial concentration of dissolved agent
C_S	Concentration of solid, crystalline or powdered, agent
C_{So}	Initial concentration of solid agent in the polymer matrix
C_W	Concentration of water in polymer matrix
C_{Wo}	Concentration of water in the reservoir
D_A	Diffusivity of agent through the polymer matrix
D_W	Diffusivity of water through the polymer matrix
ε	Matrix porosity
k	Polymer degradation rate
k_{dis}	Agent dissolution rate
L	Length of cylindrical matrix
Mw	Polymer molecular weight

Mw_o	Average initial polymer molecular weight
Mw_r	Molecular weight of release
$P(t)$	Cumulative fraction of agent retained in the matrix at time t
$R(t)$	Cumulative fraction of agent released from the matrix by time t
R_{occ}	Occlusion radius
R_p	Matrix dimension(s) across which diffusive release occurs, *e.g.* particle radius, film thickness, or critical length
σ	Variance in Mw_r
t	Time

A.2 POLYMER CHEMISTRIES

PLGA	poly(lactic-co-glycolic acid)
PLA	poly(lactic acid)
SA	sebacic ahydride
CPH	1,6-bis-*p*-carboxyphenoxy hexane
PSA	poly sebacic anhydride
PFADSA	1:1 Poly(fatty acid dimer-co-sebacic acid) anhydride
POE	Poly(ortho-ester)

BIBLIOGRAPHY

1 Siepmann, J., Elkharraz, K., Siepmann, F. & Klose, D. How autocatalysis accelerates drug release from PLGA-based microparticles: A quantitative treatment. *Biomacromolecules* **6**, 2312-2319 (2005).

2 Klose, D., Siepmann, F., Elkharraz, K., Krenzlin, S. & Siepmann, J. How porosity and size affect the drug release mechanisms from PLGA-based microparticles. *International Journal of Pharmaceutics* **314**, 198-206 (2006).

3 Berkland, C., Kim, K. & Pack, D. W. PLG microsphere size controls drug release rate through several competing factors. *Pharmaceutical Research* **20**, 1055-1062 (2003).

4 Batycky, R. P., Hanes, J., Langer, R. & Edwards, D. A. A theoretical model of erosion and macromolecular drug release from biodegrading microspheres. *Journal of Pharmaceutical Sciences* **86**, 1464-1477 (1997).

5 Takenaga, M. *et al.* A novel sustained-release formulation of insulin with dramatic reduction in initial rapid release. *Journal of Controlled Release* **79**, 81-91 (2002).

6 Cui, F. *et al.* Preparation and characterization of melittin-loaded poly (DL-lactic acid) or poly (DL-lactic-co-glycolic acid) microspheres made by the double emulsion method. *Journal of Controlled Release* **107**, 310-319 (2005).

7 Barton, C. Controlled-release: Players, Products and Prospect to 2018 (Espicom, 2009).

8 Humphreys, A. M., Rebecca;. Top 200 medicine highlights. *MedAdNews* **30** (2011).

9 Eerdekens, M., Van Hove, I., Remmerie, B. & Mannaert, E. Pharmacokinetics and tolerability of long-acting risperidone in schizophrenia. *Schizophrenia Research* **70**, 91-100 (2004).

10 Brem, H. *et al.* Placebo-controlled trial of safety and efficacy of intraoperative controlled delivery by biodegradable polymers of chemotherapy for recurrent gliomas. *Lancet* **345**, 1008-1012 (1995).

11 Jiang, W., Gupta, R. K., Deshpande, M. C. & Schwendeman, S. P. Biodegradable poly(lactic-co-glycolic acid) microparticles for injectable delivery of vaccine antigens. *Advanced Drug Delivery Reviews* **57**, 391-410 (2005).

12 Sinha, V. R. & Trehan, A. Biodegradable microspheres for protein delivery. *Journal of Controlled Release* **90**, 261-280 (2003).

13 Humphreys, A. M., Rebecca;. World's Best-Selling Medicines. *MedAdNews* (2007).

14 Mundargi, R. C., Babu, V. R., Rangaswamy, V., Patel, P. & Aminabhavi, T. M. Nano/micro technologies for delivering macromolecular therapeutics using poly(d,l-lactide-co-glycolide) and its derivatives. *Journal of Controlled Release* **125**, 193-209 (2008).

15 Fernández-Carballido, A., Herrero-Vanrell, R., Molina-Martínez, I. T. & Pastoriza, P. Biodegradable ibuprofen-loaded PLGA microspheres for intraarticular administration: Effect of Labrafil addition on release in vitro. *International Journal of Pharmaceutics* **279**, 33-41 (2004).

16 Gao, P. *et al.* Controlled release of huperzine A from biodegradable microspheres: In vitro and in vivo studies. *International Journal of Pharmaceutics* **330**, 1-5 (2007).

17 Rawat, A., Stippler, E., Shah, V. P. & Burgess, D. J. Validation of USP apparatus 4 method for microsphere in vitro release testing using Risperdal® Consta ®. *International Journal of Pharmaceutics* **420**, 198-205 (2011).

18 FDA. (ed Food and Drug Administration) 4 (Office of Communication, Training and Manufacturers Assistance, HFM-40 Center for Biologics Evaluation and Research, 2006).

19 Singh, B., Dahiya, M., Saharan, V. & Ahuja, N. Optimizing drug delivery systems using systematic "design of experiments." Part II: Retrospect and prospects. *Critical Reviews in Therapeutic Drug Carrier Systems* **22**, 215-293 (2005).

20 Singh, B., Kumar, R. & Ahuja, N. Optimizing drug delivery systems using systematic "design of experiments." Part I: Fundamental aspects. *Critical Reviews in Therapeutic Drug Carrier Systems* **22**, 27-105 (2005).

21 Rosca, I. D., Watari, F. & Uo, M. Microparticle formation and its mechanism in single and double emulsion solvent evaporation. *Journal of Controlled Release* **99**, 271-280 (2004).

22 Liggins, R. T., D'Amours, S., Demetrick, J. S., MacHan, L. S. & Burt, H. M. Paclitaxel loaded poly(L-lactic acid) microspheres for the prevention of intraperitoneal carcinomatosis after a surgical repair and tumor cell spill. *Biomaterials* **21**, 1959-1969 (2000).

23 Freiberg, S. & Zhu, X. X. Polymer microspheres for controlled drug release. *International Journal of Pharmaceutics* **282**, 1-18 (2004).

24 Alexis, F. Factors affecting the degradation and drug-release mechanism of poly(lactic acid) and poly[(lactic acid)-co-(glycolic acid)]. *Polymer International* **54**, 36-46 (2005).

25 Jain, J. P., Modi, S., Domb, A. J. & Kumar, N. Role of polyanhydrides as localized drug carriers. *Journal of Controlled Release* **103**, 541-563 (2005).

26 Lakshmi, S., Katti, D. S. & Laurencin, C. T. Biodegradable polyphosphazenes for drug delivery applications. *Advanced Drug Delivery Reviews* **55**, 467-482 (2003).

27 Grassi, M., Lamberti, G., Cascone, S. & Grassi, G. Mathematical modeling of simultaneous drug release and in vivo absorption. *International Journal of Pharmaceutics* **418**, 130-141 (2011).

28 Huang, X. & Brazel, C. S. On the importance and mechanisms of burst release in matrix-controlled drug delivery systems. *Journal of Controlled Release* **73**, 121-136 (2001).

29 Seo, S. A., Khang, G., Rhee, J. M., Kim, J. & Lee, H. B. Study on in vitro release patterns of fentanyl-loaded PLGA microspheres. *Journal of Microencapsulation* **20**, 569-579 (2003).

30 Fu, K. *et al.* A potential approach for decreasing the burst effect of protein from PLGA microspheres. *Journal of Pharmaceutical Sciences* **92**, 1582-1591 (2003).

31 Klose, D., Delplace, C. & Siepmann, J. Unintended potential impact of perfect sink conditions on PLGA degradation in microparticles. *International Journal of Pharmaceutics* **404**, 75-82 (2011).

32 Kumar, G., Sharma, S., Shafiq, N., Khuller, G. K. & Malhotra, S. Optimization, in vitro-in vivo evaluation, and short-term tolerability of novel levofloxacin-loaded PLGA nanoparticle formulation. *Journal of Pharmaceutical Sciences* **101**, 2165-2176 (2012).

33 van de Waterbeemd, H. & Gifford, E. ADMET in silico modelling: Towards prediction paradise? *Nature Reviews Drug Discovery* **2**, 192-204 (2003).

34 Bao, W., Zhou, J., Luo, J. & Wu, D. PLGA microspheres with high drug loading and high encapsulation efficiency prepared by a novel solvent evaporation technique. *Journal of Microencapsulation* **23**, 471-479 (2006).

35 Jiang, G., Thanoo, B. C. & DeLuca, P. P. Effect of osmotic pressure in the solvent extraction phase on BSA release profile from PLGA microspheres. *Pharmaceutical Development and Technology* **7**, 391-399 (2002).

36 Liu, R., Huang, S. S., Wan, Y. H., Ma, G. H. & Su, Z. G. Preparation of insulin-loaded PLA/PLGA microcapsules by a novel membrane emulsification method and its release in vitro. *Colloids and Surfaces B: Biointerfaces* **51**, 30-38 (2006).

37 Little, S. R., Lynn, D. M., Puram, S. V. & Langer, R. Formulation and characterization of poly (beta amino ester) microparticles for genetic vaccine delivery. *Journal of Controlled Release* **107**, 449-462 (2005).

38 Little, S. R. *et al.* Poly-? amino ester-containing microparticles enhance the activity of nonviral genetic vaccines. *Proceedings of the National Academy of Sciences of the United States of America* **101**, 9534-9539 (2004).

39 Chang, H. C. & Li, L. C. Sustained-release butorphanol microparticles. *Drug Development and Industrial Pharmacy* **26**, 829-835 (2000).

40 Champion, J. A. & Mitragotri, S. Role of target geometry in phagocytosis. *Proceedings of the National Academy of Sciences of the United States of America* **103**, 4930-4934 (2006).

41 Burkersroda, F., Schedl, L. & Gopferich, A. Why degradable polymers undergo surface erosion or bulk erosion. *Biomaterials* **23**, 4221-4231 (2002).

42 Rothstein, S. N. & Little, S. R. A "tool box" for rational design of degradable controlled release formulations. *Journal of Materials Chemistry* **21**, 29-39 (2011).

43 Sandor, M., Enscore, D., Weston, P. & Mathiowitz, E. Effect of protein molecular weight on release from micron-sized PLGA microspheres. *Journal of Controlled Release* **76**, 297-311 (2001).

44 Dorta, M. J., Santovena, A., Llabres, M. & Farina, J. B. Potential applications of PLGA film-implants in modulating in vitro drugs release. *International Journal of Pharmaceutics* **248**, 149-156 (2002).

45 Masters, D. B., Berde, C. B., Dutta, S., Turek, T. & Langer, R. Sustained local anesthetic release from bioerodible polymer matrices: A potential method for prolonged regional anesthesia. *Pharmaceutical Research* **10**, 1527-1532 (1993).

46 Onishi, H., Takahashi, M. & Machida, Y. PLGA implant tablet of ketoprofen: Comparison of in vitro and in vivo releases. *Biological and Pharmaceutical Bulletin* **28**, 2011-2015 (2005).

47 Ramchandani, M. & Robinson, D. In vitro and in vivo release of ciprofloxacin from PLGA 50:50 implants. *Journal of Controlled Release* **54**, 167-175 (1998).

48 Storm, P. B. *et al.* Polymer delivery of camptothecin against 9L gliosarcoma: Release, distribution, and efficacy. *Journal of Neuro-Oncology* **56**, 209-217 (2002).

49 Ehtezazi, T. & Washington, C. Controlled release of macromolecules from PLA microspheres: Using porous structure topology. *Journal of Controlled Release* **68**, 361-372 (2000).

50 Wang, F., Saidel, G. M. & Gao, J. A mechanistic model of controlled drug release from polymer millirods: Effects of excipients and complex binding. *Journal of Controlled Release* **119**, 111-120 (2007).

51 Nam, Y. S., Song, S. H., Choi, J. Y. & Park, T. G. Lysozyme microencapsulation within biodegradable PLGA microspheres: Urea effect on protein release and stability. *Biotechnology and Bioengineering* **70**, 270-277 (2000).

52 Jhunjhunwala, S., Raimondi, G., Thomson, A. W. & Little, S. R. Delivery of rapamycin to dendritic cells using degradable microparticles. *Journal of Controlled Release* **133**, 191-197 (2009).

53 Park, E. S., Maniar, M. & Shah, J. C. Biodegradable polyanhydride devices of cefazolin sodium, bupivacaine, and taxol for local drug delivery: Preparation, and kinetics and mechanism of in vitro release. *Journal of Controlled Release* **52**, 179-189 (1998).

54 Shikani, A. H. & Domb, A. J. Polymer chemotherapy for head and neck cancer. *Laryngoscope* **110**, 907-917 (2000).

55 Rahman, N. A. & Mathiowitz, E. Localization of bovine serum albumin in double-walled microspheres. *Journal of Controlled Release* **94**, 163-175 (2004).

56 Kokai, L. E. *et al.* Protein bioactivity and polymer orientation is affected by stabilizer incorporation for double-walled microspheres. *Journal of Controlled Release* **141**, 168-176 (2010).

57 Gopferich, A. Bioerodible implants with programmable drug release. *Journal of Controlled Release* **44**, 271-281 (1997).

58 Xiang, Z., Sarazin, P. & Favis, B. D. Controlling burst and final drug release times from porous polylactide devices derived from co-continuous polymer blends. *Biomacromolecules* **10**, 2053-2066 (2009).

59 Negrin, C. M., Delgado, A., Llabres, M. & Evora, C. Methadone implants for methadone maintenance treatment. In vitro and in vivo animal studies. *Journal of Controlled Release* **95**, 413-421 (2004).

60 Teomim, D. *et al.* Perivascular delivery of heparin for the reduction of smooth muscle cell proliferation after endothelial injury. *Journal of Controlled Release* **60**, 129-142 (1999).

61 Zheng, W. A water-in-oil-in-oil-in-water (W/O/O/W) method for producing drug-releasing, double-walled microspheres. *International Journal of Pharmaceutics* **374**, 90-95 (2009).

62 Eng, C. T., Lin, R. & Wang, C. H. Fabrication of double-walled microspheres for the sustained release of doxorubicin. *Journal of Colloid and Interface Science* **291**, 135-143 (2005).

63 Pollauf, E. J., Kim, K. K. & Pack, D. W. Small-molecule release from poly(D,L-lactide)/poly(D,L-lactide-co- glycolide) composite microparticles. *Journal of Pharmaceutical Sciences* **94**, 2013-2022 (2005).

64 Antheunis, H., Van Meer, J. C. D., De Geus, M., Kingma, W. & Koning, C. E. Improved mathematical model for the hydrolytic degradation of aliphatic polyesters. *Macromolecules* **42**, 2462-2471 (2009).

65 Antheunis, H., Van Der Meer, J. C., De Geus, M., Heise, A. & Koning, C. E. Autocatalytic equation describing the change in molecular weight during hydrolytic degradation of aliphatic polyesters. *Biomacromolecules* **11**, 1118-1124 (2010).

66 Berkland, C., King, M., Cox, A., Kim, K. & Pack, D. W. Precise control of PLG microsphere size provides enhanced control of drug release rate. *Journal of Controlled Release* **82**, 137-147 (2002).

67 Berkland, C. *et al.* Macromolecule release from monodisperse PLG microspheres: Control of release rates and investigation of release mechanism. *Journal of Pharmaceutical Sciences* **96**, 1176-1191 (2007).

68 Friess, W. & Schlapp, M. Release mechanisms from gentamicin loaded poly(lactic-co-glycolic acid) (PLGA) microparticles. *Journal of Pharmaceutical Sciences* **91**, 845-855 (2002).

69 Vogelhuber, W. *et al.* Programmable biodegradable implants. *Journal of Controlled Release* **73**, 75-88 (2001).

70 Luan, X. & Bodmeier, R. Influence of the poly(lactide-co-glycolide) type on the leuprolide release from in situ forming microparticle systems. *Journal of Controlled Release* **110**, 266-272 (2006).

71 Bhardwaj, R. & Blanchard, J. In vitro evaluation of Poly(D,L-lactide-co-glycolide) polymer-based implants containing the melanocyte stimulating hormone analog, Melanotan-I. *Journal of Controlled Release* **45**, 49-55 (1997).

72 Wei, G., Pettway, G. J., McCauley, L. K. & Ma, P. X. The release profiles and bioactivity of parathyroid hormone from poly(lactic-co-glycolic acid) microspheres. *Biomaterials* **25**, 345-352 (2004).

73 Sturesson, C. *et al.* Encapsulation of rotavirus into poly(lactide-co-glycolide) microspheres. *Journal of Controlled Release* **59**, 377-389 (1999).

74 Cleland, J. L. *et al.* Recombinant human growth hormone poly(lactic-co-glycolic acid) (PLGA) microspheres provide a long lasting effect. *Journal of Controlled Release* **49**, 193-205 (1997).

75 Mao, S. *et al.* Effect of WOW process parameters on morphology and burst release of FITC-dextran loaded PLGA microspheres. *International Journal of Pharmaceutics* **334**, 137-148 (2007).

76 Cross, D. P. & Wang, C. Stromal-derived factor-1 alpha-loaded PLGA microspheres for stem cell recruitment. *Pharmaceutical Research* **28**, 2477-2489 (2011).

77 Giovagnoli, S., Blasi, P., Ricci, M. & Rossi, C. Biodegradable microspheres as carriers for native superoxide dismutase and catalase delivery. *AAPS PharmSciTech* **5** (2004).

78 Panyam, J. *et al.* Polymer degradation and in vitro release of a model protein from poly(D,L-lactide-co-glycolide) nano- and microparticles. *Journal of Controlled Release* **92**, 173-187 (2003).

79 Wang, Y., Challa, P., Epstein, D. L. & Yuan, F. Controlled release of ethacrynic acid from poly(lactide-co-glycolide) films for glaucoma treatment. *Biomaterials* **25**, 4279-4285 (2004).

80 Determan, A. S., Brian G. Trewyn, Victor S.-Y. Lin, Marit Nilsen-Hamilton, Balaji Narasimhan. Encapsulation, stabilization, and release of BSA-FITC from polyanhydride microspheres. *Journal of Controlled Release* **100**, 97-109 (2004).

81 Crow, B. B., Borneman, A. F., Hawkins, D. L., Smith, G. M. & Nelson, K. D. Evaluation of in vitro drug release, pH change, and molecular weight degradation of poly(L-lactic acid) and poly(D,L-lactide-co-glycolide) fibers. *Tissue Engineering* **11**, 1077-1084 (2005).

82 Murakami, H., Kobayashi, M., Takeuchi, H. & Kawashima, Y. Utilization of poly(DL-lactide-co-glycolide) nanoparticles for preparation of mini-depot tablets by direct compression **SWELLING. *Journal of Controlled Release* **67**, 29-36 (2000).

83 Sendil, D., Wise, D. L. & Hasirci, V. Assessment of biodegradable controlled release rod systems for pain relief applications. *Journal of Biomaterials Science, Polymer Edition* **13**, 1-15 (2002).

84 Cao, H., Chen, L. B., Liu, Y. S., Xiu, H. & Wang, H. Poly-D, L-lactide and levofloxacin-blended beads: A sustained local releasing system to treat osteomyelitis. *Journal of Applied Polymer Science* **124**, 3678-3684 (2012).

85 Reeve, M. S., McCarthy, S. P., Downey, M. J. & Gross, R. A. Polylactide stereochemistry: Effect on enzymatic degradability. *Macromolecules* **27**, 825-831 (1994).

86 Joshi, A. & Himmelstein, K. J. Dynamics of controlled release from bioerodible matrices. *Journal of Controlled Release* **15**, 95-104 (1991).

87 Faisant, N. *et al.* The effect of gamma-irradiation on drug release from bioerodible microparticles: A quantitative treatment. *International Journal of Pharmaceutics* **242**, 281-284 (2002).

88 Yoshioka, S., Aso, Y. & Kojima, S. Drug release from poly(dl-lactide) microspheres controlled by γ-irradiation. *Journal of Controlled Release* **37**, 263-267 (1995).

89 Blanco-Prieto, M. J., Campanero, M. A., Besseghir, K., Heimgatner, F. & Gander, B. Importance of single or blended polymer types for controlled in vitro release and plasma levels of a somatostatin analogue entrapped in PLA/PLGA microspheres. *Journal of Controlled Release* **96**, 437-448 (2004).

90 Pettit, D. K. *et al.* Characterization of poly(glycolide-co-D,L-lactide)/poly(D,L-lactide) microspheres for controlled release of GM-CSF. *Pharmaceutical Research* **14**, 1422-1430 (1997).

91 Duvvuri, S., Gaurav Janoria, K. & Mitra, A. K. Effect of polymer blending on the release of ganciclovir from PLGA microspheres. *Pharmaceutical Research* **23**, 215-223 (2006).

92 Thomas, P. A., Padmaja, T. & Kulkarni, M. G. Polyanhydride blend microspheres: Novel carriers for the controlled release of macromolecular drugs. *Journal of Controlled Release* **43**, 273-281 (1997).

93 Schliecker, G., Schmidt, C., Fuchs, S., Wombacher, R. & Kissel, T. Hydrolytic degradation of poly(lactide-co-glycolide) films: Effect of oligomers on degradation rate and crystallinity. *International Journal of Pharmaceutics* **266**, 39-49 (2003).

94 Determan, A. S., Graham, J. R., Pfeiffer, K. A. & Narasimhan, B. The role of microsphere fabrication methods on the stability and release kinetics of ovalbumin encapsulated in polyanhydride microspheres. *Journal of Microencapsulation* **23**, 832-843 (2006).

95 Siepmann, J. & Gopferich, A. Mathematical modeling of bioerodible, polymeric drug delivery systems. *Advanced Drug Delivery Reviews* **48**, 229-247 (2001).

96 Arifin, D. Y., Lee, L. Y. & Wang, C. H. Mathematical modeling and simulation of drug release from microspheres: Implications to drug delivery systems. *Advanced Drug Delivery Reviews* **58**, 1274-1325 (2006).

97 Thombre, A. G. & Himmelstein, K. J. Simultaneous transport-reaction model for controlled drug delivery from catalyzed bioerodible polymer matrices. *AIChE Journal* **31**, 759-766 (1985).

98 Saltzman, W. M. & Langer, R. Transport rates of proteins in porous materials with known microgeometry. *Biophysical Journal* **55**, 163-171 (1989).

99 Gopferich, A., Karydas, D. & Langer, R. Predicting drug release from cylindric polyanhydride matrix discs. *European Journal of Pharmaceutics and Biopharmaceutics* **41**, 81-87 (1995).

100 Siepmann, J., Faisant, N. & Benoit, J. P. A new mathematical model quantifying drug release from bioerodible microparticles using Monte Carlo simulations. *Pharmaceutical Research* **19**, 1885-1893 (2002).

101 Raman, C., Berkland, C., Kim, K. & Pack, D. W. Modeling small-molecule release from PLG microspheres: Effects of polymer degradation and nonuniform drug distribution. *Journal of Controlled Release* **103**, 149-158 (2005).

102 Wong, H. M., Wang, J. J. & Wang, C. H. In vitro sustained release of human immunoglobulin G from biodegradable microspheres. *Industrial and Engineering Chemistry Research* **40**, 933-948 (2001).

103 Zhang, M., Yang, Z., Chow, L. L. & Wang, C. H. Simulation of drug release from biodegradable polymeric microspheres with bulk and surface erosions. *Journal of Pharmaceutical Sciences* **92**, 2040-2056 (2003).

104 He, J., Zhong, C. & Mi, J. Modeling of drug release from bioerodible polymer matrices. *Drug Delivery: Journal of Delivery and Targeting of Therapeutic Agents* **12**, 251-259 (2005).

105 Khang, G., Seo, S. A., Choi, H. S., Rhee, J. M. & Lee, H. B. Evaluation of in vitro release profiles of fentanyl-loaded PLGA oligomer microspheres. *Macromolecular Research* **10**, 246-252 (2002).

106 Anandakumar, K., Kannan, K. & Vetrichelvan, T. Development and validation of emtricitabine and tenofovir disoproxil fumerate in pure and in fixed dose combination by UV spectrophotometry. *Digest Journal of Nanomaterials and Biostructures* **6**, 1085-1090 (2011).

107 Jain, R. A. The manufacturing techniques of various drug loaded biodegradable poly(lactide-co-glycolide) (PLGA) devices. *Biomaterials* **21**, 2475-2490 (2000).

108 Shen, E. K., m. Dziadul, B. Mee-Kyung Lim, Narasimhan, B. Mechanistic relationships between polymer microstructure and drug release kinetics in bioerodible polyanhydrides. *Journal of Controlled Release* **82**, 115-125 (2002).

109 Rosas, J. E. *et al.* Biodegradable PLGA microspheres as a delivery system for malaria synthetic peptide SPf66. *Vaccine* **19**, 4445-4451 (2001).

110 Chaw, C. S., Yang, Y. Y., Lim, I. J. & Phan, T. T. Water-soluble betamethasone-loaded poly(lactide-co-glycolide) hollow microparticles as a sustained release dosage form. *Journal of Microencapsulation* **20**, 349-359 (2003).

111 Elkheshen, S. A. & Radwan, M. A. Sustained release microspheres of metoclopramide using poly(D,L-lactide-co-glycolide) copolymers. *Journal of Microencapsulation* **17**, 425-435 (2000).

112 Zong, X. H. *et al.* Structure and morphology changes in absorbable poly(glycolide) and poly(glycolide-co-lactide) during in vitro degradation. *Macromolecules* **32**, 8107-8114 (1999).

113 Hakkarainen, M., Albertsson, A. C. & Karlsson, S. Weight losses and molecular weight changes correlated with the evolution of hydroxyacids in simulated in vivo degradation of homo- and copolymers of PLA and PGA. *Polymer Degradation and Stability* **52**, 283-291 (1996).

114 Fredenberg, S., Reslow, M. & Axelsson, A. Measurement of protein diffusion through poly(D,L-lactide-co-glycolide). *Pharmaceutical Development and Technology* **10**, 299-307 (2005).

115 Mathiowitz, E., Ron, E., Mathiowitz, G., Amato, C. & Langer, R. Morphological characterization of bioerodible polymers. 1. Crystallinity of polyanhydride copolymers. *Macromolecules* **23**, 3212-3218 (1990).

116 Kipper, M. J., Seifert, S., Thiyagarajan, P. & Narasimhan, B. Morphology of polyanhydride copolymers: Time-resolved small-angle X-ray scattering studies of crystallization. *Journal of Polymer Science, Part B: Polymer Physics* **43**, 463-477 (2005).

117 Grayson, A. C. R. *et al.* Differential degradation rates in vivo and in vitro of biocompatible poly(lactic acid) and poly(glycolic acid) homo- and co-polymers for polymeric drug-delivery microchip. *Journal of Biomaterials Science, Polymer Edition* **15**, 1281-1304 (2004).

118 Gopferich, A. & Tessmar, J. Polyanhydride degradation and erosion. *Advanced Drug Delivery Reviews* **54**, 911-931 (2002).

119 Park, T. G. Degradation of poly(lactic-co-glycolic acid) microspheres: Effect of copolymer composition. *Biomaterials* **16**, 1123-1130 (1995).

120 Gopferich, A. & Langer, R. Modeling monomer release from bioerodible polymers. *Journal of Controlled Release* **33**, 55-69 (1995).

121 Saha, S. K. & Tsuji, H. Hydrolytic degradation of amorphous films of L-lactide copolymers with glycolide and D-lactide. *Macromolecular Materials and Engineering* **291**, 357-368 (2006).

122 Gopferich, A. & Langer, R. Modeling of polymer erosion in three dimensions: rotationally symmetric devices. *AIChE Journal* **41**, 2292-2299 (1995).

123 Dunne, M., Corrigan, O. I. & Ramtoola, Z. Influence of particle size and dissolution conditions on the degradation properties of polylactide-co-glycolide particles. *Biomaterials* **21**, 1659-1668 (2000).

124 Gopferich, A. Polymer bulk erosion. *Macromolecules* **30**, 2598-2604 (1997).

125 Brannon-Peppas, L. Recent advances on the use of biodegradable microparticles and nanoparticles in controlled drug delivery. *International Journal of Pharmaceutics* **116**, 1-9 (1995).

126 Rothstein, S. N., Federspiel, W. J. & Little, S. R. A unified mathematical model for the prediction of controlled release from surface and bulk eroding polymer matrices. *Biomaterials* **30**, 1657-1664 (2009).

127 Wagner, J. G. History of pharmacokinetics. *Pharmacology and Therapeutics* **12**, 537-562 (1981).

128 Rothstein, S. N., Federspiel, W. J. & Little, S. R. A simple model framework for the prediction of controlled release from bulk eroding polymer matrices. *Journal of Materials Chemistry* **18**, 1873-1880 (2008).

129 Baker, P. R. S. *et al.* Fatty acid transduction of nitric oxide signaling: Multiple nitrated unsaturated fatty acid derivatives exist in human blood and urine and serve as endogenous peroxisome proliferator-activated receptor ligands. *Journal of Biological Chemistry* **280**, 42464-42475 (2005).

130 D'Avolio, A., De Requena, M. S. D. G., Ibañez, A., Bonora, S. & Di Perri, G. An improved HPLC fluorimetric method for the determination of enfuvirtide plasma levels in HIV-infected patients. *Therapeutic Drug Monitoring* **28**, 110-115 (2006).

131 Rudolph, V. *et al.* Nitro-fatty acid metabolome: saturation, desaturation, β-oxidation, and protein adduction. *Journal of Biological Chemistry* **284**, 1461-1473 (2009).

132 Murty, S. B., Goodman, J., Thanoo, B. C. & DeLuca, P. P. Identification of chemically modified peptide from poly(D,L-lactide-co-glycolide) microspheres under in vitro release conditions. *AAPS PharmSciTech [electronic resource]* **4** (2003).

133 Hickey, T., Kreutzer, D., Burgess, D. J. & Moussy, F. Dexamethasone/PLGA microspheres for continuous delivery of an anti-inflammatory drug for implantable medical devices. *Biomaterials* **23**, 1649-1656 (2002).

134 Rafi, M., Singh, S. M., Kanchan, V., Anish, C. K. & Panda, A. K. Controlled release of bioactive recombinant human growth hormone from PLGA microparticles. *Journal of Microencapsulation* **27**, 552-560, doi:doi:10.3109/02652048.2010.489974 (2010).

135 Formiga, F. R. *et al.* Sustained release of VEGF through PLGA microparticles improves vasculogenesis and tissue remodeling in an acute myocardial ischemia-reperfusion model. *Journal of Controlled Release* **147**, 30-37 (2010).

136 Jiang, W. & Schwendeman, S. P. Stabilization of a model formalinized protein antigen encapsulated in poly(lactide-co-glycolide)-based microspheres. *Journal of Pharmaceutical Sciences* **90**, 1558-1569 (2001).

137 Rocha, F. G. *et al.* The effect of sustained delivery of vascular endothelial growth factor on angiogenesis in tissue-engineered intestine. *Biomaterials* **29**, 2884-2890 (2008).

138 Liggins, R. T. & Burt, H. M. Paclitaxel-loaded poly(L-lactic acid) microspheres 3: Blending low and high molecular weight polymers to control morphology and drug release. *International Journal of Pharmaceutics* **282**, 61-71 (2004).

139 Lao, L. L., Peppas, N. A., Boey, F. Y. C. & Venkatraman, S. S. Modeling of drug release from bulk-degrading polymers. *International Journal of Pharmaceutics* **418**, 28-41 (2011).

140 Diwan, M. & Park, T. G. Pegylation enhances protein stability during encapsulation in PLGA microspheres. *Journal of controlled release : official journal of the Controlled Release Society* **73**, 233-244 (2001).

141 Ghalanbor, Z., Körber, M. & Bodmeier, R. Improved Lysozyme Stability and Release Properties of Poly(lactide-co-glycolide) Implants Prepared by Hot-Melt Extrusion. *Pharmaceutical Research* **27**, 371-379, doi:10.1007/s11095-009-0033-x (2010).

142 Jhunjhunwala, S. *et al.* Controlled release formulations of IL-2, TGF-β1 and rapamycin for the induction of regulatory T cells. *Journal of Controlled Release* **159**, 78-84 (2012).

143 Tengood, J. E., Kovach, K. M., Vescovi, P. E., Russell, A. J. & Little, S. R. Sequential delivery of vascular endothelial growth factor and sphingosine 1-phosphate for angiogenesis. *Biomaterials* **31**, 7805-7812 (2010).

144 Tengood, J. E., Ridenour, R., Brodsky, R., Russell, A. J. & Little, S. R. Sequential delivery of basic fibroblast growth factor and platelet-derived growth factor for angiogenesis. *Tissue Engineering - Part A* **17**, 1181-1189 (2011).

145 Ding, A. G., Shenderova, A. & Schwendeman, S. P. Prediction of microclimate pH in poly(lactic-co-glycolic acid) films. *Journal of the American Chemical Society* **128**, 5384-5390 (2006).

146 Frenning, G., Brohede, U. & Strømme, M. Finite element analysis of the release of slowly dissolving drugs from cylindrical matrix systems. *Journal of Controlled Release* **107**, 320-329 (2005).

147 Ekins, S., Mestres, J. & Testa, B. In silico pharmacology for drug discovery: Methods for virtual ligand screening and profiling. *British Journal of Pharmacology* **152**, 9-20 (2007).

148 Paul, D. R. Elaborations on the Higuchi model for drug delivery. *International Journal of Pharmaceutics* **418**, 13-17 (2011).

149 Clements, C. J. & Griffiths, E. The global impact of vaccines containing aluminium adjuvants. *Vaccine* **20** (2002).

150 Vaccine Preventable Deaths and the Global Immunization Vision and Strategy, 2006--2015. *WHO Department of Immunization, Vaccines and Biologicals and UNICEF Programme Division, Health Section* **55**, 511-515 (2006).

151 Preis, I. & Langer, R. S. A single-step immunization by sustained antigen release. *Journal of Immunological Methods* **28**, 193-197 (1979).

152 Lofthouse, S. Immunological aspects of controlled antigen delivery. *Advanced Drug Delivery Reviews* **54**, 863-870 (2002).

153 O'Hagan, D. T., Singh, M. & Gupta, R. K. Poly(lactide-co-glycolide) microparticles for the development of single- dose controlled-release vaccines. *Advanced Drug Delivery Reviews* **32**, 225-246 (1998).

154 CDCP. Recommended Immunization Schedules for Persons Aged 0--18 Years--- United States, 2007. *MMWR* **55**, Q1--Q4 (2006).

155 Men, Y., Thmasin, C., Merkle, H. P., Gander, B. & Corradin, G. A single administration of tetanus toxoid in biodegradable microspheres elicits T cell and antibody responses similar or superior to those obtained with aluminum hydroxide. *Vaccine* **13**, 683-689 (1995).

156 Gupta, R. K., Alroy, J., Alonso, M. J., Langer, R. & Siber, G. R. Chronic local tissue reactions, long term immunogenicity and immunologic priming of mice and guinea pigs to tetanus toxoid encapsulated in biodegradable polymer microspheres composed of poly lactide-co-glycolide polymers. *Vaccine* **15**, 1716-1723 (1997).

157 Hanes, J., Cleland, J. L. & Langer, R. New advances in microsphere-based single-dose vaccines. *Advanced Drug Delivery Reviews* **28**, 97-119 (1997).

158 Singh, M., Chakrapani, A. & O'Hagan, D. Nanoparticles and microparticles as vaccine-delivery systems. *Expert Review of Vaccines* **6**, 797-808 (2007).

159 Jaganathan, K. S. *et al.* Development of a single dose tetanus toxoid formulation based on polymeric microspheres: A comparative study of poly(D,L-lactic-co-glycolic acid) versus chitosan microspheres. *International Journal of Pharmaceutics* **294**, 23-32 (2005).

160 Jaganathan, K. S., Singh, P., Prabakaran, D., Mishra, V. & Vyas, S. P. Development of a single-dose stabilized poly(D,L-lactic-co-glycolic acid) microspheres-based vaccine against hepatitis B. *Journal of Pharmacy and Pharmacology* **56**, 1243-1250 (2004).

161 Shi, L. *et al.* Pharmaceutical and immunological evaluation of a single-shot Hepatitis B vaccine formulated with PLGA microspheres. *Journal of Pharmaceutical Sciences* **91**, 1019-1035 (2002).

162 Jones, L. S. *et al.* Effects of adsorption to aluminum salt adjuvants on the structure and stability of model protein antigens. *Journal of Biological Chemistry* **280**, 13406-13414 (2005).

163 Yang, Z., Chen, A., Sun, H., Ye, Y. & Fang, W. Ginsenoside Rd elicits Th1 and Th2 immune responses to ovalbumin in mice. *Vaccine* **25**, 161-169 (2007).

164 Kersten, G. F. A., Donders, D., Akkermans, A. & Beuvery, E. C. Single shot with tetanus toxoid in biodegradable microspheres protects mice despite acid-induced denaturation of the antigen. *Vaccine* **14**, 1627-1632 (1996).

165 Kwon, Y. J., Standley, S. M., Goodwin, A. P., Gillies, E. R. & Fréchet, J. M. J. Directed antigen presentation using polymeric microparticulate carriers degradable at lysosomal pH for controlled immune responses. *Molecular Pharmaceutics* **2**, 83-91 (2005).

166 Liang, M. T., Davies, N. M., Blanchfield, J. T. & Toth, I. Particulate systems as adjuvants and carriers for peptide and protein antigens. *Current Drug Delivery* **3**, 379-388 (2006).

167 Moser, C. A., Speaker, T. J., Berlin, J. A. & Offit, P. A. Aqueous-based microencapsulation enhances virus-specific humoral immune responses in mice after parenteral inoculation. *Vaccine* **14**, 1235-1238 (1996).

168 Newman, K. D., Samuel, J. & Kwon, G. Ovalbumin peptide encapsulated in poly(d,l lactic-co-glycolic acid) microspheres is capable of inducing a T helper type 1 immune response. *Journal of Controlled Release* **54**, 49-59 (1998).

169 O'Hagan, D. T., Singh, M. & Ulmer, J. B. Microparticle-based technologies for vaccines. *Methods* **40**, 10-19 (2006).

170 Singh, M. *et al.* Controlled release microparticles as a single dose hepatitis B vaccine: Evaluation of immunogenicity in mice. *Vaccine* **15**, 475-481 (1997).

171 Singh, M. *et al.* Immunogenicity and protection in small-animal models with controlled-release tetanus toxoid microparticles as a single-dose vaccine. *Infection and Immunity* **65**, 1716-1721 (1997).

172 Yan, C. *et al.* Dependence of ricin toxoid vaccine efficacy on the structure of poly(lactide-co-glycolide) microparticle carriers. *Vaccine* **13**, 645-651 (1995).

173 Zhou, S., Liao, X., Li, X., Deng, X. & Li, H. Poly-D,L-lactide-co-poly(ethylene glycol) microspheres as potential vaccine delivery systems. *Journal of Controlled Release* **86**, 195-205 (2003).

174 Amorij, J. P. *et al.* Towards tailored vaccine delivery: Needs, challenges and perspectives. *Journal of Controlled Release* **161**, 363-367 (2012).

175 Vordermeier, H. M. *et al.* Synthetic delivery system for tuberculosis vaccines: Immunological evaluation of the M. tuberculosis 38 kDa protein entrapped in biodegradable PLG microparticles. *Vaccine* **13**, 1576-1582 (1995).

176 Wischke, C., Mathew, S., Roch, T., Frentsch, M. & Lendlein, A. Potential of NOD receptor ligands as immunomodulators in particulate vaccine carriers. *Journal of Controlled Release* (2012).

177 Meraz, I. M. *et al.* Activation of the inflammasome and enhanced migration of microparticle-stimulated dendritic cells to the draining lymph node. *Molecular Pharmaceutics* **9**, 2049-2062 (2012).

178 Lewis, J. S., Zaveri, T. D., Crooks, C. P. & Keselowsky, B. G. Microparticle surface modifications targeting dendritic cells for non-activating applications. *Biomaterials* **33**, 7221-7232 (2012).

179 Kanthamneni, N. *et al.* Enhanced stability of horseradish peroxidase encapsulated in acetalated dextran microparticles stored outside cold chain conditions. *International Journal of Pharmaceutics* **431**, 101-110 (2012).

180 Carrillo-Conde, B. R., Ramer-Tait, A. E., Wannemuehler, M. J. & Narasimhan, B. Chemistry-dependent adsorption of serum proteins onto polyanhydride microparticles differentially influences dendritic cell uptake and activation. *Acta Biomaterialia* **8**, 3618-3628 (2012).

181 Torres, M. P. *et al.* Polyanhydride microparticles enhance dendritic cell antigen presentation and activation. *Acta Biomaterialia* **7**, 2857-2864 (2011).

182 Jain, S., O'Hagan, D. T. & Singh, M. The long-term potential of biodegradable poly(lactideco-glycolide) microparticles as the next-generation vaccine adjuvant. *Expert Review of Vaccines* **10**, 1731-1742 (2011).

183 Goyal, A. K. *et al.* Nanodecoy system: A novel approach to design hepatitis B vaccine for immunopotentiation. *International Journal of Pharmaceutics* **309**, 227-233 (2006).

184 Johansen, P., Corradin, G., Merkle, H. P. & Gander, B. Release of tetanus toxoid from adjuvants and PLGA microspheres: How experimental set-up and surface adsorption fool the pattern. *Journal of Controlled Release* **56**, 209-217 (1998).

185 Park, E. S., Maniar, M. & Shah, J. Effects of model compounds with varying physicochemical properties on erosion of polyanhydride devices. *Journal of Controlled Release* **40**, 111-121 (1996).

186 Park, E. S., Maniar, M. & Shah, J. Water uptake in to polyanhydride devices: Kinetics of uptake and effects of model compounds incorporated, and device geometry on water uptake. *Journal of Controlled Release* **40**, 55-65 (1996).

187 Sinha, V. R. & Trehan, A. Biodegradable microspheres for parenteral delivery. *Critical Reviews in Therapeutic Drug Carrier Systems* **22**, 535-602 (2005).

188 Kemp, S. F. *et al.* Pharmacokinetic and pharmacodynamic characteristics of a long-acting Growth Hormone (GH) preparation (nutropin depot) in GH-deficient children. *Journal of Clinical Endocrinology and Metabolism* **89**, 3234-3240 (2004).

189 Serre, K. *et al.* Molecular differences between the divergent responses of ovalbumin-specific CD4 T cells to alum-precipitated ovalbumin compared to ovalbumin expressed by Salmonella. *Molecular immunology* **45**, 3558-3566, doi:10.1016/j.molimm.2008.05.010 (2008).

190 Falo Jr, L. D., Kovacsovics-Bankowski, M., Thompson, K. & Rock, K. L. Targeting antigen into the phagocytic pathway in vivo induces protective tumour immunity. *Nature Medicine* **1**, 649-653 (1995).

191 Morelli, P. A., Falkner, D., Plowey, J., Larregina, A. T. & Falo, L. D. DNA immunisation: altering the cellular localisation of expressed protein and the immunisation route allows manipulation of the immune response. *Vaccine* **22**, 447-456 (2004).

192 Cahyadi, C., Koh, J. J., Loh, Z. H., Chan, L. W. & Heng, P. W. A Feasibility Study on Pellet Coating Using a High-Speed Quasi-continuous Coater. *AAPS PharmSciTech*, doi:10.1208/s12249-012-9852-x (2012).

193 Domb, A. J. & Maniar, M. Absorbable biopolymers derived from dimer fatty acids. *Journal of Polymer Science, Part A: Polymer Chemistry* **31**, 1275-1285 (1993).

194 D'Souza, S. S. & DeLuca, P. P. Methods to assess in Vitro drug release from injectable polymeric particulate systems. *Pharmaceutical Research* **23**, 460-474 (2006).

195 Zolnik, B. S., Leary, P. E. & Burgess, D. J. Elevated temperature accelerated release testing of PLGA microspheres. *Journal of Controlled Release* **112**, 293-300 (2006).

196 Maniar, M., Domb, A., Haffer, A. & Shah, J. Controlled release of a local anesthetic from fatty acid dimer based polyanhydride. *Journal of Controlled Release* **30**, 233-239 (1994).

197 Zygourakis, K. & Markenscoff, P. A. Computer-aided design of bioerodible devices with optimal release characteristics: A cellular automata approach. *Biomaterials* **17**, 125-135 (1996).

198 Nair, L. S. & Laurencin, C. T. in *Advances in Biochemical Engineering/Biotechnology* Vol. 102 47-90 (2006).

199 Cleland, J. L. *et al.* Recombinant human growth hormone poly(lactic-co-glycolic acid) (PLGA) microspheres provide a long lasting effect. *Journal of Controlled Release* **49**, 193-205, doi:10.1016/s0168-3659(97)00075-8 (1997).

200 Ye, M., Kim, S. & Park, K. Issues in long-term protein delivery using biodegradable microparticles. *Journal of Controlled Release* **146**, 241-260 (2010).

201 Stocker, H. *et al.* Pharmacokinetics of enfuvirtide in patients treated in typical routine clinical settings. *Antimicrob Agents Chemother* **50**, 667-673, doi:10.1128/aac.50.2.667-673.2006 (2006).

202 Rockstroh, J. *et al.* Adherence to enfuvirtide and its impact on treatment efficacy. *AIDS Research and Human Retroviruses* **24**, 141-148 (2008).

203 Cohen, J. HIV/AIDS clinical trials. A powerful and perplexing new HIV prevention tool. *Science (New York, N.Y.)* **330**, 1298-1299, doi:10.1126/science.330.6009.1298 (2010).

204 M Delmedico, B. B., N Cammack et al. in *XVI International AIDS Conference.*

205 Kapoor, D. N., Katare, O. P. & Dhawan, S. In situ forming implant for controlled delivery of an anti-HIV fusion inhibitor. *International Journal of Pharmaceutics* **426**, 132-143 (2012).

206 Wei, X. *et al.* Emergence of resistant human immunodeficiency virus type 1 in patients receiving fusion inhibitor (T-20) monotherapy. *Antimicrobial Agents and Chemotherapy* **46**, 1896-1905 (2002).

207 Sluis-Cremer, N. *et al.* Anti-human immunodeficiency virus activity, cross-resistance, cytotoxicity, and intracellular pharmacology of the 3′-azido-2′,3′- dideoxypurine nucleosides. *Antimicrobial Agents and Chemotherapy* **53**, 3715-3719 (2009).

208 Berchane, N. S., Jebrail, F. F. & Andrews, M. J. Optimization of PLG microspheres for tailored drug release. *International Journal of Pharmaceutics* **383**, 81-88 (2010).

209 Choleris, E. *et al.* Microparticle-based delivery of oxytocin receptor antisense DNA in the medial amygdala blocks social recognition in female mice. *Proceedings of the National Academy of Sciences of the United States of America* **104**, 4670-4675 (2007).

210 Lawless, M. K., Hopkins, S. & Anwer, M. K. Quantitation of a 36-amino-acid peptide inhibitor of HIV-1 membrane fusion in animal and human plasma using high-

performance liquid chromatography and fluorescence detection. *Journal of Chromatography B: Biomedical Applications* **707**, 213-217 (1998).

211 Fu, K., Pack, D. W., Klibanov, A. M. & Langer, R. Visual evidence of acidic environment within degrading poly(lactic-co- glycolic acid) (PLGA) microspheres. *Pharmaceutical Research* **17**, 100-106 (2000).

212 Li, L. & Schwendeman, S. P. Mapping neutral microclimate pH in PLGA microspheres. *Journal of Controlled Release* **101**, 163-173 (2005).

213 Johnson, O. L. *et al.* The stabilization and encapsulation of human growth hormone into biodegradable microspheres. *Pharmaceutical Research* **14**, 730-735 (1997).

214 Borrego, P. *et al.* Baseline susceptibility of primary HIV-2 to entry inhibitors. *Antiviral Therapy* **17**, 565-570 (2012).

215 Ingallinella, P. *et al.* Addition of a cholesterol group to an HIV-1 peptide fusion inhibitor dramatically increases its antiviral potency. *Proceedings of the National Academy of Sciences of the United States of America* **106**, 5801-5806 (2009).

216 Program, A. R. a. R. R. (ed National Institute of Health) (2012).